System Sizing of PV-Powered DC Microgrids for Informal Settlements in South Africa

Development of a Design Framework Accelerating Electrification Efforts

Emma Shibata

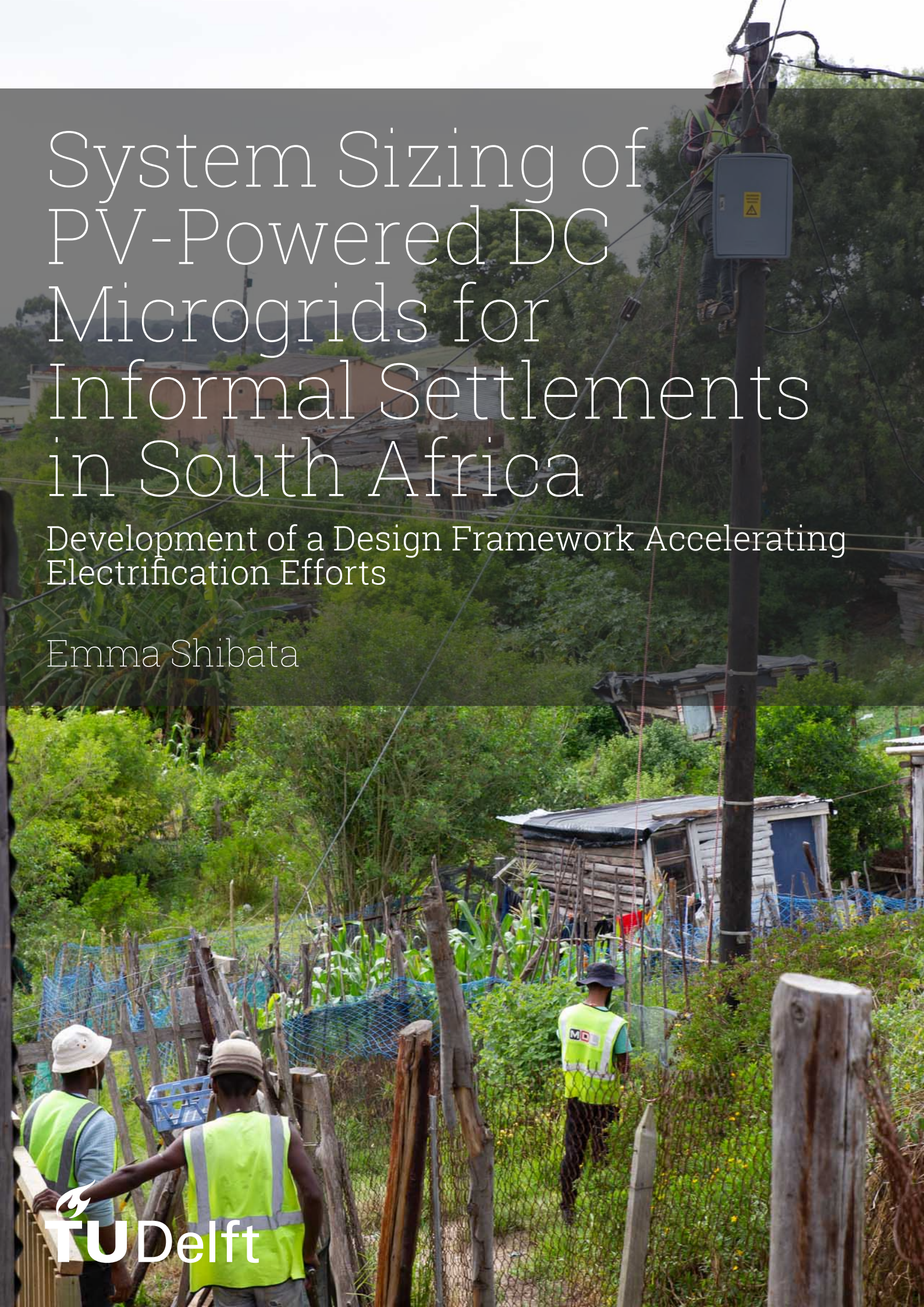

TU Delft

System Sizing of PV-Powered DC Microgrids for Informal Settlements in South Africa

Development of a Design Framework Accelerating Electrification Efforts

by

Emma Shibata

To obtain the degree of
Master of Science in Sustainable Energy Technology at
the Delft University of Technology

Student Number: 5720699

Project Duration: November 13, 2023 - July 29, 2024

Supervisor:	Dr. Patrizio Manganiello	Assistant Professor, PVMD
	Ir. Jesse Echeverry	DC Opportunities
	Dr. Ir. Laurens Mackay	DC Opportunities
Thesis Committee:	Dr. Zian Qin	Associate Professor, DCE&S
	Dr. Hesan Ziar	Assistant Professor, PVMD
	Dr. Patrizio Manganiello	Assistant Professor, PVMD
	Ir. Jesse Echeverry	DC Opportunities

TU Delft

DC pportunities

Acknowledgments

I dedicate this work to the following individuals, whose support, guidance, and encouragement have been essential throughout this journey:

- Dr. Patrizio Manganiello: The best university supervisor I could have ever wished for. Your guidance and encouragement have been instrumental in advancing my research and personal development. Thank you for exemplifying the kind of professional I strive to become.

- Ir. Jesse Echeverry: Thank you for your continuous support and belief in my abilities. Your trust in me for this project has fostered both my personal and professional growth.

- Dr. Ir. Laurens Mackay: Thank you for the continuous guidance in my thesis and accompanying me during one of the most impactful trips for me, to South Africa.

- Henry, Shoba, Andrew, Dmitry, and Arno: Your combined efforts during my trip to South Africa were invaluable to my project. Henry, your hospitality in George. Shoba, your guidance in navigating the Daveyton informal settlements and your ongoing support were instrumental. Andrew, Dmitry, and Arno, your assistance in organizing the visit to Thembalethu informal settlement and answering my questions greatly contributed to the success of this project.

- Daniel: Thank you for being there in my moments of doubts, always encouraging me to bounce back up. Our brainstorming sessions, where I could discuss even the smallest concerns, were incredibly helpful and meaningful to me.

- My Family: Any and all of my achievements are the product of your support. I am grateful for your love, support and opportunities you have given me that has shaped me to be who I am today.

Abstract

The motivation of this study stems from the reality that 2.2 million households in South Africa remain unelectrified, with the majority residing in informal settlements—communities that are remnants of the apartheid era, designed to enforce racially segregated living. While existing off-grid solutions provide basic electricity access to these households, they fail to meet the growing demand for higher levels of electricity access that local residents desire and can afford. This project aims to address this gap between the limited supply capacity of current off-grid solutions and the enhanced electricity services that communities are eager to receive.

Through site visits and consultations with local developers, specific design considerations and unique challenges were identified. These efforts revealed the limitations of existing open-source design tools, which do not comprehensively address the entire system's design requirements for the proposed solution of a PV-powered DC microgrid. Consequently, a new framework was developed, integrating open-source tools and custom Python scripts based on established methodologies.

The comprehensive design framework was applied to the informal settlements of Oudtshoorn and Daveyton, demonstrating its ability to generate feasible, scalable, and adaptable microgrid designs. Overall, this project provides a solid foundation for advancing electrification efforts in underserved communities.

Contents

1

Introduction

This introductory chapter provides an overview of the current state of electricity access in South Africa, highlighting existing challenges and complexities. The motivation to address these issues, to contribute towards enhancing electricity access levels are discussed. The approach and envisioned solution are introduced, alongside the project objectives and research questions guiding this study.

1.1. Background & Motivation

The background context necessary for understanding the current state of electricity access in South Africa is introduced in this section.

1.1.1. Call for Universal Electricity Access

The motivation of this study stems from the reality that, as of 2022, approximately 760 million people still remain unelectrified globally [1]. The wide disparity in human development as a consequence of varying levels of electricity access is evident, both between developed and developing Countries, as well as between the rich and poor within Countries [2].

The United Nations' Sustainable Development Goal (SDG) 7 addresses this issue, targeting to ensure access to affordable, reliable, sustainable, and modern energy for all by 2030 [3]. Electricity is arguably one of the most important commodities in any society of the world, adding to the importance of SDG 7 among the 17 SDGs. Electricity access is therefore critical in alleviating poverty, but also linked and fundamental to fulfilling the wider development agenda [2] [4].

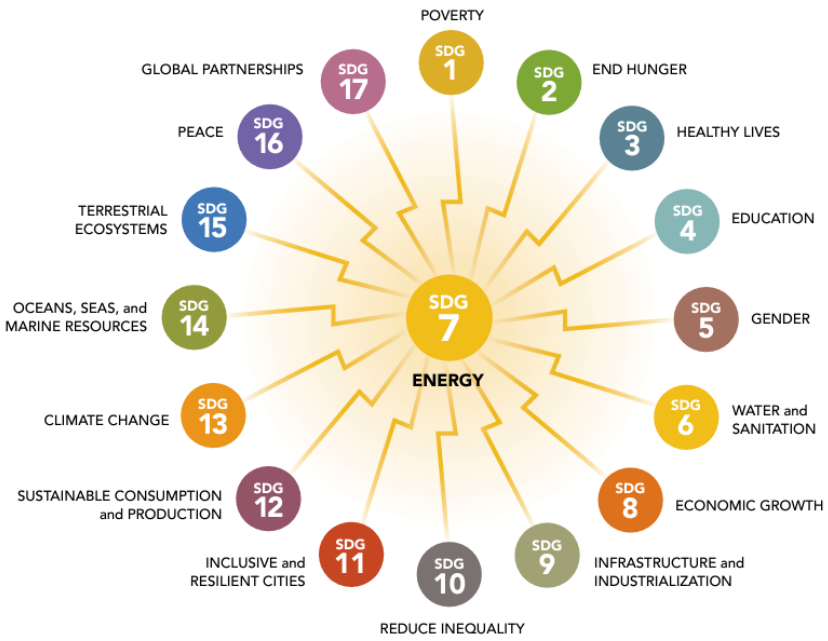

Figure 1.1: Interlinkage of SDG 7 to other SDGs [2].

1.1.2. Electrification Status of South Africa

Out of the global unelectrified population of 760 million, 598.8 million people are concentrated in Sub-Saharan Africa, as of 2023 [1]. Among these countries, South Africa has one of the highest national electrification rate of roughly 84% in 2020 [5]. The high electrification rate in comparison to the rest of Sub-Saharan Africa, visualized in Figure 1.2, is attributed to the National Electrification Programme (NEP). The NEP has facilitated over 3.4 million electrical grid connections from 1994, up to the end of 2001 [6]. This is a significant achievement that was mostly accomplished by Eskom, South Africa's energy monopoly, along with the municipalities. The electrification growth rates during the NEP were amongst the highest in the world, and was also achieved without external funding [7].

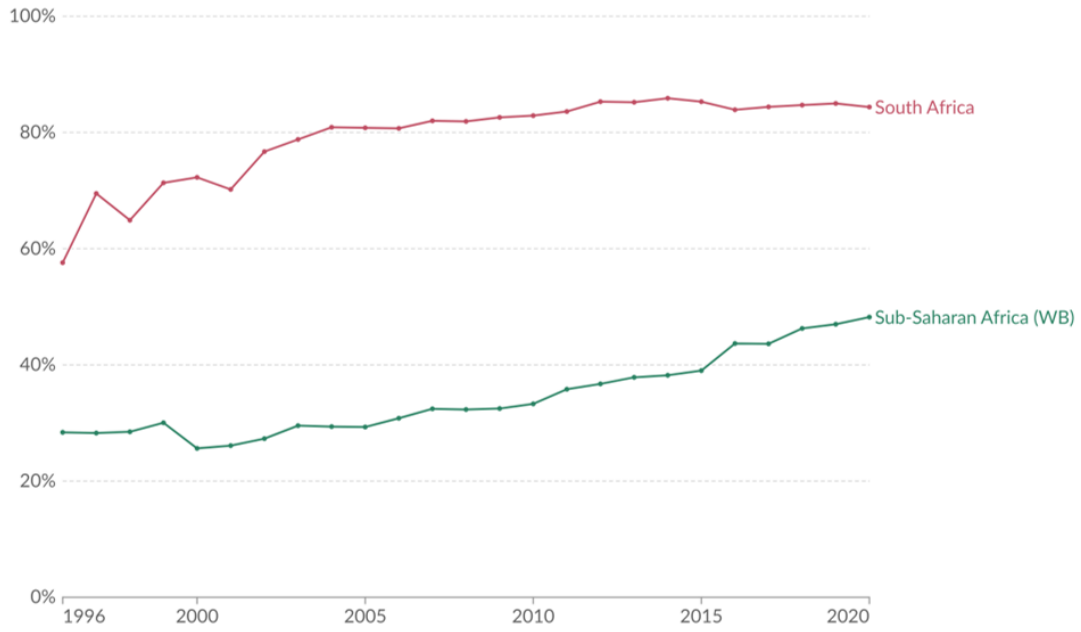

Figure 1.2: Electrification rate comparison between South Africa and Sub-Saharan Africa between 1996 and 2020 [5].

While acknowledging this achievement, it is also important to note that there are however, still 2.2 million households in South Africa that are unelectrified [8]. Additionally, the extent to which the rushed electrification meets the household electricity demand is questionable [9]. It is recorded that the project management and control processes changed throughout the NEP, initially to ensure the targeted number of new connections were met, but later to prioritize the financial viability. In order to reach connection targets efficiently while reducing the average cost per connection, one of the following two approaches were adopted:

- **The 'Blanket' Approach**
  This approach involved connecting households to the grid with a reduced 2.5 A connection, compared to the standard 60 A connection [6]. While it allowed for the immediate connection of poorer households, many of these households were not yet capable of using and paying for electricity. The welfare benefits were thus lower than expected, with monthly household consumption levels stagnating around 100 kWh rather than the anticipated 350 kWh. Because of the household electrical energy consumption stagnating below that needed to achieve financial break-even, the program was financially unviable [6].
- **The 'Targeted' Approach**
  This approach involved connecting only customers who applied and paid for a connection. While this ensured the financial viability of the program by focusing on significant electricity users, it resulted in the poorest households being connected last, or not at all.

Therefore, regardless of the approach adopted, there remains a significant population in South Africa without adequate electricity access or any access at all [10] [6]. While electrification maps such as Figure 1.3 may suggest that South Africa is only slightly behind Western societies in national electrification rates, it is important to recognize that this metric considers "having an electricity source that can provide basic lighting, and charge a phone or a radio for 4 hours a day" as being electrified. A more comprehensive consideration of electricity access levels are necessary to reveal the reality of South Africa's electrification state.

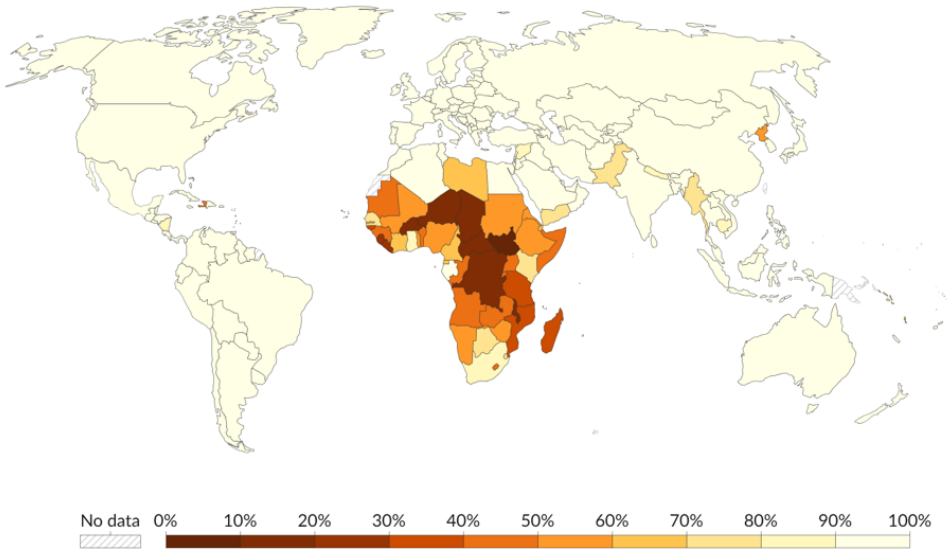

Figure 1.3: World map of national electrification rates in 2020 [5].

1.1.3. Electricity Access Metric

To avoid the misunderstanding of achieving electricity access with only limited connection that is inadequate to meet the needs of the community, the Multi-Tier Framework (MTF) is adopted as a metric for electricity access. Instead of adhering to the outdated binary measure of either having or not having a connection to electricity supply, the MTF offers a quantified categorization of electricity demand per tier, as outlined in Table 1.1. The MTF acknowledges that household electricity demand tends to increase over time. Figure 1.4 illustrates this trend, showcasing the rise in electricity demand from Tier 0 to Tier 5 through the increase in electrical appliances, their corresponding power ratings, and the improvement in the availability and reliability of electricity to power such appliances.

Table 1.1: Portion of the electricity access metric from the Multi-Tier Framework [11].

Attributes		Tier 0	Tier 1	Tier 2	Tier 3	Tier 4	Tier 5
Capacity	Power	< 3 W	> 3 W	> 50 W	> 200 W	> 800 W	> 2 kW
	Energy	< 12 Wh	> 12 Wh	> 200 Wh	> 1 kWh	> 3.4 kWh	> 8.2 kWh
Availability	Daily Availability	< 4 hours	> 4 hours		> 8 hours	> 16 hours	> 23 hours
	Evening Availability	< 1 hour	> 1 hour	> 2 hours	> 3 hours	> 4 hours	
Reliability	Number of disruptions per week	> 14				< 14	< 3 (total duration < 2 hours)

Figure 1.4: Minimal requirements by tier of electricity access [11].

1.1.4. Historical Cause of South Africa's Electricity Access Disparity

In contrast to the traditional urban-rural economic divide, South Africa presents a unique scenario of economic disparity that correlates to electricity access disparity. Within close proximity to urban areas, communities exist with lack of water, sanitation, paved roads and electricity connections, alongside elevated levels of crime and violence. These communities, "Townships", are remnants of the apartheid era designed to enforce racially segregated living [7]. Townships were established during the apartheid regime and served two purposes: to keep nonwhite people close enough to the city purely as source of cheap labor, and to enforce segregation. Townships were essentially dormitory towns for nonwhite people lacking essential services and infrastructure [7]. Despite political advancements, roughly 15 million people still inhabit South African townships [7]. Moreover, there has been a massive growth of informal settlements next to these townships, with approximately 3 million people living in worse conditions than the townships [7].

1.1.5. Limitations on the Expansion of South Africa's National Grid

Electrification via grid extension involves increasing grid capacity by connecting additional power plants and extending transmission lines to unelectrified areas. However, the lack of sufficient generation capacity, poor transmission and distribution infrastructure, high costs of supplying to rural and remote areas (due to high line losses and low usage), and the weak financial state of the utility often pose significant challenges [2]. In the case of South Africa and its national grid, challenges exist in the form of aging infrastructure, frequent load shedding, and significant tariff increases. Although electrification via the national grid will continue to play a key part in energy access solutions, these hurdles add difficulty to a successful execution.

Ageing Fossil Fuel Based Power Plants

South Africa's energy supply has historically been dominated by coal as its primary source, currently making up approximately 80% of the nations energy supply [12]. The nation's abundant supply of cheap coal enables coal to continue to remain the primary fuel source for electricity generation. Given this context, renewable energy sources currently account for less than 9.3% of South Africa's national electricity supply in 2023 [12].

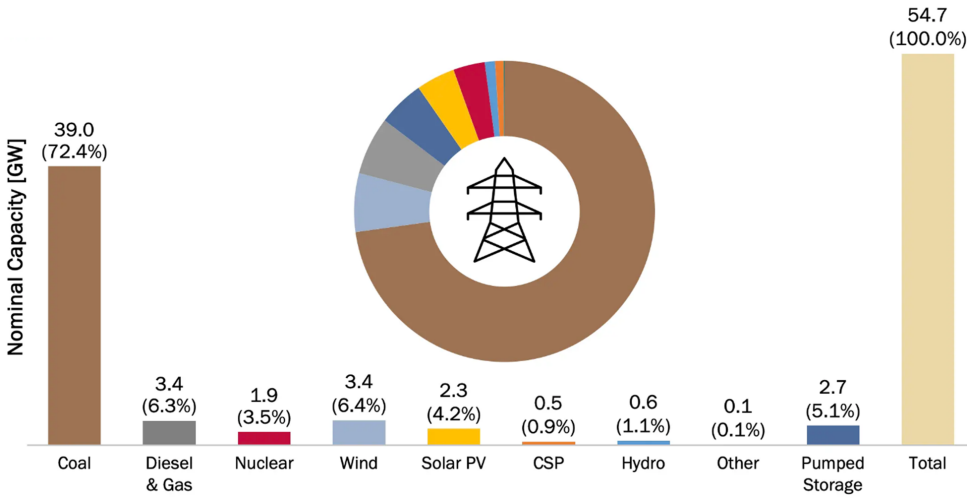

Figure 1.5: Annual energy mix of South Africa (April 2023 to March 2024) [13].

However, the share of coal continues to decrease, with a corresponding increase in unserved energy. This trend, observed in Figure 1.6, is attributed to the aging coal-fired power plant infrastructure approaching their end-of-life. The resultant increased maintenance downtime in addition to the scheduled phase-outs of these aging infrastructure is thus anticipated to cause a continuous decline in the share of coal in South Africa's energy mix [12]. Although the Renewable Energy Independent Power Producer Procurement Program (REIPPPP) aims to increase renewable shares, further increase in supply side deficiencies are expected in the near future [12].

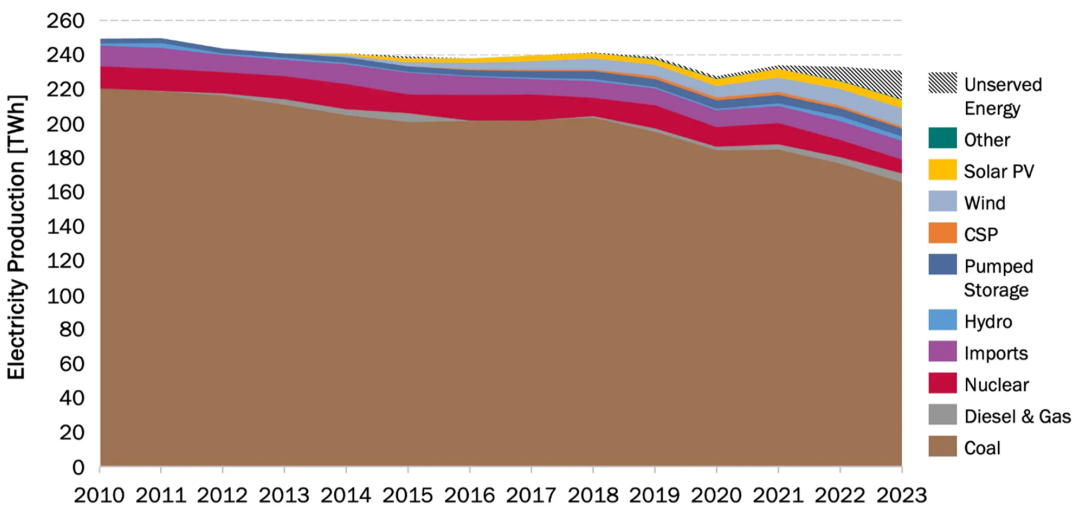

Figure 1.6: South African annual electricity production from 2010 to 2023 [13].

Load Shedding as a Result of Energy Supply Deficiency

As a result of supply side deficiencies, Eskom often resorts to load shedding, a controlled process that reduced the electricity demand via temporarily disconnecting communities from the grid. This is done to protect the electricity power system from a total blackout. As a result of of the increase in unserved energy mentioned in the previous subsection, load shedding has become a routine practice with rotational schedules that run for 2-4 hours a day [14]. Figure 1.7 visualizes the significant increase in annual hours of load shedding that was executed in the recent years.

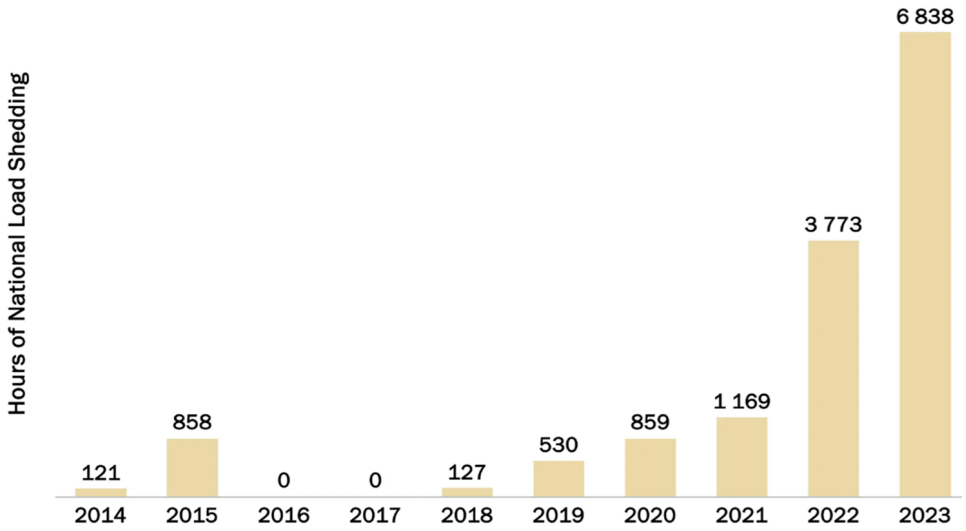

Figure 1.7: Annual hours of load shedding from 2014 to 2023 [13].

Tariff Increases to Compensate Financial Debt

Eskom has executed significant tariff increases of 653% between 2007 and 2022 to make-up for their financial challenges [15]. With a debt of ZAR 400.0 billion (USD 21.8 billion) still remaining as of 2023, Eskom is anticipated to continue increasing their tariffs [12]. This may drive consumers to detach from the grid and develop their own off-grid solutions. With South Africa having the highest income disparity in the world [16], such a shift could exacerbate disparities between those who can afford the capital cost of transitioning to self-sufficiency and those who cannot, leaving the latter group with no choice but to continue paying the increasing tariffs as their only financial option.

1.2. Addressing South Africa's lack of Electricity Access

Given the challenges imposing on South Africa’s grid-based electrification discussed in Subsection 1.1.5, it is evident that off-grid electrification must also be part of the solution to achieving universal electricity access [12].

1.2.1. Off-Grid Electrification

In contrast to the grid extension approach, off-grid electrification does not utilize the national electricity grid, but instead involves developing a localized system consisting of its own power generation and dispatch. The individual and modular designs of off-grid solution allow for rapid implementation, independent of the grid [17].

Moreover, modular off-grid solutions allow for addressing the electricity access deficit through sustainable and affordable energy technologies. Their compatibility with renewable energy technologies enables the pursuit of the Paris Agreement's goal of limiting global warming to below 2˚C, while increasing electricity access. The declining costs for renewable energy technologies offer the opportunity to leapfrog traditional fossil-fuel dependencies and be innovative about electricity access expansion [2]. As a result of this synergy between off-grid electrification and renewable energy technology, systems coupling off-grid solutions with renewable energy generation are rapidly expanding [17]. It is projected that one-third of the investments toward achieving universal electricity access by 2030 will be allocated to off-grid solutions, with 90% coming from renewable energy generation [2].

1.2.2. Limitations of Witnessed Off-Grid Electrification Initiatives

Off-grid solutions being deployed in the informal settlements were observed during a visit to South Africa in January 2024. Though the details are further discussed in Chapter 3, the main takeaways were that the observed off-grid solutions were effective in powering households in the range of Tier 1 to Tier 3 electricity access levels, depending on the solution. Local developers shared that many users are eager to further increase their electricity access and have the means to afford such enhanced services. This gap between the supply capacity of the current off-grid solutions and the capacity that the communities desire, is where this project aims to make a contribution in.

1.2.3. The proposed Solution

To bridge the gap between the current electricity access levels and the desired levels, an off-grid system that can scale alongside community development is explored. The off-grid solutions witnessed through the site visits were found to be limited up to Tier 3 access. Thus, this project aims to provide a solution that can easily scale with community needs, from Tier 3 to Tier 5 access. To achieve this, a microgrid system is designed leveraging technology from DC Opportunities (DCO), a power electronics R&D company collaborating and jointly supervising this project.

A direct-current (DC) microgrid was deemed suitable for this application over a conventional alternating-current (AC) system, given that the few electrical appliances currently owned by the users run on DC (e.g., LED lights, phone chargers, etc.). A DC solution therefore enhances the efficiency by eliminating the DC-AC-DC conversion. The decision to support the scale-up of electricity use through DC appliances is further reinforced by the market growth of efficient DC appliances in the off-grid sector [18]. In many cases, the lower system cost, achieved by reducing the system size needed to deliver the same energy services, outweighs the higher initial cost of bundling these efficient appliances, as calculated by the IEA [19]. Figure 1.8 shows an example where a 32% cost reduction is achieved by utilizing such efficient appliances, while still supplying the same level of electricity service.

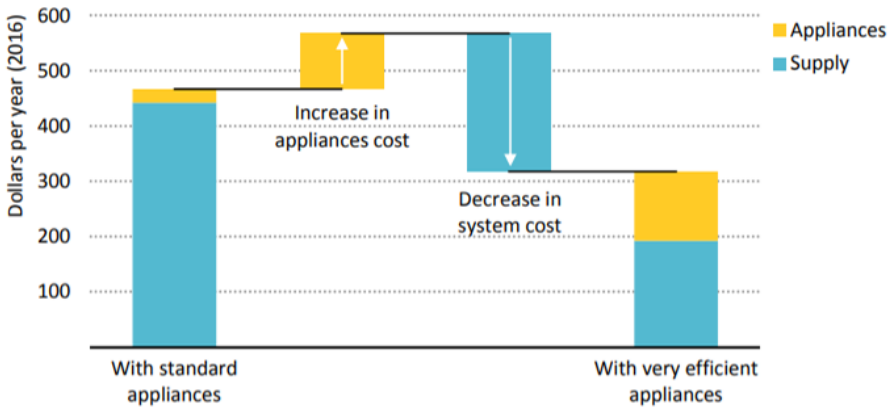

Figure 1.8: Annualised discounted cost of providing electricity access through an off-grid system, with and without very efficient appliances [19].Note: Electricity consumption is based on the average of a household gaining access in the Energy for All Case in sub-Saharan Africa in 2030, equating to 1 250 kWh per household annually with standard appliances, and 420 kWh with efficient appliances. This delivers four lightbulbs operating at five hours per day, one refrigerator, a fan operating 6 hours per day, a mobile phone charger and a television operating 4 hours per day. The costs and performance of appliances are based on 2016 prices. The anticipated price of PV in 2025 is used. A discount rate of 7% is applied.

Figure 1.9: Demonstration system of DC Opportunities with a centralized setup at the Delft University of Technology green village.

Additionally, while it is challenging to provide DC solutions in societies where AC has established as the norm, this project's unique opportunity to create a grid from start ("black start"), allows for the advantages of DC systems to be favored and applied. The advantages of a DC system include the following:

1. **Increased Efficiency**
   As the power produced and consumed are in the form of DC, eliminating DC-AC-DC conversion reduces energy losses and enhances overall efficiency. Additionally, there are no inductive or capacitive losses, as there are in AC systems [20].
2. **Thinner Conductors**
   DC voltage levels are higher compared to equivalent AC voltage levels, resulting in less necessary current for the same level of power. This allows for conductors to be sized thinner than for in AC.
3. **Quick Response of Protection**
   DC systems typically have fewer mechanical switches, replaced by semiconductor devices that allow for quicker response times.

The envisioned DC microgrid, visualized in Figure 1.10, consists of the following features:

- **Centralized Power Supply:**
  A centralized microgrid with central photovoltaic (PV) and storage system is selected to enable a greater power supply at higher voltages than in the case of a decentralized setup. The storage and converter components are to be housed in a secure, lockable cargo container. The PV modules will be mounted on top of or next to this container, depending on the system size and available space. Figure 1.9 shows a demonstration system of DCO with such a centralized setup at the Delft University of Technology Green Village. This centralized placement allows for ease of O&M and vandalism protection, while also limiting consumer interaction with the system to prevent misuse.
- **Bipolar 350V Dispatch:**
  The power supply from the PV system or batteries, is transmitted through an overhead distribution network to the connected households. A higher voltage of 350 V, as opposed to the 24 V or 48 V levels observed in the off-grid solution during the site visits, is dispatched across the network. This higher voltage is more efficient and suited for transmission. Meters for individual household

metering are to be placed at the closest pillar supporting the overhead reticulation.

Additionally, a bipolar design is chosen to allow for additional selectivity and fault isolation compared to uni-polar designs. It also allows for variable voltage connection levels; connecting the load between the positive and negative conductors results in a 700 V connection, while connecting between either positive or negative with the neutral results in a 350 V connection. Lastly, a bipolar grid necessitates less conductors in comparison to uni-polar designs to deliver the same power, as a uni-polar system needs two sets of positive and negative conductors, whereas the bipolar design utilizes just three conductors.

- **Tier 5 Infrastructure Backbone:**
  While initially tailored for Tier 3 energy access levels with a 24 V connection, a Tier 5 infrastructure backbone is to already be incorporated. This backbone allows for an easy scale-up to Tier 5, where each household will have a 350 V connection. By deploying the system with the anticipated future demand in mind, the need for extensive system upgrades with the community development is minimized.

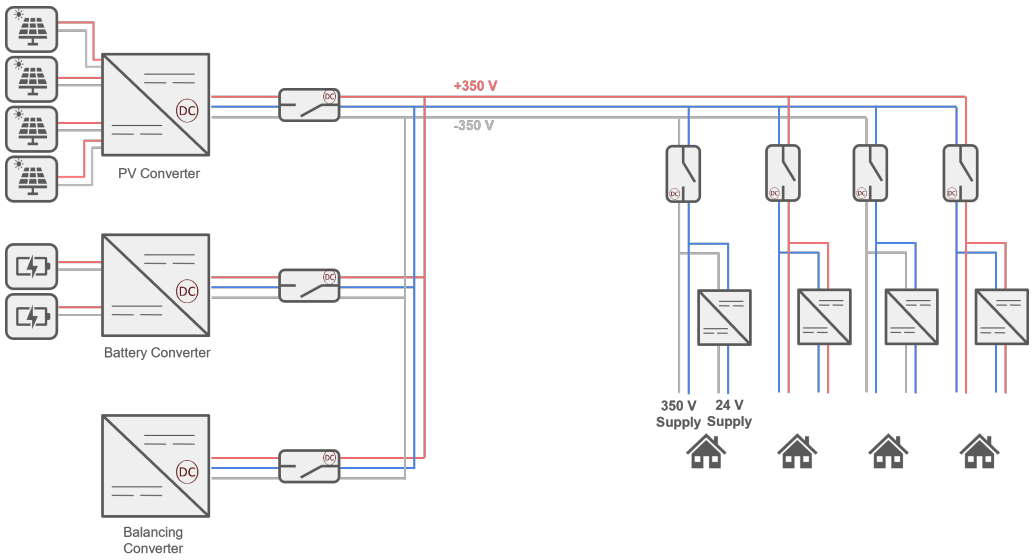

Figure 1.10: The envisioned DC microgrid design.

1.3. Project Objective

The objective of this project is to develop a comprehensive framework for designing the DC microgrid described in the previous subsection. The designed system is to serve as an electrification pathway in the context of electricity access. This project aims to make contributions in the following three ways:

1. **Apply Open-source Design Methodologies in the Context of Electricity Access**
   Unique design considerations relevant to communities with limited or unreliable access to electricity is to be identified to evaluate the suitability of existing open-source design tools and methodologies in addressing these challenges, and develop new approaches or modifications as needed.
2. **Deliver a Complete Comprehensive Design Framework**
   Deliver an automated design framework that produces a microgrid design for a given community. The necessary PV capacity, battery storage capacity, optimal grid network design are to be outputted from this comprehensive design framework. The aim is to create an automated tool that enables the rapid deployment of microgrids, thereby accelerating electrification efforts nationwide.
3. **Explore a Pathway to Community Development**
   Explore the feasibility of a microgrid design purposed to accommodate and scale with the increasing electrical demand of the developing communities.

The design framework is developed and refined through the application in two sites: the informal settlements of farmer families in Oudtshoorn, and a corner section of the Daveyton informal settlement, as depicted in Figure 1.11. The insights gained from these case studies better the design methodology and also reinforce that such designs can be replicated and implemented in similar settings across the nation.

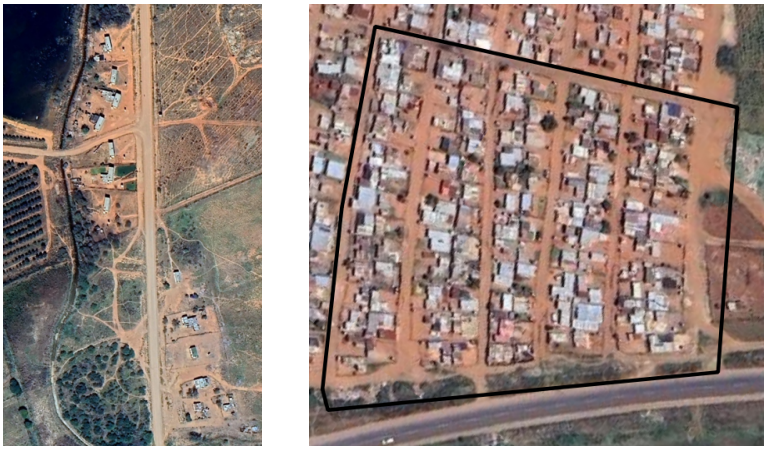

(a) Oudtshoorn Site **(b)** Daveyton Site

Figure 1.11: Targeted communities for designing a PV-powered DC microgrid in this study.

1.3.1. Research Questions

In fulfilling the objectives, the following research questions are to be answered:

1. **Are market-available open-source design tools applicable for designing feasible PV-powered DC microgrid systems in South African informal settlements?**

2. **How can a comprehensive design methodology for designing the desired PV-Powered DC Microgrid be developed, utilizing market-available design tools?**

3. **How can the developed design process be generalized and applied to diverse scopes?**

1.3.2. Report Outline

This report is composed of 7 chapters. Chapter 1 provides relevant background information on the state of electricity access in South Africa and elaborates on the project's motivation to bridge the necessary gap in achieving higher electricity access levels. The envisioned solution and approach are discussed, along with the objectives to be achieved and the research questions to be answered. A study on the technology and design theory relevant to the DC microgrid design methodology is then presented in Chapter 2, introducing PV, storage, DC technology, and system integration techniques. Next, Chapter 3 further discusses the projects with various approaches that were witnessed during the site visits to four informal settelments in South Africa. The lessons learnt from theses projects are identified to be applied for the DC microgrid solution.

The complete design process for the DC microgrid, highlighting the resources used and the applied techniques, is outlined in Chapter 4. Following this, Chapter 5 presents the findings from applying the design methodology to two specific sites: the Oudtshoorn farmer settlements and a corner section of the Daveyton informal settlement. The results obtained from applying this design methodology to the case studies is then detailed in Chapter 6. Lastly, Chapter 7 summarizes the key findings, reflecting on whether the project objectives have been met and the research questions have been answered. This chapter also discusses recommendations for the future work.

2

Literature Review of Technologies Used in Off-Grid Systems

This chapter analyses technologies applicable for off-grid electrification and their design methodologies to create an efficient and coherent system that is applicable for this project. Specifically, PV technology, storage technology, power transmission technology, and system integration methodologies are discussed. This literature review is to provide insights into the most suitable technology and integration methodology to be used in this project.

2.1. PV Technology

PV modules play a crucial role in off-grid systems as a sustainable energy source. They harnesses the potential difference generated at the junction of two semiconductor materials in response to light (photon energy) absorption above a certain material-dependant threshold frequency, to produce electricity [21]. The declining costs of this technology have enabled a rapid market growth in the recent years, as depicted in Figure 2.1 [22].

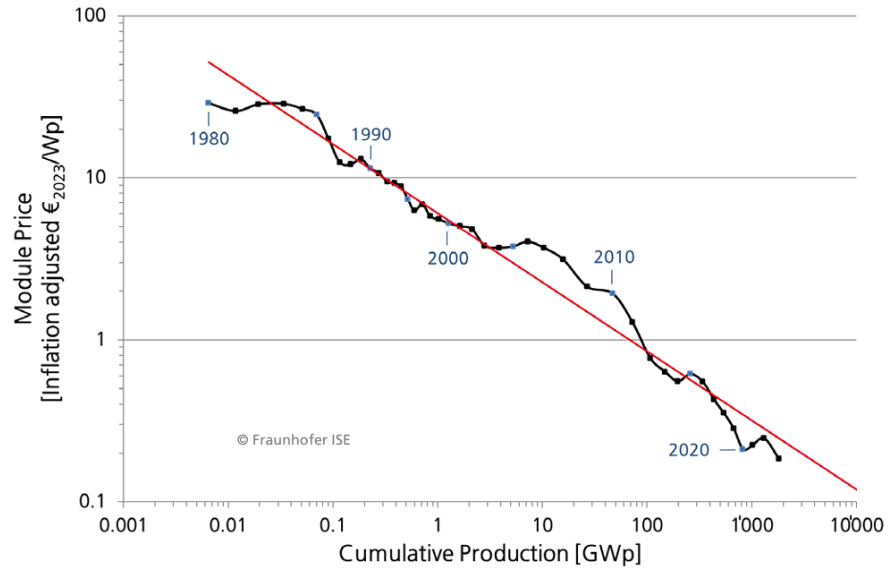

Figure 2.1: PV cumulative production vs. module price [23]

2.1.1. Types of PV Modules

The semiconductor material used in PV modules impacts its qualities and overall performance. Monocrystalline silicon is the current market-leading semiconductor material used in PV cells, making-up approximately 96% of the market, as shown in Figure 2.2 [23]. Silicon is an abundant element and has favourable properties for PV application. Specifically, its electronic band gap is optimal for terrestrial sun light absorption. Among crystalline silicon based cells, monocrystalline silicon cells have higher efficien-

cies in comparison to polycrystalline silicon, due to the absence of grain boundaries in the continuous crystal lattice which minimizes losses [21].

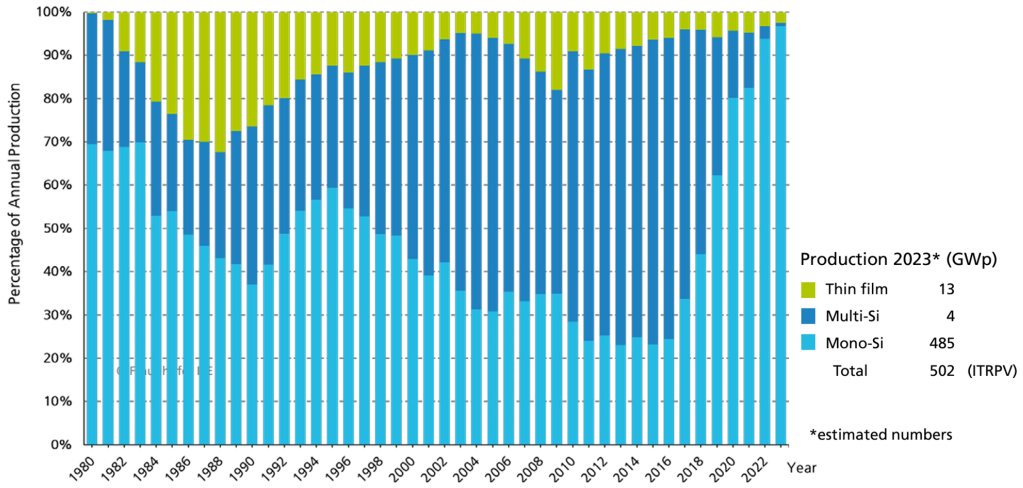

Figure 2.2: PV production by technology: Percentage of global annual production [23]

In addition to the semiconductor materials, efficiency-increasing techniques also impact the performance and suitability of a PV module for a specific application. In 2023, the monocrystalline Passivated Emitter Rear Contact (PERC) module made up 64% of the market, as shown in Figure 2.3 [24]. However, it is predicted that the market will significantly shift within the next decade, with other types of modules overtaking the market share. It is forecasted that the Tunnel Oxide Passivated Contact (TOPCon) module will increase from 29% to 53%, and the Silicon Heterojunction (SHJ) module from 5% to 19% by 2034 [24]. Thus, the current and future market-dominating PV module types - PERC, TopCon, and SHJ - are analysed to examine their suitably for use in the proposed microgrid design for this project.

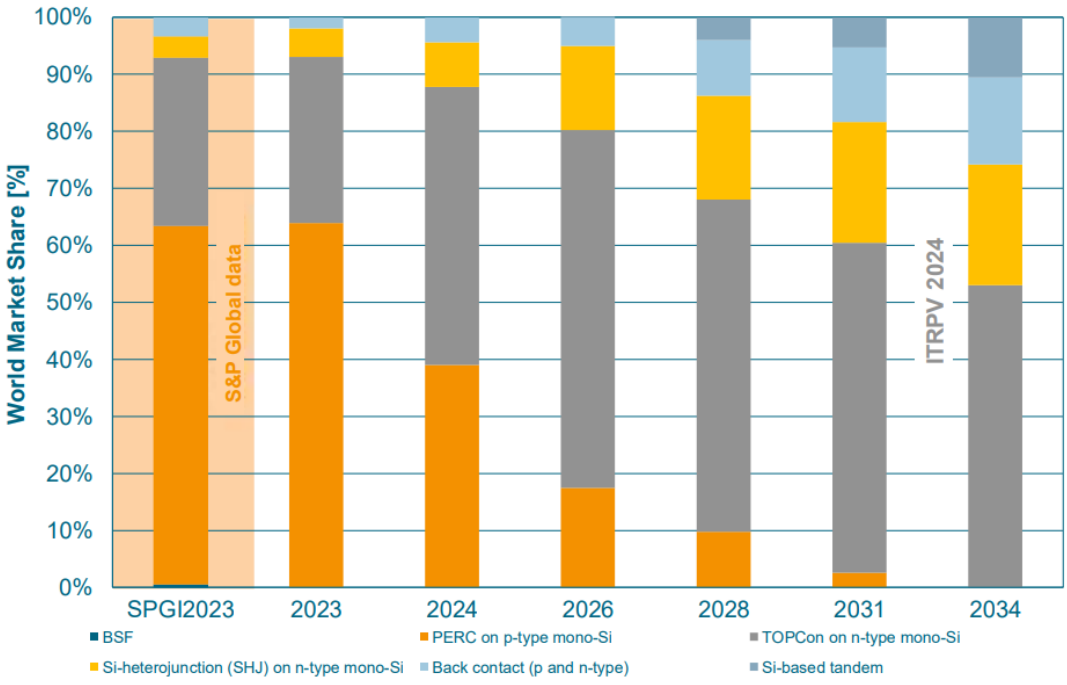

Figure 2.3: Forested PV module market shares from 2023 to 2034 [23].

- **PERC**
  The PERC architecture consists of a thermal oxide passivation layer placed between the silicon and the rear metal contact. This extra layer reflects unabsorbed light (photons with longer wavelengths) reaching the back of the cell, back across the p-n junction to generate electricity, utilizing

otherwise dissipated energy. By reducing the contact area between the rear metal contact and the semiconductor, recombination losses—caused by the recombination of electron-hole pairs—are minimized, thereby enhancing cell efficiency [21]. Due to the use of conventionally diffused front junctions and optically transparent antireflective coatings, PERC usually have short-circuit currents at STC greater than 41 mA/cm^2 [25].

- **TOPCon**
  The TOPCon architecture features an n-type silicon substrate with an ultra-thin silicon oxide layer deposited on the backside of the cell. This is followed by a layer of doped silicon, creating a passivated contact structure. The ultra-thin silicon oxide layer acts as a barrier that prevents minority carriers, such as holes in the n-type wafer base, from reaching the back contact, while allowing electrons to tunnel through with minimal loss, enhancing efficiency. Similar to PERC, TOPCon also yields high short-circuit currents in a similar range [25].
- **SHJ**
  The SHJ architecture achieves the highest open-circuit voltages among different crystalline silicon technologies by incorporating amorphous silicon passivation layers that create a heterojunction with the crystalline silicon wafer. This configuration reduces losses as the amorphous silicon, with a larger band gap energy than crystalline silicon, minimizes parasitic absorption at the front side [22]. However, despite these advantages, SHJ solar cells typically show inferior short-circuit currents due to the strong parasitic absorption at the front side [25].

2.1.2. Comparison of Types of PV Modules

The three PV modules analysed in Subsection 2.1.1 are compared to assess the best suited module type to be used for the purposed microgrid design. As the installation of the system is to be in South Africa with high temperatures and high irradiation levels, the criteria of evaluation is the performance of the modules under hot and sunny environmental conditions. Specifically, the performance parameter of interest is the internal resistance at the maximum power point (R_{MPP}) , as high internal resistance at the maximum power point performs best under hot and sunny climate conditions, according to [25]. Table 2.1 shows the comparison of the wafer R_{MPP} of PERC and SHJ from the literature, with the R_{MPP} calculated via $R_{MPP} = V_{MPP}/J_{MPP}$, where V_{MPP} and I_{MPP} are the maximum power point voltage and current respectively, and from datasheet specifications of the N158-229 TopCon wafer of a similar size [26]. The SHJ resulted with the highest R_{MPP}, attributed to the high voltage of SHJ and the high short-circuit currents of PERC and TOPCon. This indicates that the SHJ modules would be best suited for its high performance in hot and sunny environments.

Table 2.1: Comparison of internal resistance at the maximum power point of PERC, TopCon, and SHJ. The values for PERC and SHJ are obtained from [25], while the value for TopCon was calculated from the specification sheet of the N158-229 TopCon wafer [26].

	PERC	TopCon	SHJ
R_{MPP} [$\Omega \cdot cm^2$]	15.2	15.4	17.6

2.1.3. PV Power Simulation

As PV power production is dependent on local weather conditions, it is necessary to understand the power production profile that can be expected, in order to accurately size the PV system. The power produced from a PV system can be simulated based on the local meteorological data, characteristics of the selected PV module, and the PV system design. Most PV simulation and design tools in the market that perform such simulations typically consist of the following process:

1. **Retrieve Meteorological data**
   Local meteorological data is necessary input for the simulation. A time-series of data such as Diffuse Horizontal Irradiance (DHI), Direct Normal Irradiance (DNI), Global Horizontal Irradiance (GHI), ambient temperature, and wind speed are retrieved from local weather stations or Typical Meteorological Year (TMY) sources. This TMY represents a ”typical year” of weather at a particular location, constructed from multiple years of history by selecting the most typical data for each month.
2. **Calculate the Sun Path**
   Equation 2.1 and Equation 2.2 are used to calculate the sun altitude (a_S) and sun azimuth (A_S) positions. The latitude (φ_0) and longitude (λ_0) of the installation site serve as inputs, along with the location and time-dependent parameters: axial tilt (ϵ), local mean sidereal time (θ_L), and ecliptic longitude (λ_S).

$$\sin a_S = \cos\varphi_0 \cos\vartheta_L \cos\lambda_S + (\cos\varphi_0 \sin\vartheta_L \cos\varepsilon + \sin\varphi_0 \sin\varepsilon) \sin\lambda_S \tag{2.1}$$

$$\tan A_S = \frac{-\sin\vartheta_L \cos\lambda_S + \cos\vartheta_L \cos\varepsilon \sin\lambda_S}{-\sin\varphi_0 \cos\vartheta_L \cos\lambda_S - (\sin\varphi_0 \sin\vartheta_L \cos\varepsilon - \cos\varphi_0 \sin\varepsilon) \sin\lambda_S} \tag{2.2}$$

3. **Calculate the Angle of Incidence (AOI) of the Solar Vector onto the PV Module Surface**
Two design elements define the PV module installation orientation: The tilt angle (θ_M) and the azimuth angle (A_M). The tilt angle is the angle at which the PV module is fixed in relation to the ground surface (i.e., 0° representing modules that are placed flat on the surface and 90 for panels placed normal to the surface). The azimuth angle specifies the direction at which the PV panels are directed (i.e., 0° for panels facing North, 90° for East-facing panels, 180° for South-facing panels, and 270° for those facing West). These design parameters, in addition to a_M, a_S, and A_S obtained in the previous step, impact the angle of incidence (AOI) which is the angle between the PV module and the beam of the sun. Equation 2.3 is used to obtain the time-series of AOI.

$$\mathrm{AOI} = \cos^{-1}[\cos(90° - \theta_M)\cos(a_S)\cos(A_M - A_S) + \sin(a_M)\sin(a_S)] \tag{2.3}$$

4. **Calculate Plane-of-Array (POA) Irradiance**
Three components of the plane-of-array (POA) irradiance, irradiance that is transposed to the POA, are solved for and summed up to obtain the total POA irradiance:

The direct irradiance is the component of the POA irradiance that is perpendicularly reached from the Sun. It is calculated using Equation 2.4, with DNI and AOI serving as input.

$$\mathrm{G_{Direct}} = \mathrm{DNI} \cdot \cos(\mathrm{AOI}) \tag{2.4}$$

The Sky-diffuse irradiance is a component of the POA irradiance that is scattered or reflected by atmospheric components, which can be calculated using multiple established models. According to [27], the Hay/Davies and Perez transposition models were best performing, with the Sandia model only slightly behind with a relative to POA mean bias deviation of less than 2% . The better performing Hay/Davies and Perez models, however, require additional meteorological data such as extraterrestrial normal irradiance and relative airmass values, whereas the Sandia model, which is represented by Equation 2.5, only requires DHI and GHI. Thus, although the Sandia model might slightly underestimate the annual POA irradiance, its accuracy range is sufficient for practical applications and does not necessitate the additional, sometimes unattainable, weather data. Therefore, the Sandia model is assessed to be best suited for use in simulating sky-diffuse irradiance for this project.

$$\mathrm{G_{sky\ diffuse}} = DHI \times \frac{1 + \cos(\theta_M)}{2} + GHI \times \frac{(0.012A_M - 0.04) \times (1 - \cos(\theta_M))}{2}. \tag{2.5}$$

The ground-diffuse irradiation is a component of the POA irradiance that is reflected by the ground surface. It is calculated using Equation 2.6. The GHI and the module tilt angle serve as input, along with the albedo value, representing the fraction of the solar irradiation that is reflected by the Earth's surface and depends on the reflectivity of the environment [21].

$$\mathrm{G_{ground\ diffuse}} = \mathrm{GHI} \cdot \alpha \cdot \left(1 - \frac{1 + \cos(\theta_M)}{2}\right) \tag{2.6}$$

5. **Obtain PV Cell Circuit Parameters at Standard Test Conditions (STC)**
Common manufacturer datasheet specifications listed in Table 2.2, are transformed into normalized parameters listed in Table 2.3, which describe the shape of the module's I–V curve at STC [28]. These parameters construct the equivalent circuit shown in Figure 2.4, consisting of a current source that represents the photogenerated current, a single diode to model the physical p–n junction, as well as series and parallel resistances that account for non-ideal behavior of actual devices [28].

Table 2.2: Manufacturer-supplied PV module characteristics.

Description	Variable	Units
Maximum power point voltage	V_{mp}	V
Maximum power point current	I_{mp}	A
Open circuit voltage	V_{oc}	V
Short circuit current	I_{sc}	A
Temp. dependence of V_{oc}	β_{oc}	$\%/°\mathrm{C}$
Temp. dependence of I_{sc}	α_{sc}	$\%/°\mathrm{C}$
Temp. dependence of P_{mp}	γ	$\%/°\mathrm{C}$
c-Si, mc-Si, CdTe, CIS, CIGS, a-Si	Tech	n/a
Number of cells in series	N_{ser}	n/a

Table 2.3: Five circuit parameters describing the PV cell characteristics of the single diode model.

Description	Variable
Modified nonideality factor	a
Light (photogenerated) current	I_L
Diode reverse saturation current	I_o
Series resistance	R_s
Shunt (parallel) resistance	R_{sh}

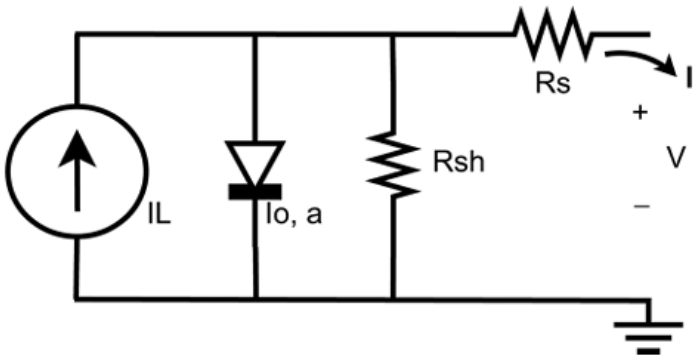

Figure 2.4: Equivalent circuit of a PV cell with series resistance R_s and shunt resistance R_{sh}.

6. **Account for PV Cell Temperature**
   The module temperature can be accounted for via thermal model to predict the associated operating temperature of the PV module [29]. Sandia Array Performance Mode is one such exemplary model, represented in Equation 2.7. Time-series of POA irradiance, ambient temperature, and wind speed, along with empirically determined coefficients (a, b) that depend both on the module construction and its mounting, serve as input to obtain the cell temperature which impacts its performance.

$$T_m = E \cdot \left\{ e^{a+b \cdot WS} \right\} + T_a \tag{2.7}$$

7. **Obtain PV Cell Circuit Parameters at Effective Irradiance and Cell Temperature**
   As depicted in Figure 2.5, the effective irradiance and cell temperature affect the I-V curve shape. Thus, the normalized parameters that describe the module's I–V curve at STC must be adjusted in the context of varying irradiance and temperature. The same five parameter values, listed in Table 2.3, can be derived via CEC model for the non-standard rating conditions, at effective irradiance and cell temperature. Thus the POA irradiance and the module temperature obtained in the previous step, serve as input.

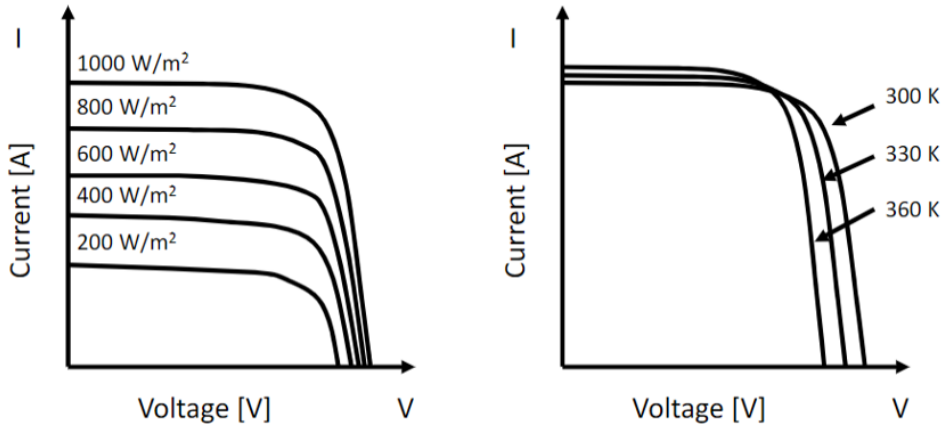

Figure 2.5: IV curve depicting effect of irradiance and temperature [30].

8. **Maximum Power Point (MMP) Calculation**
   Lastly, the five parameter values at effective irradiance and cell temperature are inputted to the single diode model to calculate the I-V curve, obtaining the MPP. Figure 2.6 illustrates the MPP on the I-V curve.

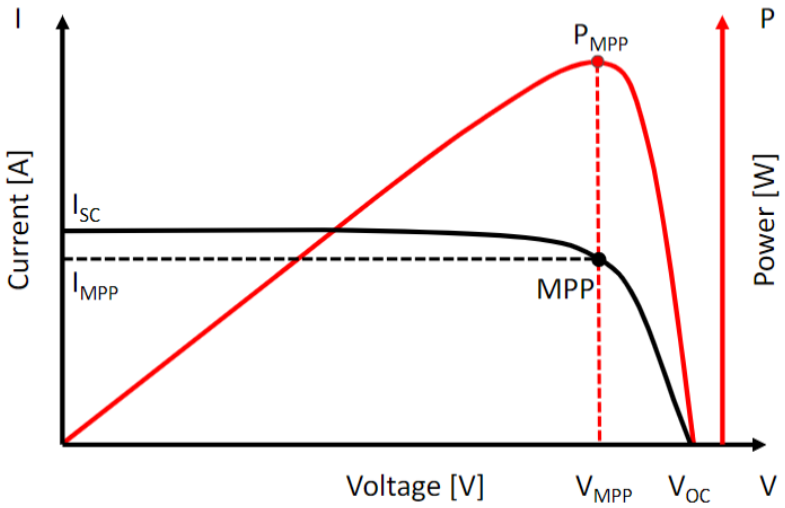

Figure 2.6: IV curve highlighting MPP [30].

Table 2.4 compares some notable market-available PV simulation and design tools in terms of their functionality, and Table 2.5 in terms of the models used in their calculations.

Table 2.4: Comparison of PV simulation and design tools.

	Accessibility	Simulation			Optimization	System Design
		Minimum Resolution	Account for Shading	Account for Cable Losses	Solve for optimal θ_M & A_M	PV System Sizing Method
SAM [31]	Open Source	minute	yes	yes	yes	usable area
PvSyst [32]	Closed Source	hour	yes	yes	yes	usable area Load profile
Helio-Scope [33]	Closed Source	hour	yes	yes	yes	usable Area
PV Watts [34]	Open Source	hour	no	default percentage	no	usable area
PVGIS [35]	Open Source	hour	use terrain shadows	default percentage	yes	-
PV*SOL [36]	Closed Source	minute	yes	yes	yes	Usable area load profile
HOMER Pro [37]	Closed Source	hour	no	no	no	load profile economic-analysis
PV Lib [38]	Open Source	input dependant	function selection dependant	no	possible	-

Table 2.5: Models used by the PV simulation and design tools.

	Irradiance transposition Model	Cell Temperature Model	IV Curve Model
SAM [31]	Perez, Isotropic, HDKR	Sandia, NOCT	CEC ,Sandia
PVsyst [32]	Hay & Davies, Perez	Diffusion cell temperature	Single diode, PVsyst module-performance
Helio-Scope [33]	Hay & Davies, Perez	Sandia, Diffusion cell temperature	Single-diode
PV Watts [34]	Perez	Fuentes	Simplified estimation
PVGIS [35]	Perez, Hay & Davies, etc.	Huld	NOCT
PV*SOL [36]	Reindl, Perez etc.	Dynamic thermal	PV*SOL, Single-diode
HOMER Pro [37]	HDKR	Simplified estimation	NOCT
PV Lib [38]	Perez, Hay & Davies, Klucher, Reindl, King and Isotropic	SAPM, PVSyst cell temperature	CEC single diode, SAPM, PVWatts DC

Upon reviewing market-available PV simulation and design tools listed in Table 2.4, PV Lib, the open source library of modelling functions purposed for simulating PV performance, developed by the PVPMC and Sandia National Laboratories [38], is deemed most suitable for the use in this project. Although it requires programming knowledge making it a less user-friendly approach compared other alternatives, it being open source and its flexibility in modelling a purely DC system reinforced the selection of PV Lib. Additionally, studies have been performed showing that PV Lib is one of the most accurate prediction models in determining the modelled DC power output [39], further supporting the utilization of this model for this project.

2.2. Storage Technology

Energy storage is a critical component for off-grid systems that have an intermittent power source as its sole generation source. Chemical storage in the form of batteries is currently the primary energy

storage technology used in off-grid systems [22].

2.2.1. Types of Batteries

Batteries significantly affect the design, cost, and reliability of an off-grid system, thus, it is important to select the battery type and size best suited for the desired application. The current and future market dominating battery technologies are Lithium-ion and Lead-acid batteries, as shown in Figure 2.7 [40]. Therefore, these two battery types are further evaluated for potential use in this the proposed microgrid design.

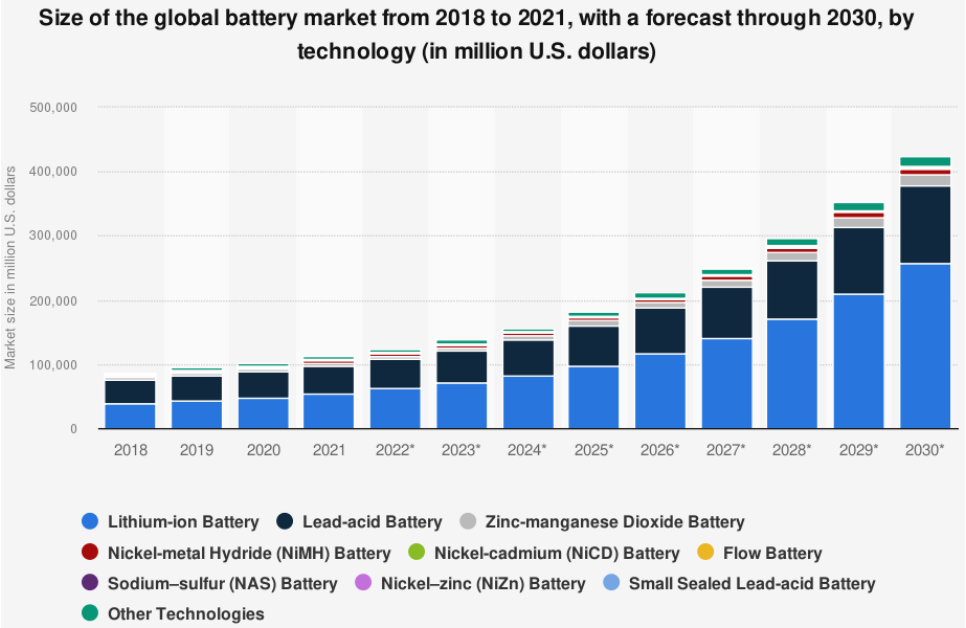

Figure 2.7: Global battery market breakdown of technology from 2018 to 2021, and forecast through 2023 [40].

- **Lead-Acid Batteries**
  Lead acid batteries have a well-established and mature technology base. They are low-cost and tolerant to overcharge, but have a shorter lifespan and lower energy density compared to other battery types [41]. They also require frequent maintenance. Lead acid batteries typically have energy efficiencies in the range of 70–80 % [42].
- **Lithium-Ion Batteries**
  Lithium-ion batteries are superior than other battery types in terms of high energy efficiency and power density, which allow for lighter and smaller modules. They also have broad temperature range of operation, rapid charge capability, and relatively long cycle life. They are however, susceptible to deep discharge/overcharge [41]. Lithium-ion batteries have high energy efficiencies in the range of 85–95 % [42].

2.2.2. Battery Type Comparison

Based on the characteristics of the two battery types discussed in Subsection 2.2.1, the lithium-ion battery is assessed to be most suitable for use in the purposed microgird design due to its high efficiencies, longer life time, and reduced need of maintenance. Additionally, its shortcoming regarding the sensitivity to deep discharge/overcharge can be mitigated by DCO's battery converter, protection modules, and droop control technology.

2.2.3. Battery Charging/Discharging Behavior

Understanding the charging and discharging behavior of a battery is essential for efficient storage system design and management. Key parameters such as State of Charge (SOC) and Depth of Discharge (DOD) play crucial roles in this process.

SOC is the percentage of the current charge level of the battery relative to its maximum capacity, while DOD is its inverse, indicating the percentage of the battery's capacity that has been used. It is common practice in the industry to maintain SOC levels within the 20-80% range, to prolong the battery life cycle [43]. Monitoring SOC levels thus sheds insight in the sizing of the battery system, as relatively constant high SOC levels indicate an over-size of the battery system, while low levels indicate under-sizing. Ideal

battery system size would results in fluctuating SOC levels within the desired 20-80% range.

2.3. Distribution Network

The design of the distribution network, which encompasses the power transmission from the power and storage sources to the households, is a crucial aspect of microgrid design. For this project, the distribution network is to connect all households to the central container housing the batteries and electrical components, and where the PV modules are to be mounted. It is to consist of overhead cabling supported by pillars, as local contacts share that it is the economically preferred option to underground cabling. The cable routing, pillar placement and cable sizing are crucial design elements that must be considered to ensure the overall performance and economic viability of the system.

2.3.1. Distribution Network Design Approaches

Efficiency, reliability, and cost-effectiveness should be considered in the planning of the microgrid layout for an effective solution. There are several approaches and tools available for designing distribution networks:

- **Market-available tools**
  Market-available tools such as PowerLines Pro, Automated Utility Design, and PLS-CADD automates the distribution system design process [44]. These tools provide advanced functionalities such a optimal pillar placement and structural analysis of power lines. However, these tools are closed source with expensive licenses, and also have a steep learning curve requiring thorough training to use effectively.
- **Engineering Intuition**
  Intuitive pillar placement based on ”engineering intuition” has also classically been used. While this method can be quick and is based on practical knowledge, the intuitive pillar placement does not always lead to cost-effective cable routing [45].
- **Graph Theory Based Pathfinding Algorithms**
  Within the study of graph theory, ”pathfinding” is the search for the optimal (shortest, cheapest, etc.) path between two points. This process utilizes a graph consisting of nodes (points) and edges (connections between two nodes), each with a weighted value (distance, cost, etc). Given a starting node and a target node, the algorithm determines the optimal path based on the specified criteria. The application of pathfinding algorithms to the context of rural electrification has been made in [45], where cost-effective power line routes between villages were explored through a pathfinding algorithm.

2.3.2. Distribution Network Design Methodology Comparison

Among the possible distribution network design approaches discussed in Subsection 2.3.1, the graph theory based approach best aligns with this project’s objectives. The objective to utilizing open-source tools rules out the option of the closed-source, costly and training-requiring market-available tools. Additionally, the intuitive approach is also avoided as the end deliverable of this project, the comprehensive microgrid design framework, should not rely on user expertise.

On the other hand, the application of pathfinding algorithms via open-source python library NetworkX [46] seems promising for identifying the shortest cable path between the central container and each houshold, thereby minimizing the cabling costs that scale with cable length. However, though this technique can successfully determine the cost-optimal individual cable rout from the central container to each household for this project, combining these individual paths does not result in the cost-optimal overall network layout. This is because the costs of pillars and the varying cable cost per unit length that is dependent on the cable sizes needed for carrying multiple loads (i.e., when sharing the same paths) are not considered. Therefore, the proposed approach is to couple this pathfinding algorithm with a Integer Linear Programming (ILP) optimization. The pathfinding algorithm is to first identify a set of possible cable paths to each household. Subsequently, a ILP optimization is applied to select the cable path for each household that results in the cost-optimal overall network layout. This approach therefore accounts for the costs resulting from the combination of the selected paths. It is also important to acknowledge the computational complexity of pathfinding algorithms, thus data processing techniques to reduce the computational effort should also be applied [45].

2.4. System Integration

System integration involves combining the various components of an off-grid system in an effective way to achieve optimal performance and reliability. Thus, in this section, approaches to integrate the

technologies discussed in Section 2.1, Section 2.2, and Section 2.3 to the overall microgrid design are evaluated.

2.4.1. Load Assessment

To design a reliable off-grid system that meets energy demand, it is essential to assess the energy consumption profile (load profile) and use it as a basis for sizing the generation and storage capacity. Load profiles encapsulate the power demand with respect to time, playing a crucial role in accurately sizing an off-grid PV system to meet momentary power demands, over time. Accurate demand forecasting ensures the system is designed to meet actual energy needs, avoiding over-sizing, which would result in unnecessary high costs, and under-sizing, which would cause the system to fail in meeting the loads at times[18].

Recorded data is thus ideal for this purpose. However, in the case of this project, recorded data was not available. For off-grid electrification projects faced with the same situation, estimating energy consumption behaviour through interviews and surveys has been a typical alternative [18]. However, studies show that modeled load profiles relying purely on interview-based data is inaccurate and should be avoided [47]. For this reason, a load profile model that incorporate consumption behaviour trends of a similar electricity access level shows the most promise in obtaining the load profile that is to serve as a starting point for the systems design and sizing of the other components.

2.4.2. Cable Sizing of the Distribution Network

The cables dispatching power from the central container to the households must be sufficiently sized to manage cable losses to a reduced level, while avoiding unnecessary high costs as a result of over-sizing. The cable sizing thus follows the design guideline of Equation 2.8. The two temperature correction factors, F_1 and F_2, account for the conditions of use to appropriately size the cables. Specifically, F_1 is the ambient temperature correction factor, determined using Figure 2.8, obtained from Article 310 of the National Electrical Code (NEC) [48]. The sum of the ambient temperature (T_H) and the ambient temperature adjustment for cables exposed to sunlight (T_0) is used to find the appropriate F_1 value for the installation site. The value of T_0 is identified from Table 2.7 [48]. On the other hand, F_2, the adjustment factor for the number of current-carrying conductors in a cable, is found from Figure 2.9 [48]. The cable ampacity requirement calculated with Equation 2.8 and the temperature correction factors, is used for sizing the cables according to Table 2.6.

$$\text{Cable Ampacity Requirement} = \frac{1.56 \times I_{SC}}{F_1 \times F_2} \tag{2.8}$$

Table 2.6: Conductor cross-section area and maximum current rating based on UL 486E and IEC 60998-1 [49].

Conductor Cross-Section Area [mm^2]	Maximum Rating [A]
2.5	15
6	30
10	50
16	65
25	85
35	115
50	145
70	195
90	220

For ambient temperatures other than 30°C (86°F), multiply the ampacities specified in the ampacity tables by the appropriate correction factor shown below.

Ambient Temperature (°C)	Temperature Rating of Conductor			Ambient Temperature (°F)
	60°C	75°C	90°C	
10 or less	1.29	1.20	1.15	50 or less
11—15	1.22	1.15	1.12	51—59
16—20	1.15	1.11	1.08	60—68
21—25	1.08	1.05	1.04	69—77
26—30	1.00	1.00	1.00	78—86
31—35	0.91	0.94	0.96	87—95
36—40	0.82	0.88	0.91	96—104
41—45	0.71	0.82	0.87	105—113
46—50	0.58	0.75	0.82	114—122
51—55	0.41	0.67	0.76	123—131
56—60	-	0.58	0.71	132—140
61—65	-	0.47	0.65	141—149
66—70	-	0.33	0.58	150—158
71—75	-	-	0.50	159—167
76—80	-	-	0.41	168—176
81—85	-	-	0.29	177—185

Figure 2.8: Ambient temperature correction factors [48].

Table 2.7: Ambient temperature for cables exposed to sunlight [48].

Distance Above Roof to Bottom of Raceway of Cable	Temperature Adder
< 13 mm	33 °C
< 90 mm	22 °C
< 300 mm	17 °C
< 900 mm	14 °C

Number of Conductors*	Percent of Values in Table 310.16 Through Table 310.19 as Adjusted for Ambient Temperature if Necessary
4—6	80
7—9	70
10—20	50
21—30	45
31—40	40
41 and above	35

Figure 2.9: Adjustment factors for more than three current-carrying conductors in a raceway or cable [48].

Additionally, the cable related power loss must be accounted for in the design phase, by sizing the PV and battery capacities to compensate for these losses. Thus, accurately estimating these cable losses ensures that the system is designed to provide sufficient energy to meet the demand after all losses are considered.

An open-source python library, pandapower is a network calculation program that automatizes power system analysis via Newton-Raphson method [50]. Use of this available tool was examined, however, it was found to be aimed for use in static analysis of three-phase power systems, thus was not usable for this project. The lack of available tools for automatically calculating cable losses for purely DC networks pushed forward the approach to create a python script that calculates the power losses of the designed distribution network for this study using Equation 2.9. From the equation, it is observed that the losses are proportional to cable length (L_{cable}) and inversely proportional to the cross-sectional area of the cable (A_{cable}), and dependant on the material's conductivity (ρ_{cable}).

$$P_{\text{cable loss}} = I^2 \cdot R^2_{\text{cable}} = \frac{I^2 \cdot \rho_{cable} \cdot L_{cable}}{A_{cable}} \tag{2.9}$$

2.4.3. PV & Battery System Sizing

PV and battery sizing is crucial for optimizing the performance and cost-efficiency of hybrid energy systems. The battery should be sized large enough to store excess PV power and supply power to loads during periods of PV power deficit, while avoiding excessive costs associated with over-sizing. There are a range of performance indicators for sizing the PV and battery systems for a hybrid project. Figure 2.10 shows the share of sizing criteria for hybrid systems, with the economic and reliability indicators dominating the shares. Thus, the sizing methods utilizing reliability and economic indicators are evaluated in the following:

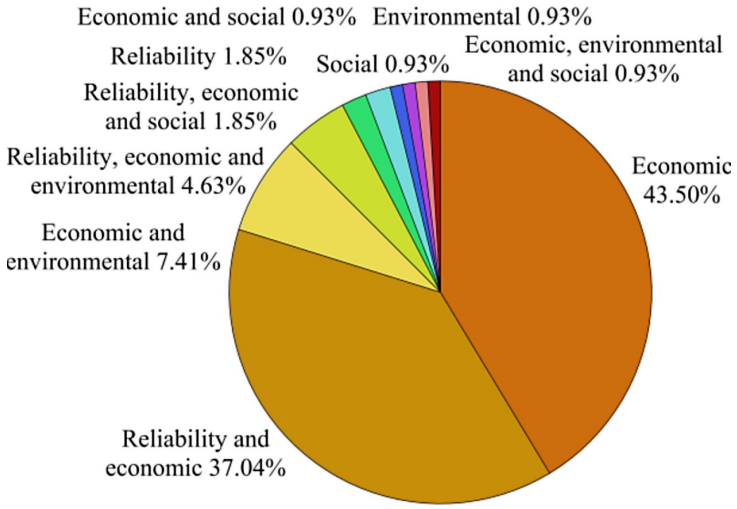

Figure 2.10: Utilized sizing criteria of hybrid renewable energy systems [51].

- **Intuitive Method: Number of Autonomous Days**
  One of the simpler methods is to determine the duration that the system should meet the demand with only the battery supply. A reserve energy capacity should be planned to account for anticipated poor weather conditions. This reserve allows for the system to be independent of the PV power production a certain duration, refereed to as "days of autonomy (d_A)". Table 2.8 lists the recommended number of autonomous days at several latitudes, though project specific considerations should further influence d_A. For this project's case of installation in South Africa, based on the latitude, d_A in the range of 10-12 would be chosen.

Table 2.8: Recommended number of autonomous days at several latitudes [21].

Latitude (°)	Recommended Number of Autonomous Days: d_A
0-30	5-6
20-50	10-22
50-60	15

With a defined d_A, Equation 2.10 can be applied to solve for the necessary battery capacity (E_{Battery}). The total daily DC energy requirement of the system (E_{Load}), also including system losses, are multiplied by d_A. In order to account for measures to prolong the battery life, it is recommended to divide the value by the restricted DOD of 80% [21].

$$E_{\text{Battery}} = \frac{d_A \times E_{\text{Load}}}{\text{DOD}_{\max}} \tag{2.10}$$

Furthermore, the intuitive method can be applied to size the PV array as well. The size of the PV array can be determined by the average energy produced during the design period, ensuring it exceeds the load demand by a safety factor (SF). This safety factor is often chosen based on the designer's experience, which may introduce some inaccuracy. The size of the PV array can be calculated using Equation 2.11, where C_{PV} is the PV system capacity, η_{system} is the system efficiency, and ESH is the equivalent sun hours of a given instalation site.

$$C_{\text{PV}} = \frac{E_{\text{Load}}}{ESH \cdot SF \cdot {}_{system}} \tag{2.11}$$

It is important to note that the intuitive method, while simple and quick, may result in low reliability or increased capital, operational, and maintenance costs. Therefore, it is more suitable for initial and rough approximations rather than the sole system sizing methodology.

- **Commercial Software Tools**
  Various software tools are also available for the optimal sizing of standalone hybrid systems, with the most commonly utilized tools being Hybrid Optimization Model for Electric Renewables (HOMER) and RETScreen [52]. These tools facilitate the design and analysis of renewable energy systems by simulating system performance, assessing economic viability, and optimizing configurations based on specific criteria.

  However, HOMER does not allow users to modify component specifications, while RETScreen has limited data retrieval options and lacks time series data input capabilities. These shortcomings adds difficulty for use in this project [52].

- **Numerical Method: Performance Analysis of Loss of Load Probability (LLP)**
  An analysis of simulating the performance of the off-grid system can be used to identify and validate the necessary battery size to meet the reliability requirement. LLP, the fraction of the energy demand which is not met by the system, is one of the most common evaluation metric for this approach [51]. The power mismatch between the generated PV power and the load, along with the remaining energy capacity within the battery is assessed for each timestamp to determine when the system cannot deliver the required load. The total amount of energy that the system failed to meet the demand (E_{fail}) is divided by the total annual energy demand, as shown in Equation 2.12, to solve for the LLP. The battery should be sized to achieve a LLP that is within the desired LLP of the system. Table 2.9 lists recommended LLP values. For this project, a 5 % LLP is appropriate, balancing between domestic illumination and appliance usage, which are the primary electrical needs in the targeted communities. This higher LLP, compared to the strictly domestic illumination application, helps minimize costs while still meeting the essential energy requirements of these communities.

$$\text{LLP} = \frac{E_{\text{fail}}}{\int_{\text{year}} P_L(t)\mathrm{d}t} \tag{2.12}$$

Table 2.9: Recommended LLP for some applications [21].

Application	Recommended LLP
Domestic Illumination	10^{-2}
Appliances	10^{-1}
Telecommunications	10^{-4}

3

Electricity Access Initiatives

This chapter presents insights gained from the examination of various informal settlements during the site visit to South Africa, mentioned in Subsection 1.2.2. The various electrification approaches, as well as the key lessons learnt are discussed, as they are crucial in enhancing the solution that this project proposes.

3.1. Witnessed Off-Grid Electrification Solutions

Four informal settlements, indicated in Figure 3.1, were visited in January 2024. The extent of electricity access of the community, as well as the off-grid electrification solutions that were deployed were observed during these visits.

Figure 3.1: Map of South Africa highlighting the visited informal settlements.

Thembalethu informal settlement: PV-powered AC microgrid pilot project

In a section of the Thembalethu informal settlement, an AC microgrid consisting of 6.6 kWp PV, 30 kWh battery storage, and overhead reticulation at 48V had been installed, as visualized in Figure 3.2. The project is being run by a local developer, Specialized Solar Systems (SSS), who offer energy package subscriptions with a Pay-As-You-Go billing strategy. The newly connected 12 homes that had previously been relying on illegal connections to the national grid — a common practice in South Africa [53] — are now subscribed to a basic, upgradable plan of 2 kWh of electricity a day with a 5 A connection.

Figure 3.3a shows one of the newly connected homes, Figure 3.3b displays the installed PV system, and Figure 3.3c illustrates the system interface installed in each household.

Figure 3.2: Map of the distribution network of Thembalethu PV-Powered AC microgrid. The PV system is depicted by blue blocks at the bottom-left corner. The overhead pillar-to-pillar reticulation cables are illustrated in black lines, while the pillar-to-household cables are visualized in red lines.

(a) One of the newly connected homes

(b) PV installation

(c) Household connection point

Figure 3.3: Images from the Thembalethu site visit

Oudtshoorn informal settlement: Failed solar home system (SHS)

Commissioned by the local municipality, SSS had also supplied SHS's to the informal settlement of farmer homes in Oudtshoorn. Unfortunately, the system had failed within 2 years of installation due to the residents overloading the battery. However, since then, the residents have replaced the original battery with a second-hand battery and are re-using the single PV module system to power minimal loads such as indoor lighting and phone charging. Figure 3.4a shows one of the farmer homes while Figure 3.4b illustrates the state of the SHS with the adaptation of a second-hand battery.

(a) One of the farmer homes

(b) The adoption of a second-hand battery

Figure 3.4: Images from the Oudtshoorn site visit

Daveyton informal settlement: Mobile PV panel system

A family member of a local contact, living in the informal settlement of Daveyton, demonstrated her mobile and small-scale PV module and battery system that was distributed by the local municipality. Similar to the Oudtshoorn site, this system is the sole electricity source that is used for indoor lighting and phone charging. Figure 3.5a shows one of the homes in the Daveyton informal settlement, Figure 3.5b visualizes the small-scale PV module, and Figure 3.5c displays the battery device.

(a) One of the homes in the Informal Settelment

(b) The mobile PV module

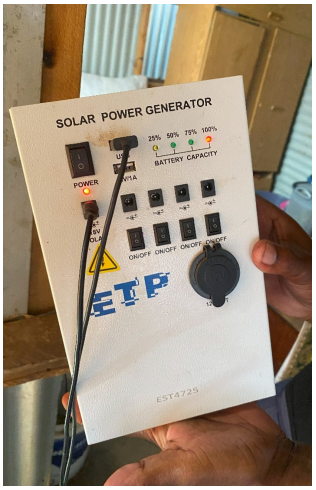

(c) The battery device

Figure 3.5: Images from the Daveyton site visit

Diepsloot informal settlement: Utility-based PV-tower management framework

In Diepsloot township and informal settlement, an utility-based energy management framework designed by SSS and operated by DC-GO was visited. Approximately 500 PV-towers, consisting of 800 Wp of PV and 5 kWh of battery storage have been deployed to offer energy bundle subscriptions. Each PV-tower can power up to 16 homes, providing connections of 24 V or 4 8V, depending on the energy bundles of the connecting homes. Figure 3.6a visualizes the installed PV-towers in the community, Figure 3.6b shows the household connection interface, and Figure 3.6c depicts the PV-tower structure.

(a) Aerial view of an installed PV-tower

(b) Household connection point

(c) Ground view of an installed PV-tower

Figure 3.6: Images from the Diepsloot site visit

3.2. Considerations for Initiatives in Informal Settlements

Through observing the various off-grid systems and discussing lessons learned with local developers, several design considerations unique to electrification solution development in South African informal settlements were identified. Notable aspects that should be accounted in order to achieve an effective and successful solution deployment are discussed in the following:

- **Theft Prevention:**
  Theft appeared to be one of the most significant concerns in service deployment in informal settlements. Social factors such as poverty, unemployment, lack of competent law enforcement in the communities are considered root causes of violence and theft that occur frequently [54]. Therefore, theft prevention must be a key consideration in solutions to be adapted in these communities.

  A notable example of theft prevention is the PV-tower design deployed in Diepsloot. The components are elevated to a height of 4 meters to add difficulty in accessing the expensive components of the system. Despite this precaution, a DC-GO O&M employee shared that a few incidents of theft were still unavoidable. Additionally, he mentioned that mixed copper-aluminum cables were also adopted in some areas as a precaution to copper cable theft, which is common due to the high resale value of copper.

- **System Misuse:**
  System misuse is another common cause of system failure, as observed in Oudtshoorn. When components are placed within homes, residents may tamper with the devices, leading to failures. Therefore, it is crucial to limit the interface between users and the system to ensure its prolonged lifespan.

- **Community Relationships**
  Community relationships are also of significance. Offering a service to only a small section can cause friction amongst the community. Neighbors who are not given access to the service could possibly tap into the service infrastructure, similar to how many locals currently connect to the national grid illegally, potentially causing system overload. Alternatively, the neighbors could act violently towards the homes with service access. Thus system deployment must be carefully thought with local leadership so as to avoid community friction.

- **Ownership & Accountability:**
  Accountability is another important aspect. A DC-GO employee mentioned that clients sometimes do not pay for 2-3 months and yet expect to receive power after paying the next month's bundle fee. This makes management of the system challenging, thus is crucial to keep clients accountable for their ownership of the system and subscription. One way to do this is by introducing a reconnection fee, similar to that applied by Eskom for the national grid, which charges a 5500 rand fee for reconnection.

4

Methodology

In this chapter, the PV-powered DC microgrid design methodology is outlined. Recall that for this project, the desired solution is initially tailored to Tier 3 energy access, but can easily scale up to Tier 5. This is to minimize the system upgrade needed when the community progresses towards higher energy access tiers. To obtain this desired microgrid design, first, a microgrid catered for Tier 5 electricity demand (”Tier 5 Microgrid”) is designed. Subsequently, the Tier 5 microgrid is modified to initially cater to Tier 3 electricity requirements, while retaining the Tier 5 microgrid infrastructure backbone (”Tier 3 Microgrid”).

The microgrid design process consists of multiple interconnected design domains. Figure 4.1 visualizes the overall design methodology of the microgrid design process, showcasing the interconnection of the design domains. The following sections discusses the detailed procedure of each design domain:

1. Demand Forecasting (Section 4.1)
2. PV String Sizing & Modelling (Section 4.2)
3. Distribution Network Design & Loss Calculation (Section 4.3)
4. PV & Battery Sizing (Section 4.4)

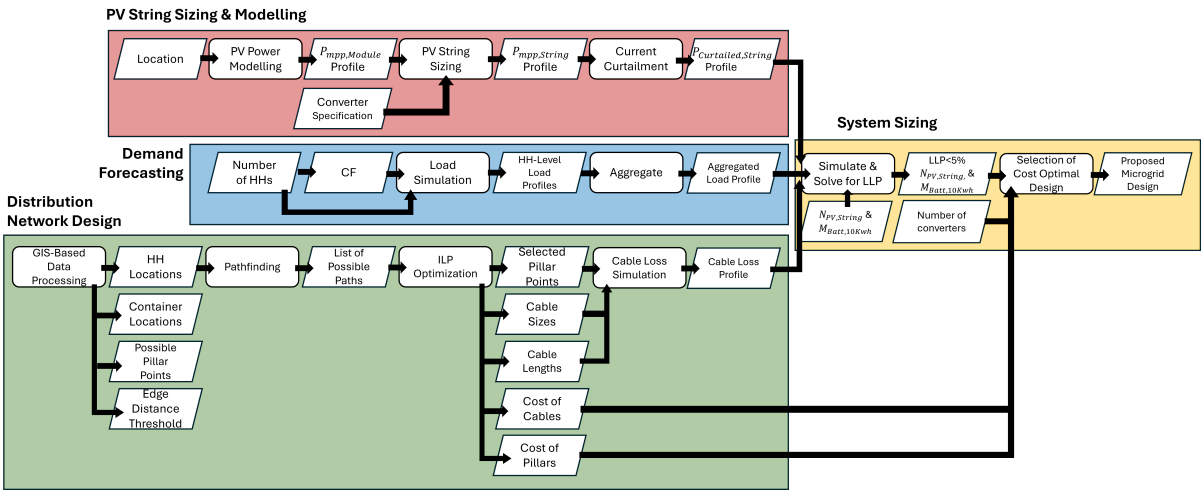

Figure 4.1: Flowchart of overall design procedure. Note: HH refers to household. $N_{PV,String}$ denotes the number of PV strings, and $M_{Batt,10kWh}$ represents the number of 10 kWh battery units.

4.1. Demand Forecasting

The design process begins with generating the load profile for the microgrid. Although recorded consumption data is the ideal system sizing reference, as noted in Subsection 2.4.1, the unavailability of consumption data for the targeted communities of this project has led to a load profile generating model to be utilised instead. The model selection rational, the load profile generation methodology of the selected model, and the application method is discussed in the following subsections.

4.1.1. Selected Load Profile Generator

Dr. Narayan 's load profile generating model [18] is utilized, as it was assessed to be most suitable for this project due to the following aspects:

- **Application for the energy access context:**
  The produced load profiles adhere to the electricity access classifications outlined in the MTF in terms of the quality and quantity of the energy services [18]. Thus, the model enables the generation of Tier 3 and Tier 5 load profiles necessary for this project's application.
- **Modeled based on DC appliances:**
  All appliances used in the construction of the load profiles are DC appliances listed in Appendix A [18]. This aligns with this project's focus on designing a DC microgrid tailored to accommodate such appliances.
- **Incorporates real-world variability:**
  While there is consistency with the daily time frame in which a load is used, the number of load usages and the cycle times are assigned randomly within the allowable range, embodying uncertainty [18]. This randomness, combined with adherence to typical consumption trends, aids in modelling realistic household electricity consumption behaviours.

4.1.2. Load Profile Construction Methodology

The model takes a bottom-up approach, constructing load profiles per load type (j) and summing them up to obtain the overall load profile. First, parameters listed in Table 4.1 and the specifications shown in Appendix A serve as inputs to the model, constraining the load profiles to abide to the MTF-defined energy quality and quantity attributes, as well as general consumption patterns.

Table 4.1: Input parameters for the load profile generation model.

Input Parameter	Notation	Definition
Load type	j	Type of appliance in use
Rated power	P	Rated power of appliance
Maximum Usage	$T_{\max}$	Maximum number of hours a load is operational in a day
Instances	n_j	Number of times a load j is operated in the allowed usage window
Usage window Limits	W	The allowed time window within which the loads are expected to be used
Quantity of loads	q	The number of loads of each type
Load occurrence Limits	$n_{j,\text{min}}, n_{j,\text{max}}$	Limit of number of load occurrence
Coincidence Factor	CF	Likelihood of appliances functioning simultaneously

Load usages are then randomly constructed within constraints by stochastically generating internal parameters listed in Table 4.2. For every j, a number of instances (n_j) of load occurrence during the day is randomly generated within the allowable range of $n_{j,\text{min}}$- $n_{j,\text{max}}$. In the case of Figure 4.2 that illustrates an example of the randomly generated internal parameters for a single load type that is rated at 150W, n_j is randomly assigned as 2, thus the corresponding two load occurrences are depicted in the two grey blocks. The start time (t_{ji}) of every load instance (i) for each j, is randomly assigned within the allowed windows (W). The cycle time (T_{ji}) is also randomly generated for each i, and for every j.

Table 4.2: Generated parameters within the load profile generation model.

Generated Parameters	Notation	Definition
Start Time	t_{ji}	Start time of a load instance within the usage window
Cycle Time	T_{ji}	Duration for which a load is operational
Peak Window	W_{peak}	The usage window where multiple appliances can be operated simultaneously

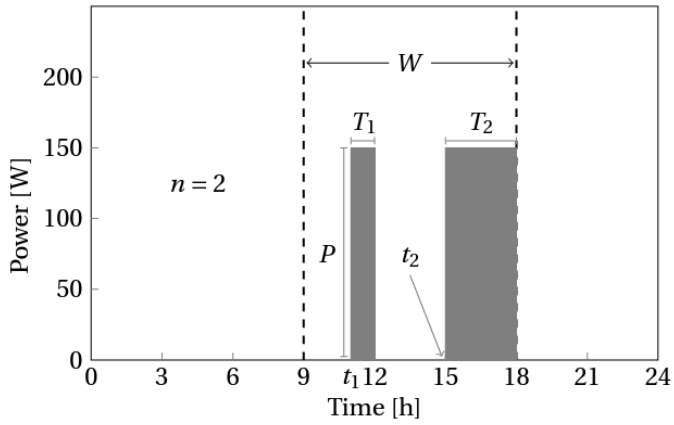

Figure 4.2: Example showcasing the load occurrences (n) randomly generated within the load usage window (W) [18].

The peak window (W_{peak}), an intersection of load usage windows of other loads, is also generated. A constraint ensures that at least one load occurrence from each load type falls within this W_{peak}. The probability of load occurrence start times (t_{ij}) within the peak window follow a normal distribution with the mean centered around the middle of the peak window. As illustrated in Figure 4.3, the coincidence factor (CF) influences the shape of the distribution, with a high CF corresponding to a narrow distribution compared to that of a lower CF. In this model, CF is limited to a value between $(CF_{\text{min}}, 1)$. These limits are depicted in Figure 4.3 as a blue dotted line for the case of $CF = 1$, implying that all load occurrences begin at the center of W_{peak}. CF_{min}, shown in a black line, is set to enable a normal distribution that fits within three standard deviations (3σ) from the mean (μ).

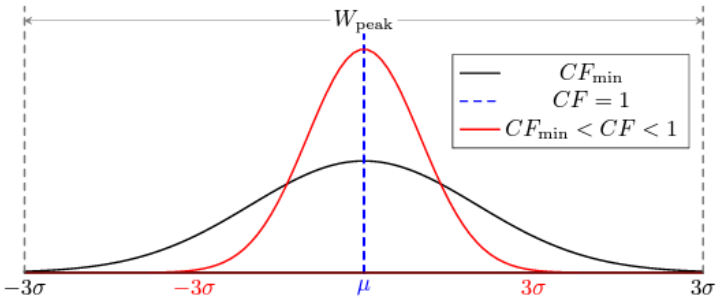

Figure 4.3: Load occurrence normal probability distribution in the peak window [18].

The end time of the load usage, calculated by adding the cycle time (T_{ij}) to the start time (t_{ij}), is subsequently evaluated. T_{ij} is cut short in the case that t_{ij}+ T_{ij} exceeds the allowed time window (W_{j}), or if the total operational hours of a load type ($T_{\text{total,j}}$) exceeds the maximum allowed usage hours ($T_{\text{max,j}}$). In this way, a day long time interval showing the precise time stamps when the load is active or inactive, is generated for all existing quantities (q) of each j. Combining all time intervals result in the overall daily load profile. This process is repeated for 365 days to construct a yearly load profile.

4.1.3. Application of the Load Profile Generating Model

The model is utilized with a modified CF suitable for the targeted communities, as suggested by Dr. Narayan [18]. This value is obtained through the relationship between the diversity factor and the aggregation level that is depicted in Figure 4.4, provided by Dr. Tindemans [55]. The diversity factor is the inverse value of the CF, and the aggregation level represents the number of households considered within a given scope. The relationship implies that the larger the size of the community, the lower the CF, signifying that it is less probable for load usages across the entire community to overlap.

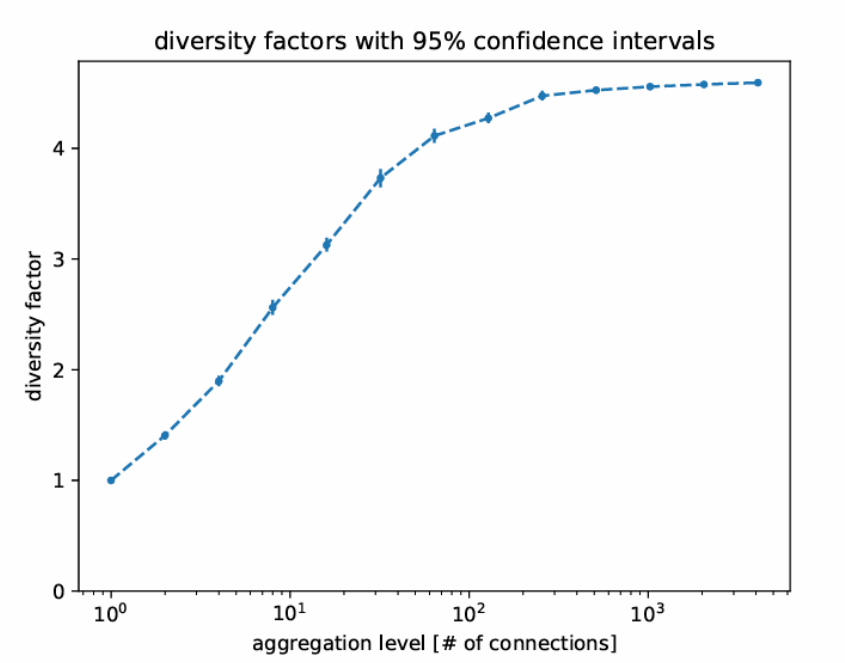

Figure 4.4: Relationship between diversity factor and aggregation level

Note that the model produces varying load profiles with the same set of input data constraints, due to its stochastic nature. Thus, the model is run for the necessary number of households to generate distinct load profiles for each household. These load profiles are then summed to obtain the aggregated community level load profile.

4.2. PV System Design, String Sizing & Curtailment

Similar to demand forecasting in Section 4.1, the power generation profile of a string of PV modules is modeled to serve as a reference for the final system sizing design stage. The required number of PV strings for the system to meet the load is determined based on the PV string power generation profile simulated in this design domain.

The following subsection discusses the PV simulation tool selection. The proceeding subsections then outlines the process of selecting the optimal orientation for the PV modules, simulating the power output of various PV modules, determining the maximum feasible PV string size, and curtailing the PV string power output in accordance with the solar converter specifications.

4.2.1. PV Simulation Tool Selection

As concluded from the evaluation of market-available PV simulation and design tools in Subsection 2.1.3, the open source Python library PV LIB [38], is selected for use in this project. The meteorological data for input is sourced from PVGIS, a free web application providing solar radiation data [35]. TMY data of DHI, DNI, GHI, ambient temperature, and wind speed, is retrieved.

4.2.2. Solving for Optimal PV Module Orientation

As outlined in Subsection 2.1.3, the POA irradiance is dependant on the PV system orientation, defined by θ_M and A_M of the PV modules. In this step, the system orientation that yields the highest annual irradiation is solved for.

- **The sky diffuse irradiance** is solved for with the *king* function which represents the simple sandia sky diffuse model [56], among the six irradiance transposition models offered by PV Lib listed in Table 2.5, due to the evaluation discussed in Subsection 2.1.3.
- **The ground diffuse irradiance** is estimated using the *get_ground_diffuse* function. Values for albedo are obtained from the NASA Langley Research Center (LaRC) Prediction of Worldwide Energy Resource (POWER) Project [57]. The albedo values of 0.13 and 0.15 are applied for the Oudtshoorn and Daveyton sites, respectively.
- **The direct irradiance** is estimated using the *poa_components* function that combines DNI with sky diffuse and ground diffuse irradiance.

By summing these three components and aggregating the hourly values over the year, the total annual irradiation is obtained. The optimal tilt angle is obtained by selecting the θ_M in the range of 0° to 90° that result in the highest annual irradiance. Note that A_M is fixed at north-facing, as it is the direction receiving the most light for Southern Hemisphere locations.

4.2.3. PV Power Output Simulation on Module Level

Given the optimal θ_M and A_M that was obtained in the previous step, the power output of a single PV module is computed. Although the evaluation of PV module types suggested the use of SHJ type PV modules in Subsection 2.1.2, the selection of PV modules for this project is restricted to that offered by SSS, listed in Table 4.3, which only consist of PERC modules. This study addresses real-world scenarios and considers practical constraints, such as the limited PV module selection available from the local developer on whom the system installation will depend. Therefore, though deemed less suitable due to their slightly lower R_{MPP} than SHJ modules, they are to be considered for this project.

The Sandia model is first utilized via *temperature.sapm_module* function to estimate the operating temperature of the glass/glass module mounted on an open-rack. This choice is based on the fact that all selected PV modules are glass-glass, and the anticipated PV system is designed for open mounting. However, these parameters can be adjusted to reflect different installation characteristics, such as glass/backsheet modules or non-open-rack systems, if the system employs such configurations.

Next, the *ivtools.sdm.fit_cec_sam* function is then used to convert manufacturer datasheet specifications listed in Table 4.3, into the normalized parameters introduced in Table 2.3. Subsequently, *pvsystem.calcparams_cec* function is used to calculate five parameter values for the single diode equation at effective irradiance and cell temperature. Finally, the function *pvsystem.max_power_point* calculates the maximum power point.

Table 4.3: Specifications of PV modules offered by SSS.

Power Rating of PV Module [W]	Canadian Solar HiKu6 Mono PERC			EnerSol Mono PERC	
	405	550	455	420	555
Vmp, module [V]	31	41.7	41.3	31.93	42.11
Imp, module [A]	13.07	13.2	11.02	13.15	13.18
Voc, module [V]	37	49.6	49.3	38	50.05
Isc, module [A]	13.93	14	11.66	13.87	14.07
α_{sc} [%/°C]	0.05	0.05	0.05	0.04	0.04
β_{oc} [%/°C]	-0.26	-0.26	-0.26	-0.3	-0.3
γ_{pmp} [%/°C]	-0.34	-0.34	-0.34	-0.4	-0.4
Cells in Series	108	108	144	144	144

4.2.4. PV String Sizing

The next step is to evaluate the maximum PV string size (i.e., number of PV modules per string), and to simulate the power output of this string. This maximum string size is restricted by electrical specifications of DCO's solar converter to which the PV modules are to be connected. These specifications are shown in Table 4.4.

Table 4.4: Solar converter specifications.

	Solar Converter Specifications
$P_{\text{converter, rated}}$ [W]	11000
$I_{\text{converter, SC}}$ [A]	15
$I_{\text{converter, Operational, Max}}$ [A]	13
$V_{\text{converter, Max}}$ [V]	760
$V_{\text{MPPT, Max}}$ [V]	608
$V_{\text{MPPT, Min}}$ [V]	100

The rule of thumb for string sizing are depicted in Equation 4.1 - Equation 4.4. Note that parallel PV string connections at the converter inputs are not possible given the I_{SC} of the PV modules and the $I_{\text{converter, SC}}$. Thus, the number of strings per converter input ($M_{\text{strings per input}}$) is set to 1, reforming Equation 4.1 to $I_{\text{converter,Max}} > I_{\text{module,sc}}$ as the design equation for currents. Furthermore, this restriction

is already embedded in the selection process of PV modules, as only PV modules with short-circuit current lower than the maximum input current of the solar converter are considered.

$$I_{\text{converter,Max}} > I_{\text{module,sc}} \cdot M_{\text{strings per input}} \tag{4.1}$$

$$V_{\text{converter,Max}} > N_{\text{modules per string}} \cdot V_{\text{module,oc}} \tag{4.2}$$

$$V_{\text{MPPT,min}} < N_{\text{modules per string}} \cdot V_{\text{module,mp}} < V_{\text{MPPT,min}} \tag{4.3}$$

$$V_{\text{converter,max}} > N_{\text{modules per string}} \cdot V_{\text{module,oc}} \cdot (1 - ((T_{STC} - T_{\text{ambient,min}}) \cdot \beta_{V_{oc}}/100) \tag{4.4}$$

The maximum string size is solved based on Equation 4.2, dividing $V_{\text{converter, Max}}$ by the $V_{\text{oc, module}}$. This string size is further evaluated by checking if the MPP voltage of the string is between the MPPT voltage range of the converter, ensuring that the number of panels per string satisfies Equation 4.3. The temperature effect is also considered via Equation 4.4, ensuring that the $V_{\text{oc, module}}$ at the lowest ambient temperature of the site does not exceed $V_{\text{converter, Max}}$.

The obtained value for $N_{\text{modules per string}}$ next serves as input to the *scale_voltage_currentpower* function to obtain the power output timeseries for the string of PV modules. This function scales the produced power of a single PV module to that of a string by multiplying the current with $N_{\text{modules per string}}$.

4.2.5. PV String Power Output Curtailment

In the last step, the power output timeseries of the string of PV modules is curtailed. The solar converter limits the current output of a string to the maximum operational current ($I_{\text{converter, Operational, Max}}$) of 13A, thus, the power profile is curtailed accordingly. The current output of the PV string is examined for each timestamp, and if the value exceeds the threshold, it is replaced by this limit. Note that the voltage shift due to the current curtailment is not accounted for, making the simulated curtailed power output to scale linearly with this curtailed current. This implies that the simulation slightly underestimates the power output of the PV string. However, this effect is expected to be negligible due to the small shift of voltage levels during this curtailment.

4.3. Distribution Network Designing

This section discusses the distribution network design domain. The design process of the distribution network that delivers the power from the central container to all the households involves layout optimization and cable sizing. Based on the evaluation of the possible distribution network design approach discussed in Section 2.3 , it was decided to apply the graph theory based pathfinding algorithm methodology. This approach entailed GIS based data processing, graph theory based overhead cabling pathway identification, and integer linear programming (ILP) optimization for the overall layout cost. Additionally, the cable losses of the designed distribution network is simulated, using the approach proposed in Subsection 2.4.2, to serve as input for the PV and battery sizing.

4.3.1. GIS based data processing

Quantum GIS (QGIS) [58], an open source GIS software is used to dissect the geographical locations that serve as input to the proceeding steps in designing the overhead cabling network. Layer files containing the geographical locations of the following points are created and exported as shapefiles:

1. The households that the microgrid is to power
2. The central container
3. Possible pillar points
   (i.e., locations where pillars supporting the overhead cables can be placed)

The households and container locations are manually identified on the map, while the identification method for the possible pillar points varies depending on the geographical scope of the design site. For a design site with long-spanning households, such as the Oudtshoorn site, a grid of equally spaced points within the geographical scope of the project is created. The area occupied by the households, container, and roads are extracted, leaving a grid of feasible points for pillar installation. However, for sites with narrow roads threading through highly dense clusters of households, such as in the case of the Daveyton site, the extraction of the areas occupied by the households, container, and roads was not precise enough. Consequently, manually identifying potential pillar points was found to be more effective.

4.3.2. Cable Path Identification

Proceeding with the coordinates of the households, container, and possible pillar points, graph theory based pathfinding algorithms are then applied to create possible cable routes. Graph theory is a branch of mathematics that studies graphs, which are made up of nodes and edges. In this project, an open-source python package, NetworkX [46], is used to create and manipulate graphs where the households, container, and possible pillar points make up the nodes, and the edges represent the cabling of the distribution system. The following outlines the process of generating a set of cabling routes that serve as decision variables in the proceeding ILP optimization:

1. **Create a Complete Graph**
   First, a graph with nodes consisting of the households, container, and possible pillar points is created. To mitigate significant electrical power losses and mechanical cable sagging across long distances, maximum threshold distances are enforced based on practices from the Thembalethu AC microgrid system introduced in Figure 3.1. Edges are added between node pairs according to the following maximum threshold distances:
   - (Household - Possible pillar point) pairs within a 20m radius
   - (Container - Possible pillar point) pairs within a 30m radius
   - (Possible pillar point - Possible pillar point) pairs within a 30m radius

   Note that household-to-household and household-to-container connections are not considered.
2. **Compute Shortest Paths**
   Given the complete graph from the previous step, the shortest path from the container to each household is computed using the *"shortest_path"* function with the dijkstra method from NetworX [46]. This algorithm finds the path with the minimal sum of edge lengths. The number of nodes traversed in the shortest path is recorded and used as the cutoff value in the subsequent step. A subgraph consisting only of the nodes and edges in these shortest paths is created, referred to as the ”Dijkstra’s graph.”
3. **Add Neighboring Nodes**
   Neighboring nodes, which are nodes not included in Dijkstra’s graph but share an edge with any nodes within it, are identified and added to Dijkstra’s graph. This creates a larger graph, referred to as ”Dijkstra’s + neighbors graph.”
4. **Identify All Possible Paths**
   Lastly, given the dijkstra’s + neighbors graph, the *"all_simple_paths"* function is employed to generate all paths connecting the container to each household without repeating nodes. The cutoff, set to the number of nodes in the shortest path, limits the search depth. This process is repeated for each household, creating a set of paths for each household. Setting a minimal cutoff value reduces the size of the set of paths and minimizes the computational power needed for this step and the subsequent ILP optimization.

Note that while it is possible to skip steps 2 and 3 and directly search for possible paths within the complete graph, the computation time for the pathfinding algorithm is factorial (O(n!)) in the complete graph of order n. Steps 2 and 3 filter out nodes distant from the shortest path, reducing the number of nodes that the pathfinding algorithm must search through and thus optimizing computational efficiency.

4.3.3. ILP Optimization

In this step, layout costs are optimized. This is done by formulating and solving an integer linear programming problem via open-source python library, Pulp [59]. The ILP optimization problem is constructed with optimization objective, decision variables, and constraints described in the following:

- **Objective:**
  The objective function is to minimize the overall layout costs. This consists of the following:
  1. Node cost:
     The cost of installing the pillars in the selected points. The fixed cost coefficient of 1000 euros is multiplied by the total number of pillar points within the selected paths. This node cost coefficient is based on estimated material and installation costs shared by SSS.
  2. Edge Costs:
     The cost of overhead cabling. This cost depends on the edge distance and the necessary cable size. While the edge distance is a straight-forward parameter, the size of the cable is determined by the current requirement for each edge. The current requirement is calculated using Equation 2.8. One of the input parameters of this equation, the maximum current that

the cable is expected to carry, is taken as the peak current obtained from the household-level load profiles, multiplied by the number of households that rely on a certain edge (further refereed to as ”edge occurrence”). Consequently, the more loads an edge carries, the greater the ampacity requirement, leading to the need for larger sized cables.

For this project, Draka installation cables of sizes listed in Table 4.5, represented by the visual in Figure 4.5 are considered. These cables consist of four conductors necessary for the DC microgrid: positive, neutral, negative, and communication. They are the most economical option offered by Rexel, the cable supplier for DCO. Although mixed copper-aluminum cables were initially considered as an additional measure for theft prevention, their unavailability in a range of sizes prevented their use, necessitating the use of copper cables instead.

When the required ampacity exceeds the threshold of the maximum current rating of the thickest cable, an additional cable is allocated to carry the overflow current. This means that multiple cables can be allocated for a single edge of the distribution network. As a result, heavily load-carrying edges will consist of multiple cables to dispatch the power effectively.

Table 4.5: Specifications of the considered cables for this study.

Conductor Cross-Section Area [mm^2]	Cost per Length [€/m]	Conductor Resistance [Ω/km]
2.5	2.65	7.41
6	5.96	3.08
10	9.78	1.83
16	15.06	1.15
25	23.70	0.727
35	34.08	0.524
50	45.84	0.387
70	64.20	0.268
90	92.40	0.193

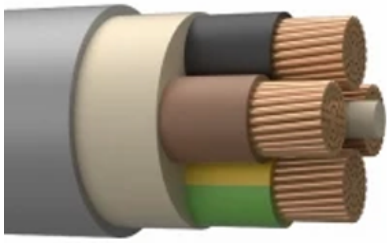

Figure 4.5: Visual of Draka installation cable considered for this project.

- **Decision Variable:**
  All simple paths connecting each target node to the container, generated in the previous step, are the decision variables. A path within the set of all possible paths for each household is either selected or not.
- **Constraints:**
  For each household, only one cable path is selected from its corresponding set of all possible paths.

Through this ILP problem, a distribution network connecting all households with the central container via overhead reticulation with pillar placement that results in the minimal cost is obtained. Specifically, the number of pillars, their installation locations, and the necessary cable sizes and lengths are obtained.

4.3.4. Calculating Cable Losses

The final step of the distribution network design domain is to calculate the power losses of the distribution network designed in Subsection 4.3.3. As discussed in Subsection 2.4.2, the lack of available

open-source tools for automatically calculating cable losses for DC networks led to the decision to create a python script to do so. The cable loss simulation takes the following procedure:

1. Each household is allocated its own individual household-level load profile generated in Section 4.1.
2. For each edge in the distribution network, the load profiles of the housdholds that use the edge is summed to get the load profile of each edge.
3. Starting from the outer edges (”edge occurrence”= 1), Equation 2.9 is used to calculate the cable losses, given the cable sizes determined in Subsection 4.3.3, and the hourly load. This cable loss is then added to the load of the edges connected towards the central container of the path.
4. Proceeding with edges with ”edge occurrence” of incremental increase ensures that cable losses of the outer edges are always added to the inner edges before the cable losses calculations.

Repeating these steps for each hourly increment allows for the simulation of cable losses throughout the project. It is acknowledged that the voltage drop due to these losses are not considered in this simulation. While this is a point for future work, as mentioned in Section 7.3, to introduce a backward/forward sweep technique, the voltage drop effect is assumed to be minimal for the relatively small low voltage levels of the system and the small scale of the study cases.

4.4. System Sizing

The last design domain is sizing the power generation and storage capacity of the microgrid. The task of sizing stand-alone power supply systems is finding the best compromise between reliability and cost [60]. In this project, this task is tackled in two stages:

1. Restrict the system sizing options to that which achieve an acceptable level of reliability.
2. Out of the sizing options from step 1, select the most economical option.

These steps are elaborated upon in the following subsections.

4.4.1. PV & Battery Sizing for Reliability

To determine the necessary combination of PV power supply and battery capacity to achieve a desired level of reliability, a Python script is developed based on the numerical sizing method which entails a LLP performance analysis, as decided as the most suitable approach for this project in Subsection 2.4.3.

Table 4.6: Battery and converter parameters used in the simulation.

Parameter	Description
P_{PV}	Generated power from PV system
P_{Load}	Aggregated load
P_{Loss}	Power loss due to cables
$P_{Mismatch}$	Power mismatch between P_{PV} and the sum of P_{Load} and P_{Loss}
E_{Batt}	Momentary energy capacity of the battery
$E_{Batt,Max}$	80% of the rated energy capacity of the battery system (upper operational limit of the battery)
$E_{Batt,Min}$	20% of the rated energy capacity of the battery system (lower operational limit of the battery)
$P_{Batt,Charge,Max}$	Chargeable capacity in the battery: $E_{Batt,Max}$ - E_{Batt}
$P_{Batt,Discharge,Max}$	Dischargeable capacity in the battery:E_{Batt} - $E_{Batt,Min}$
$P_{Conv,Max}$	Maximum converter discharge/charge rate. This value is the rated power of the converter (11 kW) multiplied by the number of units.
η_{Batt}	Power efficiencies of battery system. A value of 0.96%, benched marked from SSS battery selection, is used for this study.
η_{Conv}	Power efficiencies of DCO’s 11 kW battery converter. A value of 0.95%, inquired from DCO, is used for this study.

The aggregated load profile, the power production profile of a string of PV modules, and the power loss profile, in addition to the battery and battery converter specifications, serve as input to this script.

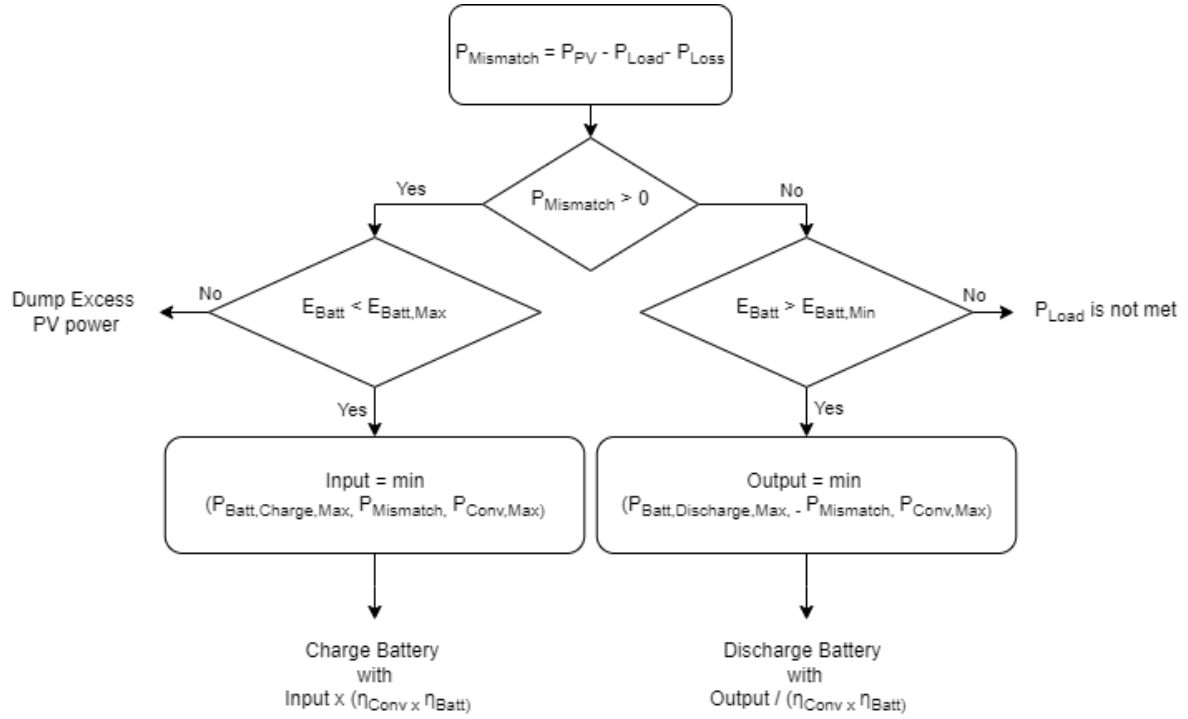

Figure 4.6: Concept illustration of system behaviour modeled in LLP Solver

A 10 kWh lithium-ion battery is selected for the base unit for this simulation, as discussions in Subsection 2.2.2 led to the conclusion that this battery type would be best suited for this project. The power produced from the PV string, the load and the losses, along with the remaining energy capacity within the battery is assessed for each timestamp. Based on these evaluations, the script determines the battery's charge/discharge state.Table 4.6 summarizes the parameters used in this simulation, and the model functionality is visualized in Figure 4.6.

The function iterates over each hour of the year to simulate the operation of the microgrid system. For each hour: $P_{Mismatch}$ is calculated. If there is excess PV power (i.e., $P_{mismatch}$ > 0), the battery is charged if there is chargeable capacity in the batteries (i.e., E_{Batt} < $E_{Batt,Max}$). Otherwise, excess power is dumped. The input power to the battery is the minimal value of the following: $P_{Batt,Charge,Max}$, $P_{mismatch}$, and $P_{Conv,Max}$. The battery is charged with the limiting value of the three, multiplied by the system efficiency (η_{Batt} x η_{Conv}). On the other hand, if there is a deficit in PV power (i.e., $P_{mismatch}$ < 0), the battery discharges to cover the deficit if there is available energy in the battery (i.e., if E_{Batt} > $E_{Batt,Min}$). The output power of the battery is the minimal value of the following: $P_{Batt,Discharge,Max}$, -$P_{mismatch}$, and $P_{Conv,Max}$. The demand is not met if the limiting value of the three, divided by the system efficiency, is less then $P_{mismatch}$.

At the end of the simulation, the LLP is calculated as the ratio of energy deficit to the total energy demand. This simulation is run for various numbers of PV strings ($N_{\text{PV String}}$), and various numbers of 10 kWh battery units (M_{10kWh}), to solve for a pair of ($N_{\text{PV String}}$, M_{10kWh}) that yields a LLP of less than 5%.

4.4.2. System Sizing for Economic Feasibility

After solving for the combination of PV and battery capacity that satisfy the LLP requirement, the most economical ($N_{\text{PV String}}$, M_{10kWh}) pair is selected. This is done by comparing the overall material cost of the PV strings, solar converter, battery units, and battery converters. Table 4.7 shows the cost of the components. Note that the PV module costs were obtained from SSS, converter prices were provided by DCO, and the 10 kWh battery unit cost was calculated based on the worldwide lithium-ion battery price of the 2023 market [61].

Table 4.7: Material cost of components for system sizing

Component	Cost per Unit [€]
CS 455W PV Module	97.20
CS 550W PV Module	110.00
CS 405W PV Module	95.55
EnerSol 420W PV Module	92.61
EnerSol 555W PV Module	138.47
Battery Market Price of 10 kWh Lithium-ion	1278.8
11kW Solar Converter	1100
11kW Battery Converter	1100

5

Results

This chapter presents the results of applying the microgrid design methodology outlined in Chapter 4 to the two sites, Oudtshoorn and Daveyton. It includes both the Tier 5 and Tier 3 microgrid designs for each site.

5.1. Simulated Demand

The household-level and community-level aggregated load profiles for the two sites were simulated via method discussed in Subsection 4.1.3. The resultant annual energy consumption and peak power, for both Tier 5 and Tier 3 levels, at the Oudtshoorn and Daveyton sites are shown in Table 5.1 and Table 5.2, respectively. As expected, there is a significant increase in the annual consumption and peak power from Tier 3 to Tier 5 for both sites. Additionally, the significant difference in scale between the Oudtshoorn site which consists of 13 households and Daveyton site that is made up of 119 households is also expected.

Table 5.1: Annual energy consumption and peak power of the simulated Tier 3 and Tier 5 load profiles for the Oudtshoorn site.

	Tier 3	Tier 5
Annual Aggregated Community-Level Energy Consumption	4.64 MWh	45.05 MWh
Peak Power of Aggregated Community-Level Load	1.16 kW	23.36 kW

Table 5.2: Annual energy consumption and peak power of the simulated Tier 3 and Tier 5 load profiles for the Daveyton site.

	Tier 3	Tier 5
Annual Aggregated Community-Level Energy Consumption	42.09 MWh	410.69 MWh
Peak Power of Aggregated Community-Level Load	10.04 kW	198.12 kW

Figure 5.1 and Figure 5.2 shows the aggregated load profiles for the Tier 3 (in orange) and Tier 5 (in blue) levels for the Oudtshoorn site, and Figure 5.3 and Figure 5.4 shows that of the Daveyton site. It is noticed that both load profiles consist of two peaks in a single day, one wider peak in the morning and a narrow peak in the evening.

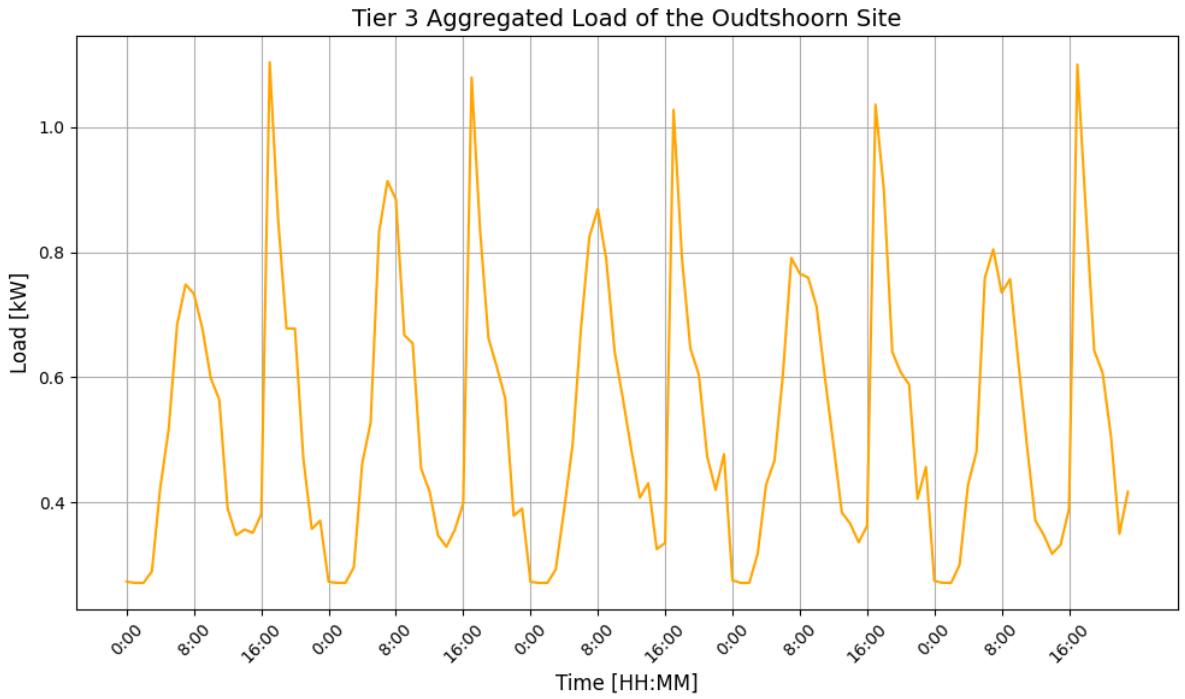

Figure 5.1: Simulated Tier 3 aggregated community-level load for the Oudtshoorn site. An exemplary 5-day period is presented.

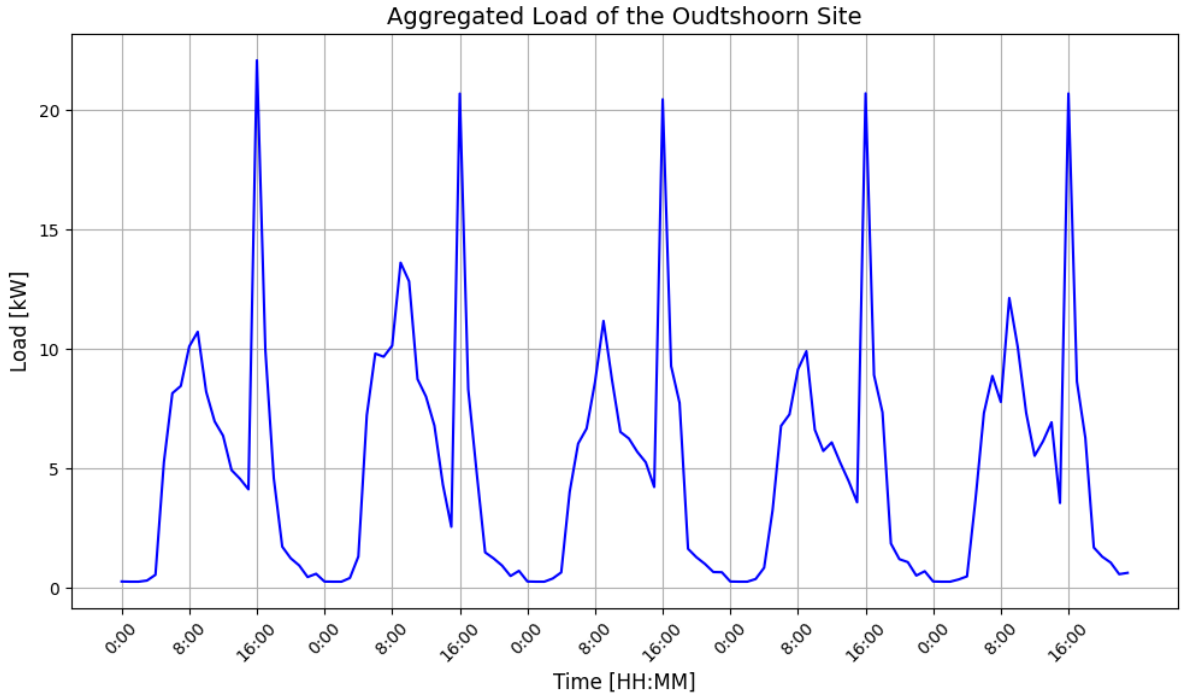

Figure 5.2: Simulated Tier 5 aggregated community-level load for the Oudtshoorn site. An exemplary 5-day period is presented.

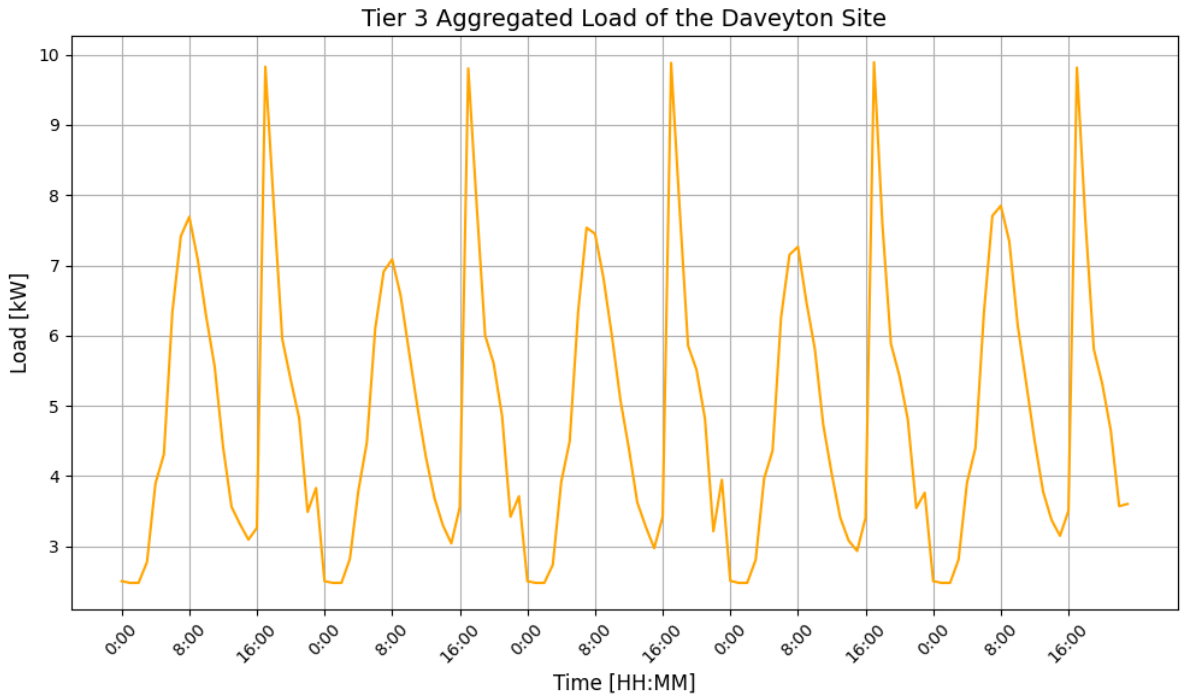

Figure 5.3: Simulated Tier 3 aggregated community-level load for the Daveyton site. An exemplary 5-day period is presented.

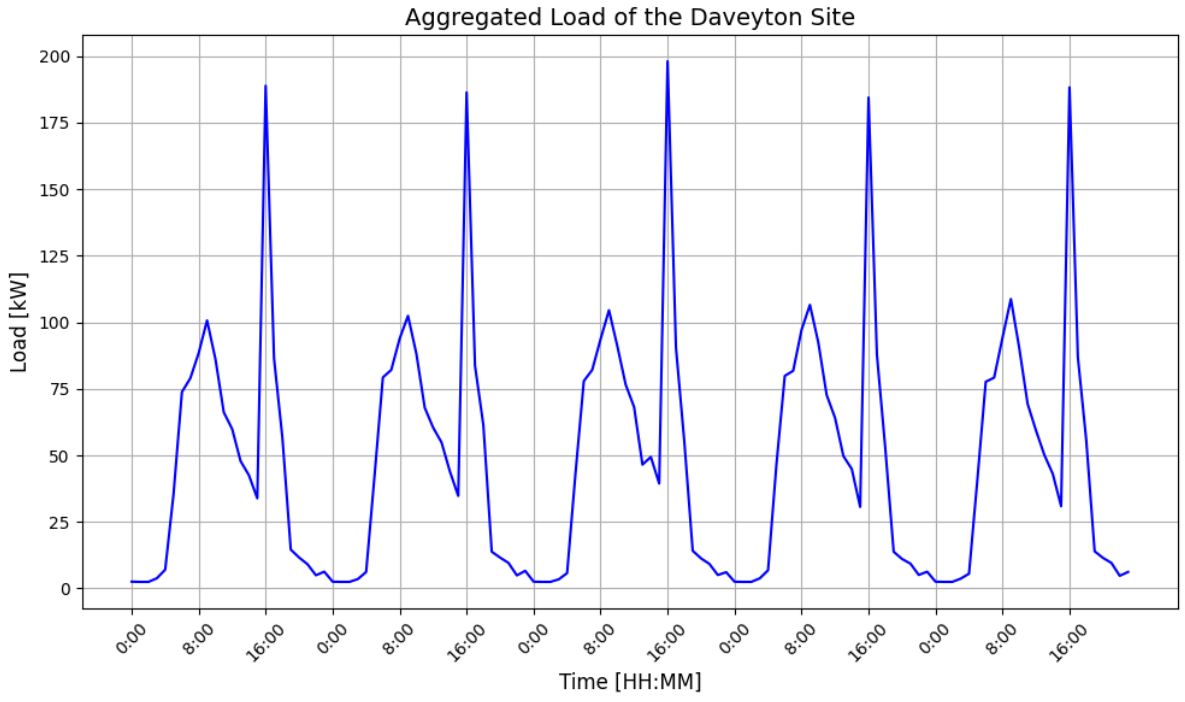

Figure 5.4: Simulated Tier 5 aggregated community-level load for the Daveyton site. An exemplary 5-day period is presented.

5.2. PV System Design

This section discusses the optimal orientation for PV modules, the sizing of PV strings, and the impact of curtailment.

5.2.1. Optimal PV Module Orientation

Following the procedure outlined in Subsection 4.2.2 for solving for the optimal orientation of the PV system yielded the results summarized in Table 5.3. Given the geographical data and albedo values

also presented in the table, the optimal tilt angle was found to be 41° for the Oudtshoorn site and 37° for the Daveyton site. This slight difference in the optimal tilt angles are mainly attributed to the variation in latitude. The resulting annual POA global irradiation at these optimal tilt angles were 2.13 MWh/m^2 and 2.10 MWh/m^2 respectively. Also note that the maximum ambient temperature obtained from the meteorological data was 38.19°C for the Oudtshoorn site and 33.46 °C for the Daveyton site.

Table 5.3: PV system orientation results.

	Oudtshoorn Site	Daveyton Site
Latitude [°]	-33.5334	-26.1435
Longitude [°]	22.2272	28.4455
Albedo [-]	0.13	0.15
Optimal Tile Angle [°]	41	37
Annual POA Global Irradiation at Optimal Tilt [MWh/m^2]	2.13	2.10

5.2.2. PV String Sizing

Table 5.4 presents the maximum string size, the corresponding rated PV string capacity, and the corresponding annual energy yield for a string of the all considered PV modules at each site. These values were determined using the methodology outlined in Subsection 4.2.4. It is observed that the PV string size for each PV module option is the same for both sites. This indicates that the variation in local ambient temperatures did not impact the string sizing via Equation 4.4. The simulated annual energy yields are thus similar values in both sites for the same PV module option, with the Oudtshoorn site having a slightly higher value, consistent with the annual POA global irradiation variance.

Table 5.4: PV string sizing results.

	Oudtshoorn Site					Daveyton Site				
Power Rating of PV Module [W]	Canadian Solar HiKu6 Mono PERC			EnerSol Mono PERC		Canadian Solar HiKu6 Mono PERC			EnerSol Mono PERC	
	405	550	455	420	555	405	550	455	420	555
Maximum String Size	18	13	13	17	13	18	13	13	17	13
PV String Capacity [kWp]	7.29	7.15	5.92	7.14	7.22	7.29	7.15	5.92	7.14	7.22
Annual Energy Yield of PV String Before Curtailment [MWh]	14.64	14.35	11.87	14.13	14.26	14.45	14.17	11.72	13.96	14.09

5.2.3. Curtailment Effect

Next, the effect of the PV string current curtailment, detailed in Subsection 4.2.5, is presented in Table 5.5. For each PV module option for each site, the fraction of time that the curtailment in executed in a year, the annual energy yields after curtailment, and the annual energy loss due to curtailment are also shown. Results show that the Oudtshoorn site was impacted more by the curtailment than the Daveyton site, resulting in slightly greater losses. It is also noticed that the strings of Canadian Solar 455 W modules for both sites were not effected by the curtailment, as this module has a lower rated current than the other modules. Figure 5.5 shows the variation in current curtailment impact on the annual current output for the PV strings made up of Canadian Solar 455 W modules and the Canadian Solar 550 W modules. The difference in string current levels between the two sites can also be observed.

Table 5.5: Current curtailment results on PV strings for consisting of the various PV modules at both sites.

	Oudtshoorn					Daveyton				
Power rating of PV Module [W]	Canadian Solar HiKu6 Mono PERC			EnerSol Mono PERC		Canadian Solar HiKu6 Mono PERC			EnerSol Mono PERC	
	405	550	455	420	555	405	550	455	420	555
Fraction of the Year when Curtailment is Executed [%]	2.80	3.26	0	2.80	3.16	1.59	2.05	0	1.61	1.96
Annual Energy Yield of PV String After Curtailment [MWh]	14.58	14.29	11.87	14.08	14.2	14.43	14.14	11.72	13.94	14.07
Annual Energy Loss of PV String due to Curtailment [%]	0.36	0.45	0	0.36	0.43	0.14	0.2	0	0.14	0.19

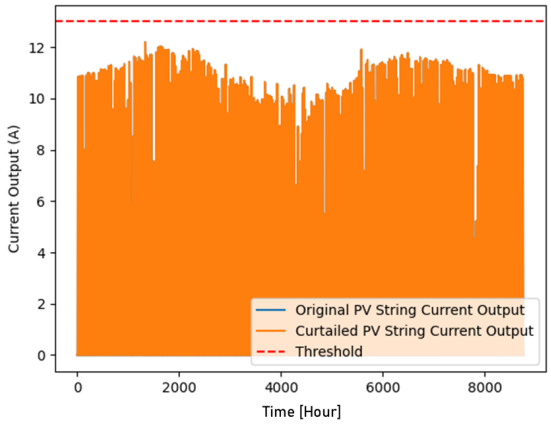

(a) Annual current output of a PV string consisting of Canadian Solar 455 W modules in Oudtshoorn site. Note that the orange lines overlap the blue lines as the curtailment did not affect the PV string current output.

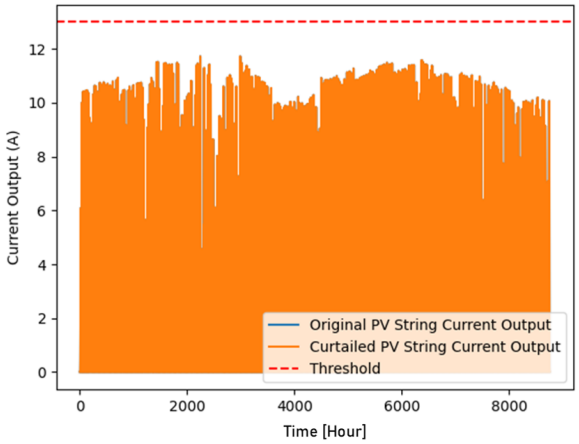

(b) Annual current output of a PV string consisting of Canadian Solar 455 W modules in Daveyton site. Note that the orange lines overlap the blue lines as the curtailment did not affect the PV string current output.

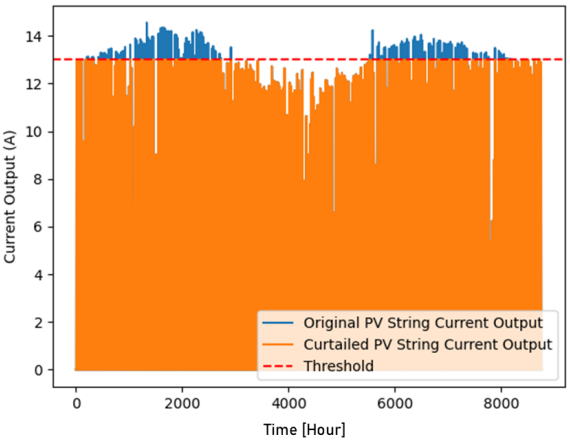

(c) Annual current output of a PV string consisting of Canadian Solar 550 W modules in Oudtshoorn site.

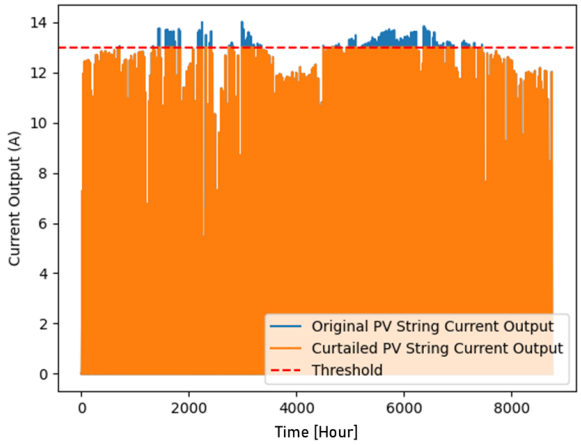

(d) Annual current output of a PV string consisting of Canadian Solar 550 W modules in Daveyton site.

Figure 5.5: The effect of PV current curtailment on the annual current output of PV strings for the Oudtshoorn and Daveyton sites. Results for the PV strings consisting of Canadian Solar 455 W and 550 W modules are presented.

5.3. Distribution Network Design

This section presents the extracted geographical data used as input for the graph manipulation process, provides an example of the graph manipulation, and details the optimal distribution network layout

and structure.

5.3.1. Processed Geographical Data

In the distribution network design domain, multiple scenarios were considered. Figure 5.6 shows the two considered scenarios for the Oudtshoorn site: a 10m spaced grid (Oudtshoorn Scenario-A) and a 8m spaced grid (Oudtshoorn Scenario-B) for the possible pillar point locations. The central container is shown as a red node and the households are shown in yellow nodes for both. The green nodes in Figure 5.6a represent the 10m spaced grid of possible pillar point locations and the pink nodes in Figure 5.6b represent that of a 8m spaced grid. The possible pillar point grid was created within the defined scope of the installation site using the internal tool functions of QGIS.

(a) Oudtshoorn scenario-A: 10m grid for possible pillar points shown in green nodes.

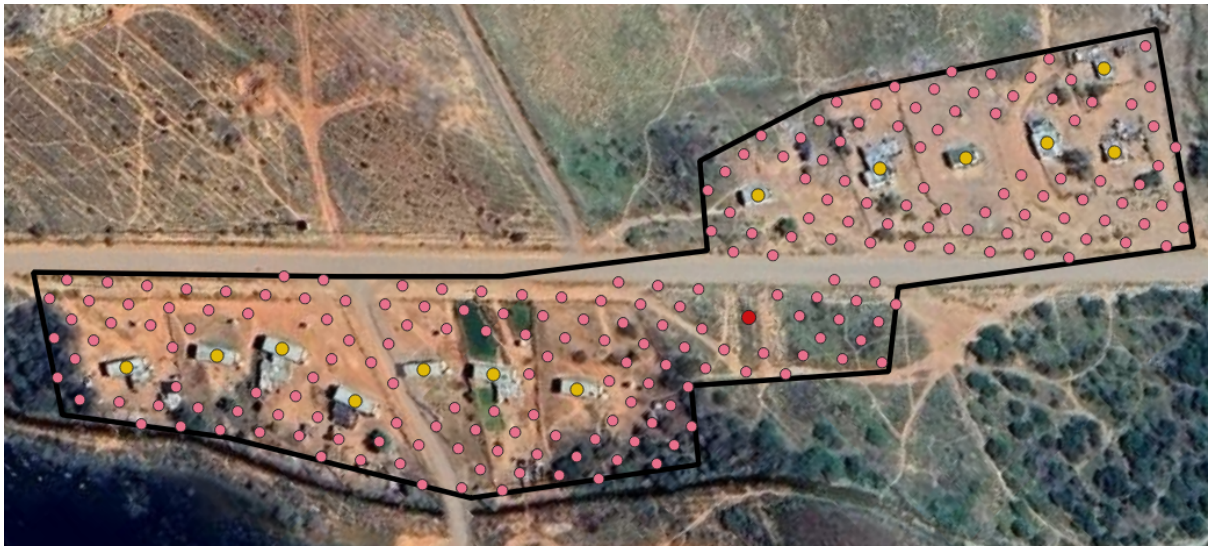

(b) Oudtshoorn scenario-B: 8m grid for possible pillar points shown in pink nodes.

Figure 5.6: Extracted geographical data from QGIS for the Oudtshoorn site.
The central container and the households are shown in red and yellow, respectively.

For the Daveyton site, the manually identified pillar points are consistent among the two considered scenarios, instead, the central container is placed at different locations. Daveyton Scenario-A places the central container at the East end of the community, while Daveyton Scenario-B places it at the South end. The central container and households are again shown in red and yellow, respectively, with the red central container marker placed differently in Figure 5.7a and Figure 5.7b. The locations of the possible pillar points are represented in green and are the same for both scenarios.

(a) Daveyton scenario-A: East central container location.

(b) Scenario B: South central container location.

Figure 5.7: Extracted geographical data from QGIS for the Daveyton site.
The central container, the households, and the possible pillar points are shown in red, yellow, and green, respectively.

5.3.2. Graph Manipulation

The geographical data was then manipulated through the application of graph theory based concepts that are outlined in Subsection 4.3.2. Figure 5.8 provides an exemplary visual of the evolution of the graphs for scenario B of the Daveyton site. The households, central container, and possible pillar points are represented in red, dark-blue, and light-blue, respectively. Figure 5.8a shows the starting point of the process, the complete graph consisting of all pairs of nodes connected via edge (shown in black lines) when located within the maximum allowed distances. Next, within this complete graph, the shortest path connecting the central container to each household is identified via dijkstra method. Figure 5.8b shows the resultant graph containing only these shortest paths (shown in red lines). In the third step, the neighboring nodes are added to the Dijkstra's graph, as seen in Figure 5.8c. Lastly, a list of all possible paths connecting to the central container via the allowed number of node connections are identified for all households. This list of possible paths serve as input to the ILP optimization outlined in Subsection 4.3.3, that solves for the cost optimal selection of paths, finally yielding the optimal graph shown in Figure 5.8d. The selected paths are represented in blue lines, and the selected pillar points as well as the container are shown in grey.

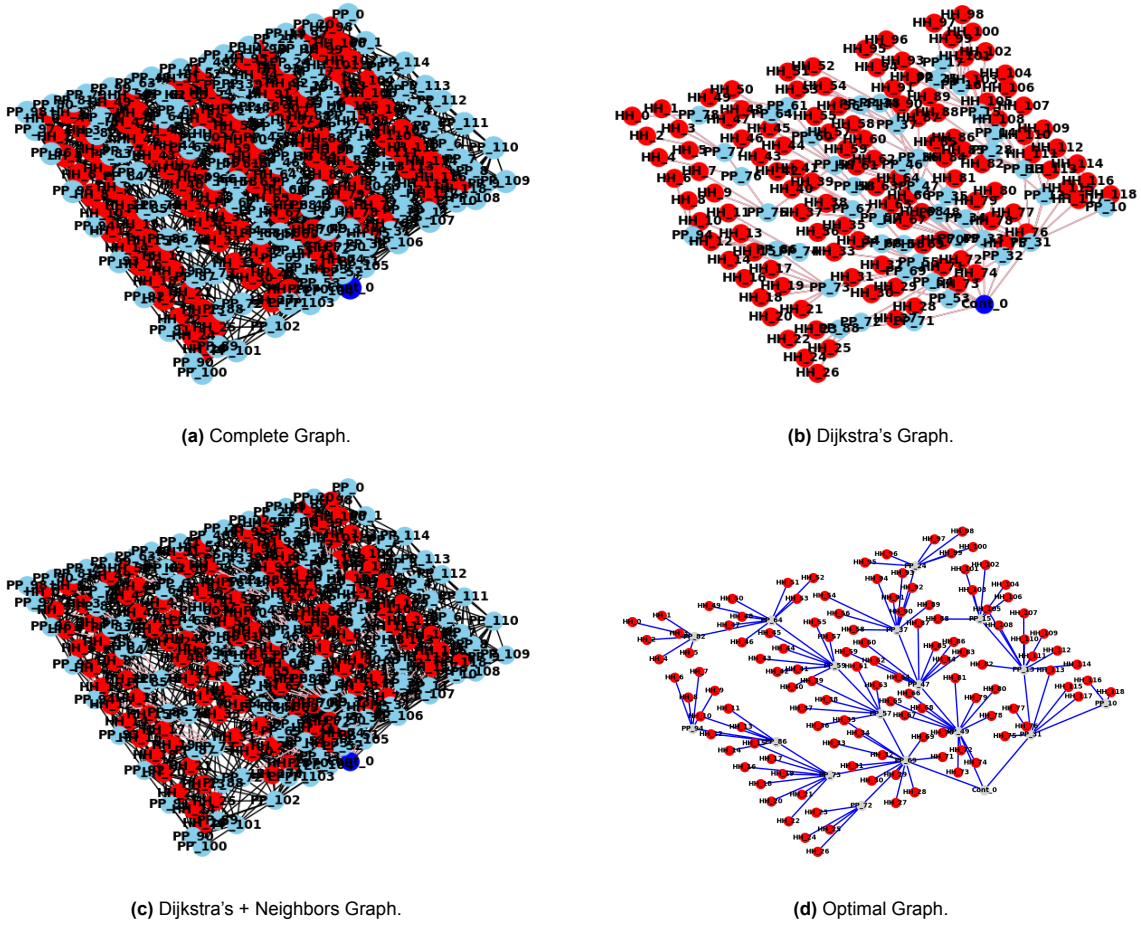

(a) Complete Graph.

(b) Dijkstra's Graph.

(c) Dijkstra's + Neighbors Graph.

(d) Optimal Graph.

Figure 5.8: Intermediate outputs of graph manipulation for the Daveyton scenario-B distribution network. The households, central container, and possible pillar points are represented in red, dark-blue, and light-blue, respectively in Figure 5.8a, Figure 5.8b, and Figure 5.8c. In Figure 5.8d, the selected paths are represented in blue lines, and the selected pillar points as well as the container are shown in grey.

5.3.3. Optimal Distribution Network Layout

The allocation of cable size within the ILP optimization was conducted following the methodology outlined in Subsection 4.3.3, with the necessary parameters for Equation 2.8 presented in Table 5.6. The peak current was obtained from the household-level load profiles, and the maximum ambient temperature (T_H) was obtained from the meteorological data used in Section 4.2. The temperature adder for ambient temperature adjustment for cables exposed to sunlight (T_0) is set as 14 °C as it is assumed that the cables have a distance of 300mm - 900mm above the roofs in Table 2.7. The ambient temperature correction factor (F_1) was then obtained from Figure 2.8 for the temperature value of $T_H + T_0$. As mentioned in Subsection 2.4.2, the adjustment factor for more than three carrying conductors in a cable set to 1 as the bipolar dispatch of the system only has two conductors that simultaneously are energized.

Table 5.6: Cable sizing parameters.

	Oudtshoorn Site	Daveyton Site
Maximum Load of a Single Household [W]	2069.6	2099.5
Maximum Ambient Temperature [°C]	38.19	33.46
Added Temperature [°C]	14	14
$T_H + T_0$ [°C]	52.19	47.46
F_1	0.76	0.82

The resultant optimal distribution network layouts for scenario A and B of Oudtshoorn and Daveyton are shown in Figure 5.9, Figure 5.10, Figure 5.11and Figure 5.12. Note that the households, central container, and the selected pillar points are represented in orange, red, and blue, respectively. The corresponding network structure and costs are summarized in Table 5.7 and Table 5.8 for Oudtshoorn, and Table 5.9 and Table 5.10 for Daveyton.

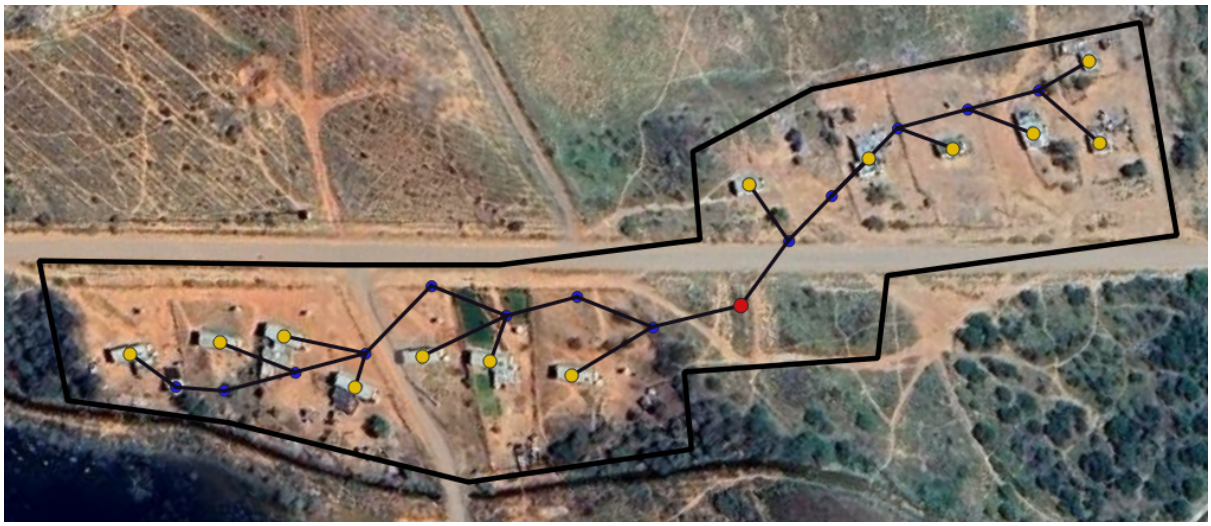

Figure 5.9: Generated distribution network for scenario A of Oudtshoorn site.

Figure 5.10: Generated distribution network for scenario B of Oudtshoorn site.

Table 5.7: Oudtshoorn distribution network structure.

	Oudtshoorn Scenario-A (10m)	Oudtshoorn Scenario-B (8m)
Number of of Pillars	13	12
Number of Edges	26	25
Number of Cables	26	25
Maximum Number of Households Connected to a Single Edge	7	6
Maximum Number of Households Connected to a Single Cable	7	6
Total Cable Length	558.98 m	605.31 m
Required Length of 2.5 mm^2 Cable	290.47 m	341.63 m
Required Length of 6 mm^2 Cable	44.06 m	29.71 m
Required Length of 10 mm^2 Cable	103.36 m	88.30 m
Required Length of 16 mm^2 Cable	22.03 m	86.53 m
Required Length of 25 mm^2 Cable	99.06 m	59.14 m
Required Length of 35 mm^2 Cable	0.00 m	0.00 m
Required Length of 50 mm^2 Cable	0.00 m	0.00 m
Required Length of 70 mm^2 Cable	0.00 m	0.00 m
Required Length of 90 mm^2 Cable	0.00 m	0.00 m

Table 5.8: Oudtshoorn distribution network costs.

	Oudtshoorn Scenario-A (10m)	Oudtshoorn Scenario-B (8m)
Cable Material Cost [€]	4722.66	4807.41
Cost of Pillars [€]	1300	1200
Total Cost [€]	6022.66	6007.41

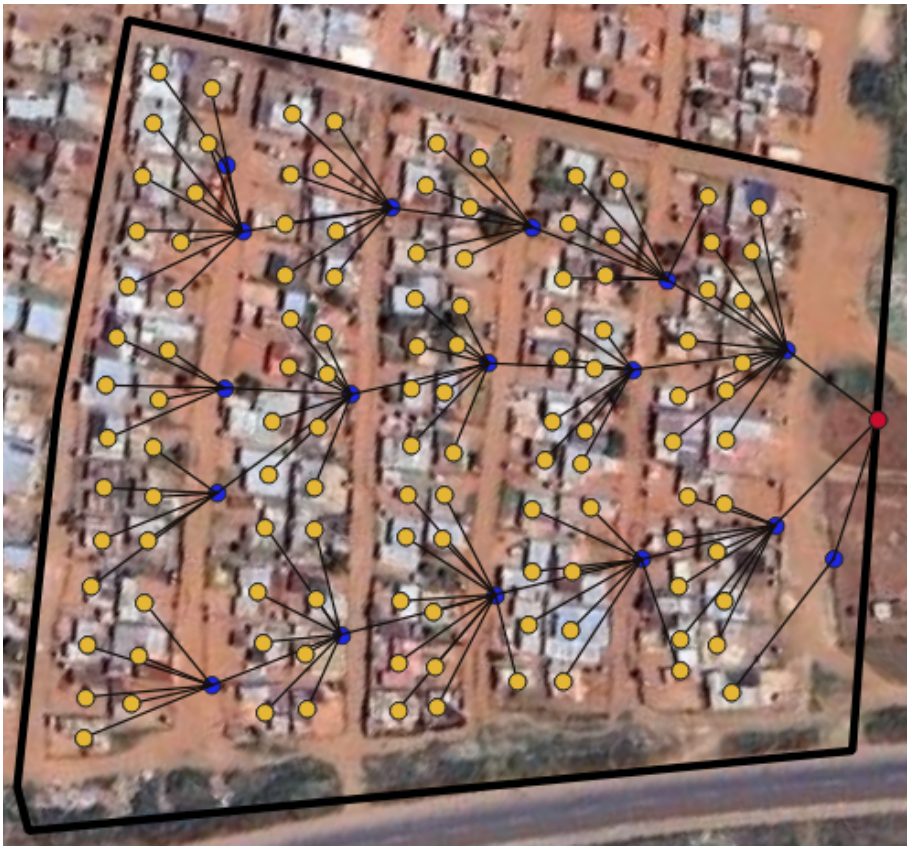

Figure 5.11: Generated distribution network for scenario-A of Daveyton site

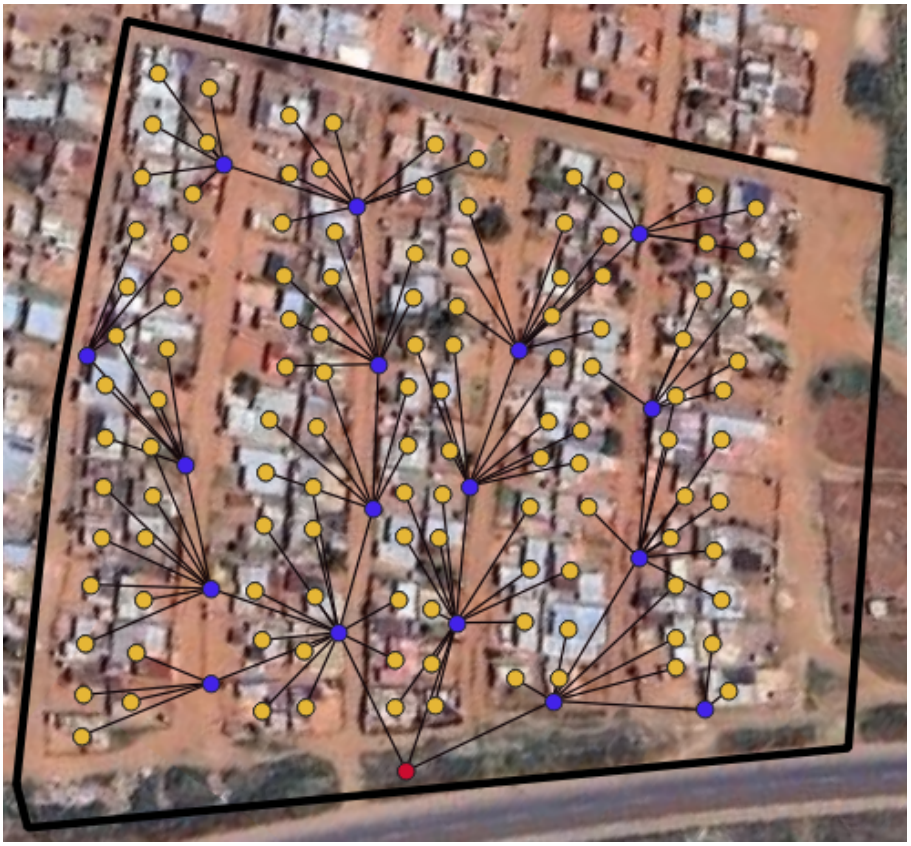

Figure 5.12: Generated distribution network for scenario-B of Daveyton site

Table 5.9: Daveyton distribution network structure.

	Daveyton Scenario-A (10m)	Daveyton Scenario-B
Number of of Pillars	17	17
Number of Edges	135	135
Number of Cables	155	143
Maximum Number of Households Connected to a Single Edge	77	59
Maximum Number of Households Connected to a Single Cable	19	19
Required Length of 2.5 mm^2 Cable	2248.95 m	2169.46 m
Required Length of 6 mm^2 Cable	0.00 m	59.28 m
Required Length of 10 mm^2 Cable	26.09 m	110.71 m
Required Length of 16 mm^2 Cable	53.39 m	24.98 m
Required Length of 25 mm^2 Cable	83.00 m	84.17 m
Required Length of 35 mm^2 Cable	56.14 m	46.8 m
Required Length of 50 mm^2 Cable	27.68 m	0.00 m
Required Length of 70 mm^2 Cable	84.46 m	139.38 m
Required Length of 90 mm^2 Cable	363.85 m	221.53 m

Table 5.10: Daveyton distribution network costs.

	Daveyton Scenario-A (10m)	Daveyton Scenario-B
Total Cable Length	2943.56 m	2856.31 m
Cost of Cables [€]	51209.59	40568.87
Cost of Pillars [€]	1700	1700
Total Cost [€]	52909.59	42268.87

5.3.4. Simulated Cable Losses of the Distribution Network

The cable losses of each distribution network scenario were simulated through the methodology discussed in Subsection 4.3.4. The resultant annual energy losses are presented in Table 5.11 and Table 5.12. Additionally, visuals from the cable loss calculation process for the Tier 5 Oudtshoorn Scenario-A distribution network, given as an example, are presented in Figure 5.13 and Figure 5.14, with Figure 5.15 showing the overall system cable loss.

Table 5.11: Annual energy loss due to cabling of the Oudtshoorn distribution network.

	Tier 3		Tier 5	
	Oudtshoorn Scenario-A	Oudtshoorn Scenario-B	Oudtshoorn Scenario-A	Oudtshoorn Scenario-B
Total Annual Loss	1249.2 Wh	1239.76 Wh	0.2 MWh	0.21 MWh
Total Anmual Loss Percentage [%]	0.03	0.03	0.44	0.47

Table 5.12: Annual energy loss due to cabling of the Daveyton distribution network

	Tier 3		Tier 5	
	Daveyton Scenario-A	Daveyton Scenario-B	Daveyton Scenario-A	Daveyton Scenario-B
Total Annual Loss	4390.96 Wh	4314.12 Wh	0.7 MWh	0.73 MWh
Total Anmual Loss Percentage [%]	0.01	0.01	0.18	0.18

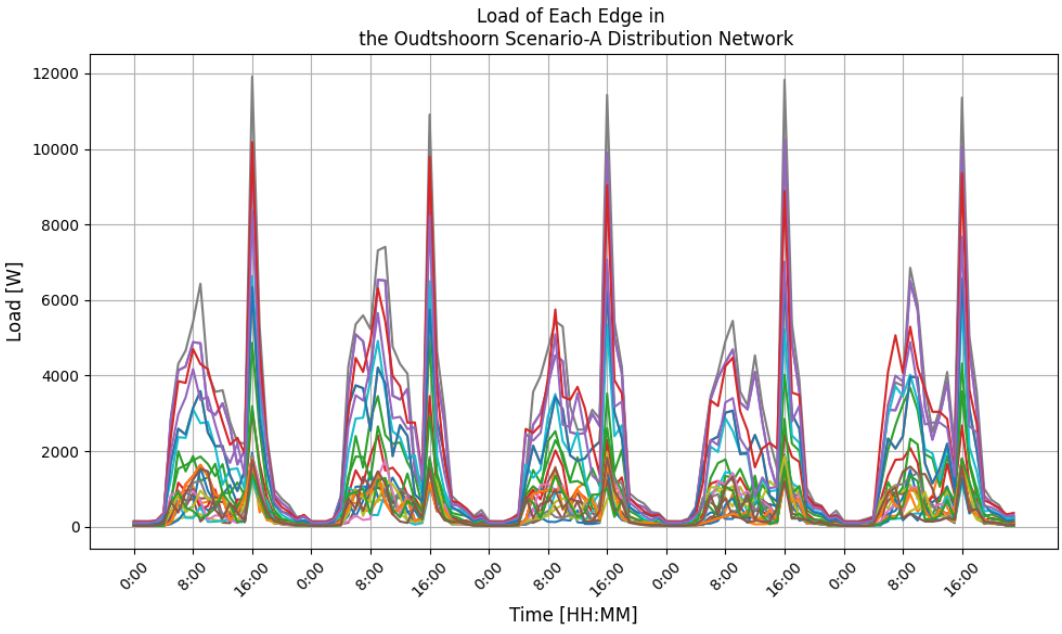

Figure 5.13: The Load of each edge of the Tier 5 Oudtshoorn Scenario-A distribution network.

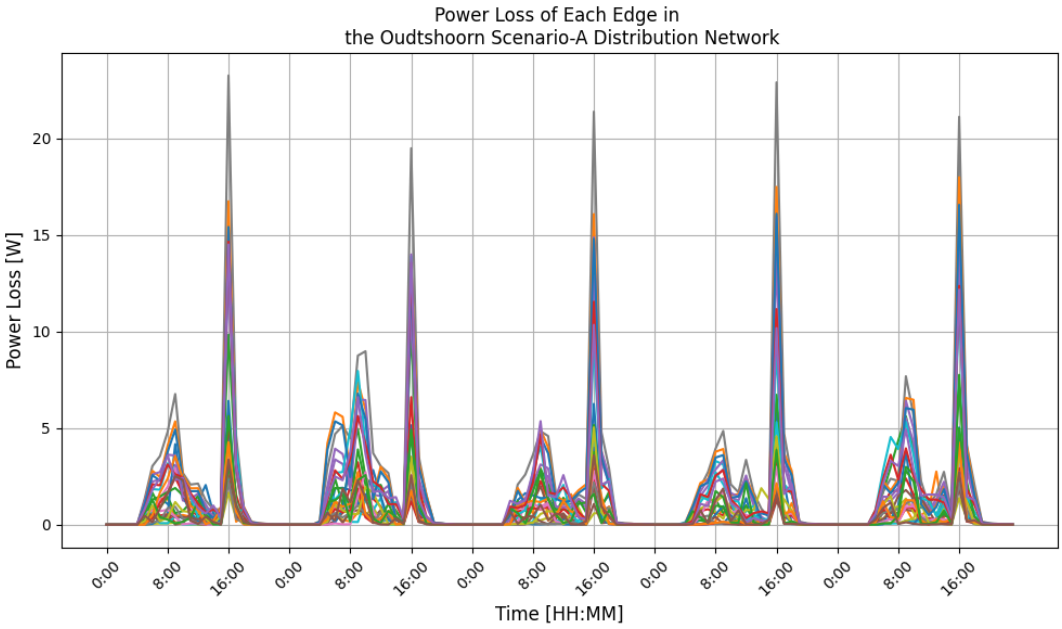

Figure 5.14: The cable losses of each each edge of the Tier 5 Oudtshoorn scenario-A distribution network.

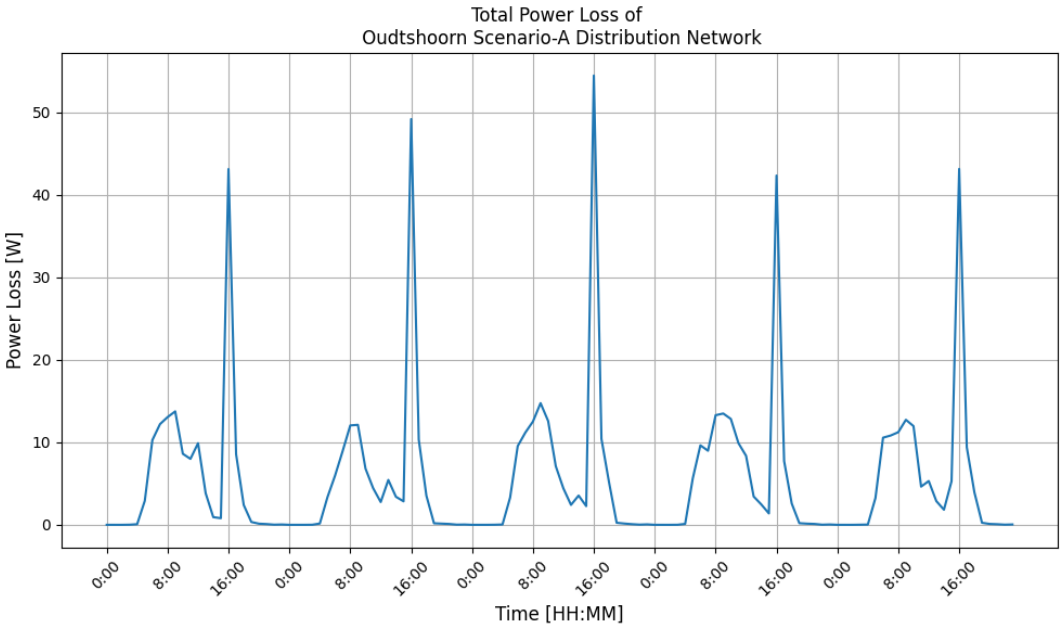

Figure 5.15: The total cable losses of the Tier 5 Oudtshoorn scenario-A distribution network.

It is observed that the resultant annual losses due to the distribution network cabling are kept at small values. Tier 5 distribution networks had annual energy losses of roughly 0.2 - 0.5%. Additionally, as expected, the annual energy losses for Tier 3 loads through distribution networks sized for Tier 5 load, resulted in extremely small losses.

5.4. System Sizing

This section details the PV and battery sizing, the simulated system behavior, and the overall material costs of the microgrid design.

5.4.1. PV & Battery Sizing

Given the PV power profile, load profile, and power loss profiles obtained throughout the previous design domains, the necessary power and storage capacities were solved for, via the methodology described in Section 4.4.

Table 5.13 and Table 5.14 presents the system component breakdown of the cost optimal system that achieves the desired LLP for the Tier 3 and Tier 5 systems for the Oudtshoorn site. For the Daveyton site, the corresponding breakdowns are shown in Table 5.15 and Table 5.16. Additionally, illustrative visuals depicting the changes in cost and LLP with varying PV and battery capacities for the scenario-B distribution network using Canadian Solar 550 W PV modules are provided for Tier 3 Oudtshoorn (Figure 5.16), Tier 5 Oudtshoorn (Figure 5.18), Tier 3 Daveyton (Figure 5.19), and Tier 5 Daveyton (Figure 5.17). Note only PV and Battery sizing scenarios that achieve a LLP < 5% are shown in the figures, and that a star symbol marks the cost optimal scenario. The total material cost of the cost-optimal design is bolted.

Table 5.13: Component breakdown of the cost optimal Tier 3 microgrid that is sized to achieve LLP <5% for the Oudtshoorn site

	Oudtshoorn Scenario-A					Oudtshoorn Scenario-B				
Power rating of PV Module [W]	Canadian Solar HiKu6 Mono PERC			EnerSol Mono PERC		Canadian Solar HiKu6 Mono PERC			EnerSol Mono PERC	
	405	550	455	420	555	405	550	455	420	555
Number of PV Strings	1	1	2	1	1	1	1	2	1	1
Number of 10kWh Battery Units	1	1	1	1	1	1	1	1	1	1
Number of Solar Converter	1	1	1	1	1	1	1	1	1	1
Number of Battery Converters	1	1	1	1	1	1	1	1	1	1
LPP [%]	4.78	4.88	3.25	4.93	4.9	4.78	4.88	3.25	4.93	4.9
Total Material Cost [k€]	5.23	**4.91**	5.96	5.05	5.28	5.23	**4.91**	5.96	5.05	5.28

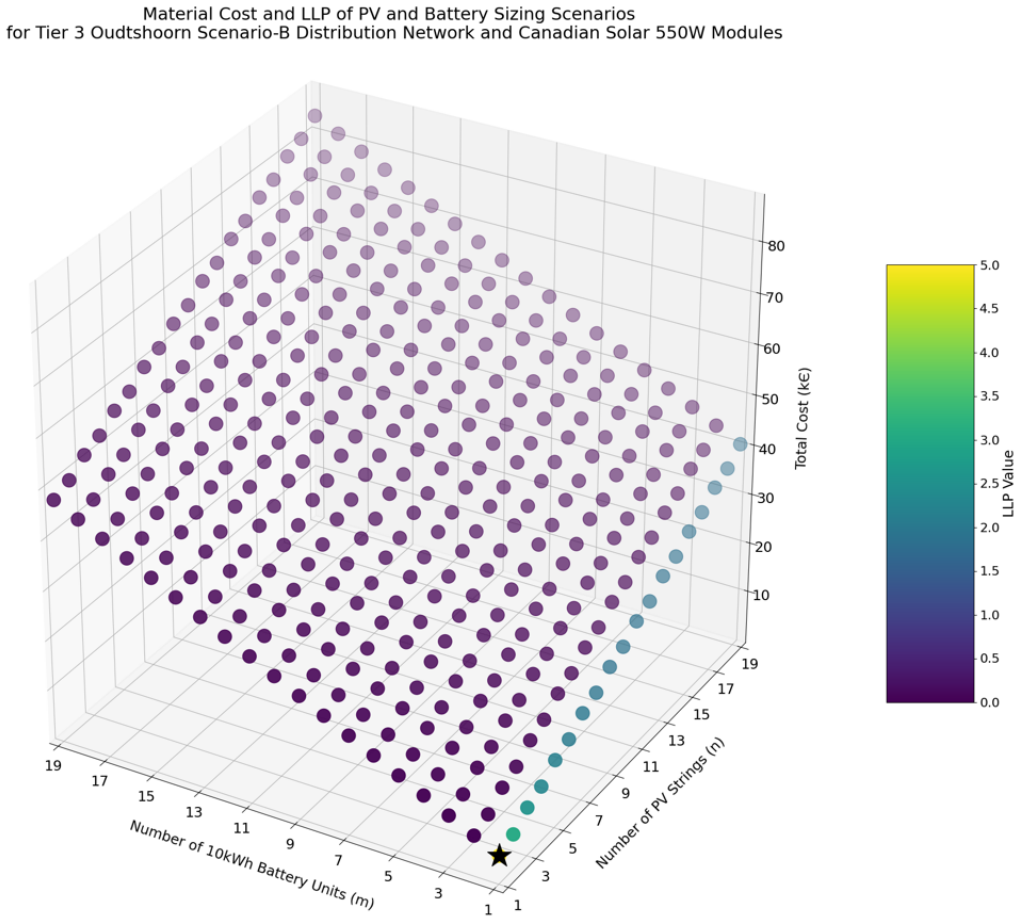

Figure 5.16: LLP and Cost as a result of PV and battery sizing for the Tier 3 Oudtshoorn Scenario B Distribution Network. Displayed is one of the the two cost optimal cases: Scenario-B and Canadian Solar 550 PV module strings.

Table 5.14: Component breakdown of the cost optimal Tier 5 microgrid that is sized to achieve LLP <5% for the Oudtshoorn site

	Oudtshoorn Scenario-A					Oudtshoorn Scenario-B				
Power rating of PV Module [W]	Canadian Solar HiKu6 Mono PERC			EnerSol Mono PERC		Canadian Solar HiKu6 Mono PERC			EnerSol Mono PERC	
	405	550	455	420	555	405	550	455	420	555
Number of PV Strings	4	5	5	6	5	4	5	5	6	5
Number of 10kWh Battery Units	9	8	9	8	8	9	8	9	8	8
Number of Solar Converter	2	3	3	3	3	2	3	3	3	3
Number of Battery Converters	9	8	9	8	8	9	8	9	8	8
LPP [%]	4.83	4.97	4.64	3.63	5	4.82	4.97	4.64	3.63	5
Total Material Cost [k€]	30.61	**29.48**	30.92	31.78	31.33	30.61	**29.48**	30.92	31.78	31.33

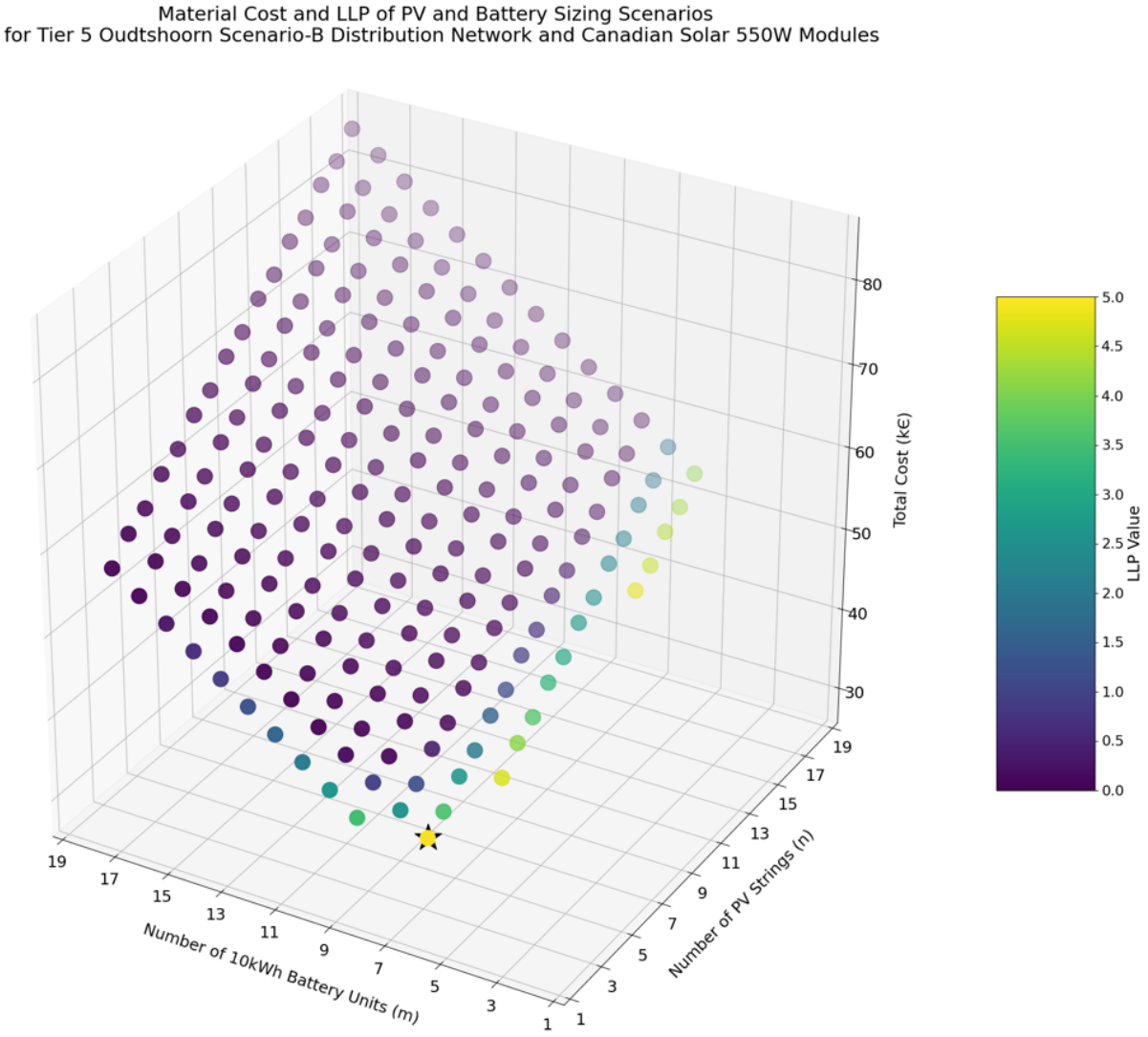

Figure 5.17: LLP and Cost as a result of PV and battery sizing for the Tier 3 Daveyton Scenario B Distribution Network. Displayed is one of the the two cost optimal cases: Scenario-B and Canadian Solar 550 PV module strings.

Table 5.15: Component breakdown of the cost optimal Tier 3 microgrid that is sized To achieve LLP <5% for the Daveyton site

	Oudtshoorn Scenario-A					Oudtshoorn Scenario-B				
Power rating of PV Module [W]	Canadian Solar HiKu6 Mono PERC			EnerSol Mono PERC		Canadian Solar HiKu6 Mono PERC			EnerSol Mono PERC	
	405	550	455	420	555	405	550	455	420	555
Number of PV Strings	4	4	6	4	4	4	4	6	4	4
Number of 10kWh Battery Units	11	11	10	11	11	11	11	10	11	11
Number of Solar Converter	21	22	25	21	22	22	22	26	22	22
Number of Battery Converters	75	74	76	76	74	73	74	75	74	74
LPP [%]	4.04	4.32	3.87	4.48	4.36	3.6	3.85	4.8	4.01	3.9
Total Material Cost[k€]	35.37	**34.09**	34.54	34.66	35.57	35.37	**34.09**	34.54	34.66	35.57

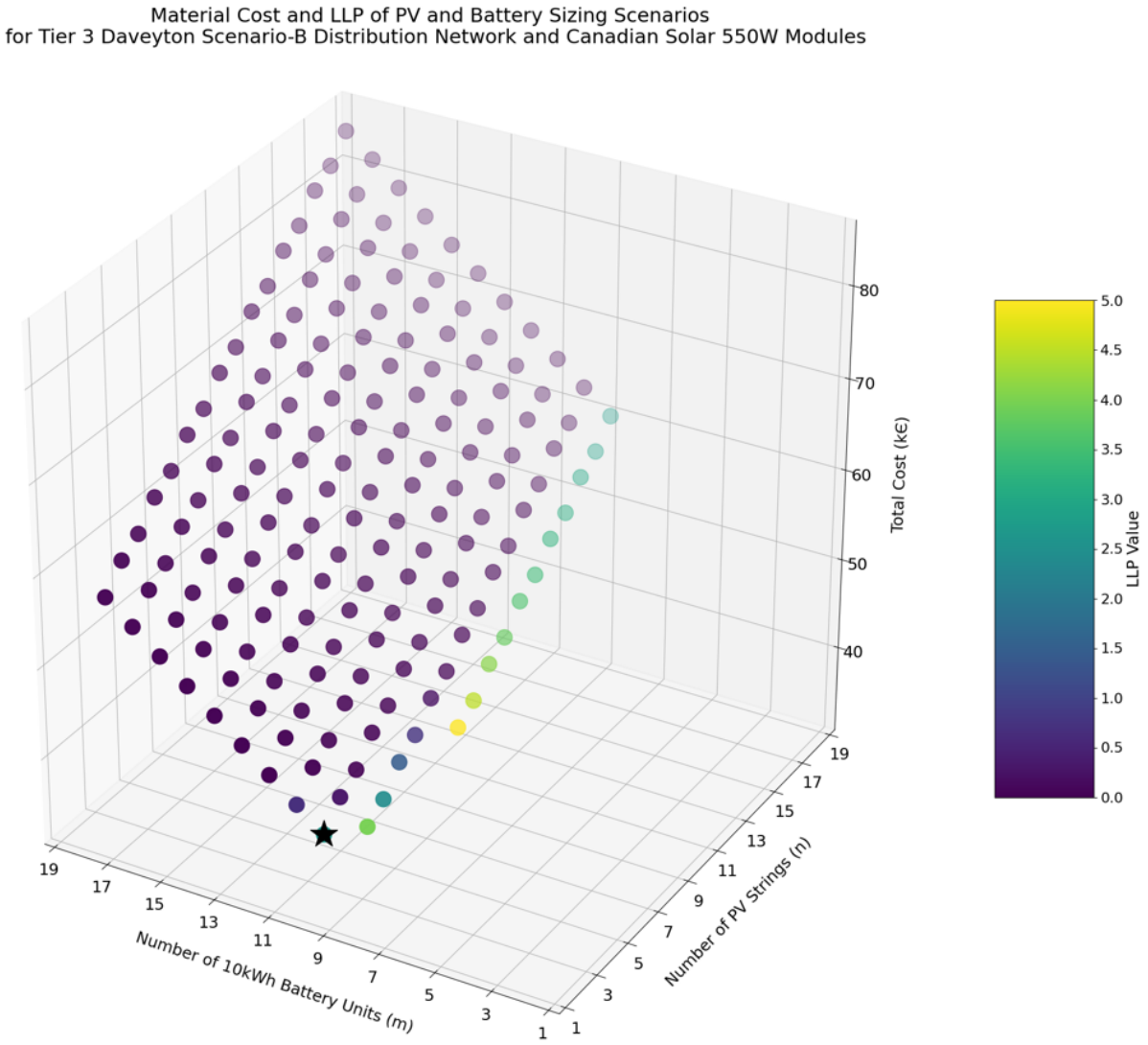

Figure 5.18: LLP and Cost as a result of PV and battery sizing for the Tier 3 Oudtshoorn Scenario B Distribution Network. Displayed is one of the the two cost optimal cases: Scenario-B and Canadian Solar 550 PV module strings.

Table 5.16: Component breakdown of the cost optimal Tier 5 microgrid that is sized To achieve LLP <5% for the Daveyton site

	Oudtshoorn Scenario-A					Oudtshoorn Scenario-B				
Power rating of PV Module [W]	Canadian Solar HiKu6 Mono PERC			EnerSol Mono PERC		Canadian Solar HiKu6 Mono PERC			EnerSol Mono PERC	
	405	550	455	420	555	405	550	455	420	555
Number of PV Strings	40	38	47	42	38	38	40	47	42	38
Number of 10kWh Battery Units	72	74	73	71	74	73	72	73	71	74
Number of Solar Converter	21	22	25	21	22	22	22	26	22	22
Number of Battery Converters	75	74	76	76	74	73	74	75	74	74
LPP [%]	4.80	4.95	4.98	4.98	4.99	4.97	4.98	4.94	4.94	4.94
Total Material Cost [k€]	263.3	251.3	258.4	258.1	265.3	261.6	**250.5**	258.4	258.1	265.3

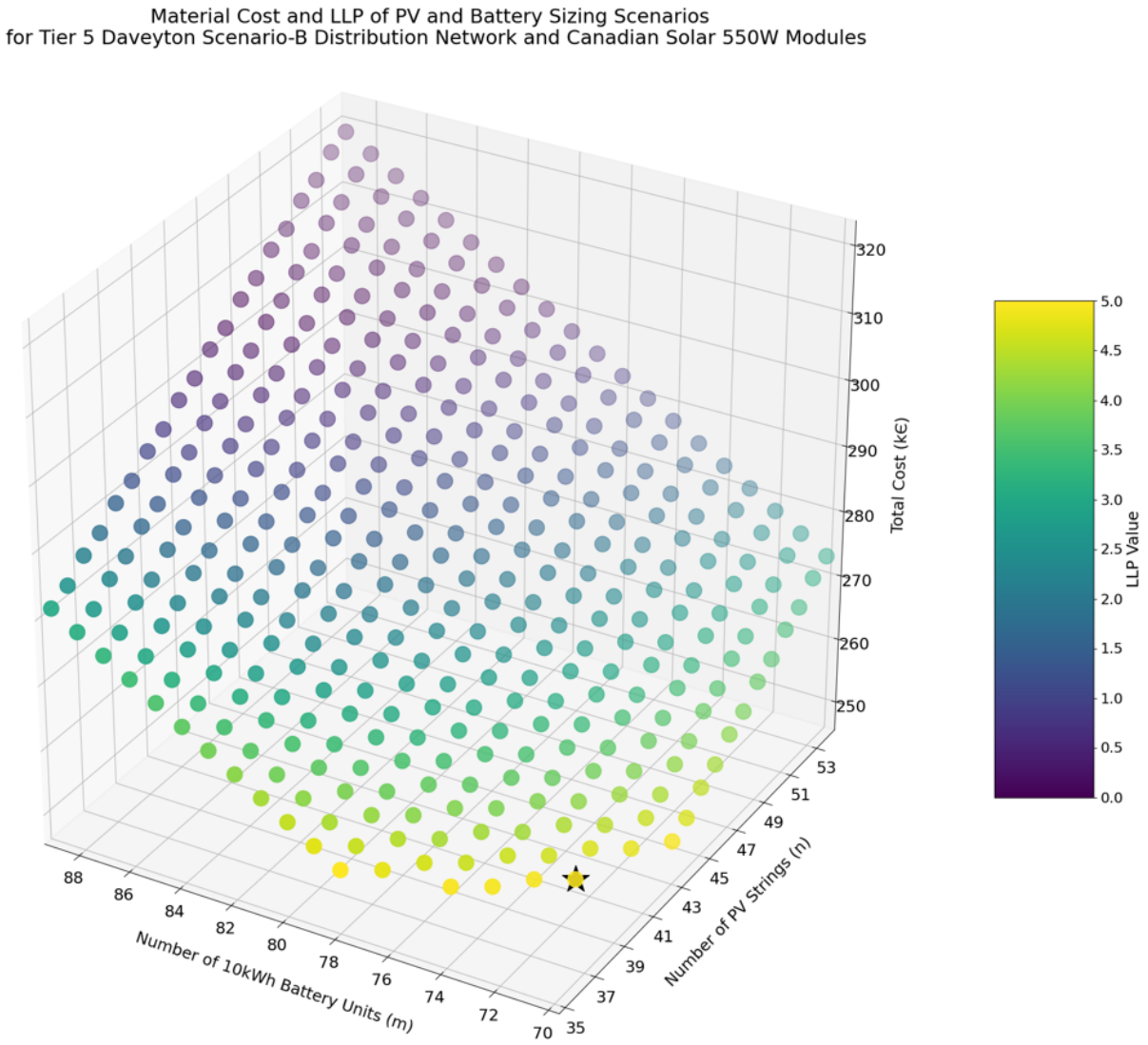

Figure 5.19: LLP and Cost as a result of PV and battery sizing for the Tier 3 Daveyton Scenario B Distribution Network. Displayed is one of the the two cost optimal cases: Scenario-B and Canadian Solar 550 PV module strings.

5.4.2. Simulated System Behaviour

An exemplary 5-day period showcasing the simulated system behavior and battery system SOC levels are presented for the Oudtshoorn and Daveyton sites. For the Oudtshoorn site with Scenario-

B distribution network using Canadian Solar 550W PV modules, the simulated system behavior and SOC levels for Tier 3 are shown in Figure 5.20 and Figure 5.21, respectively, while those for Tier 5 are depicted in Figure 5.22 and Figure 5.23, respectively. For the Daveyton site, also with Scenario-B distribution network using Canadian Solar 550W PV modules, the corresponding figures are Figure 5.24 and Figure 5.25 for Tier 3, and Figure 5.26 and Figure 5.27 for Tier 5, respectively.

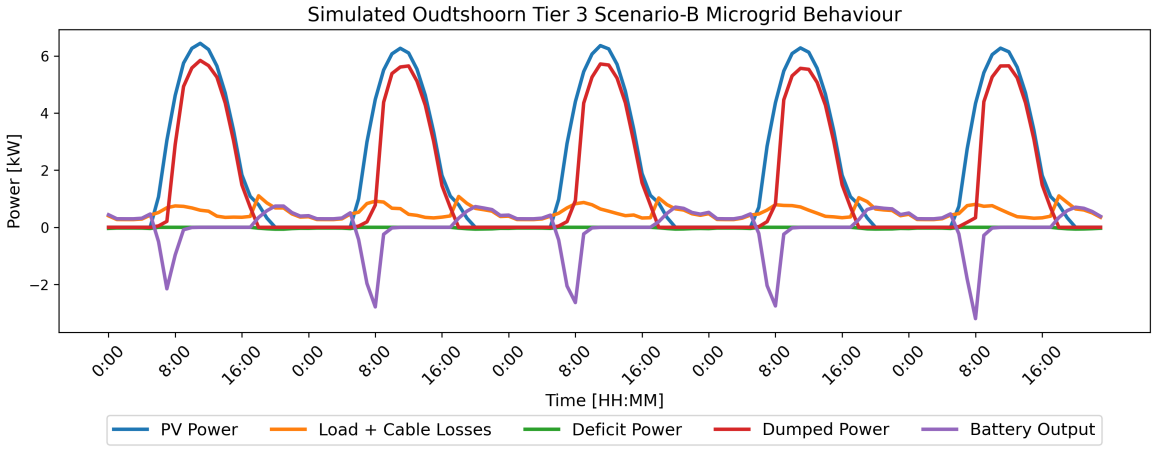

Figure 5.20: Simulated system behavior for the Tier 3 Oudtshoorn Scenario-B distribution network using Canadian Solar 550W PV modules.

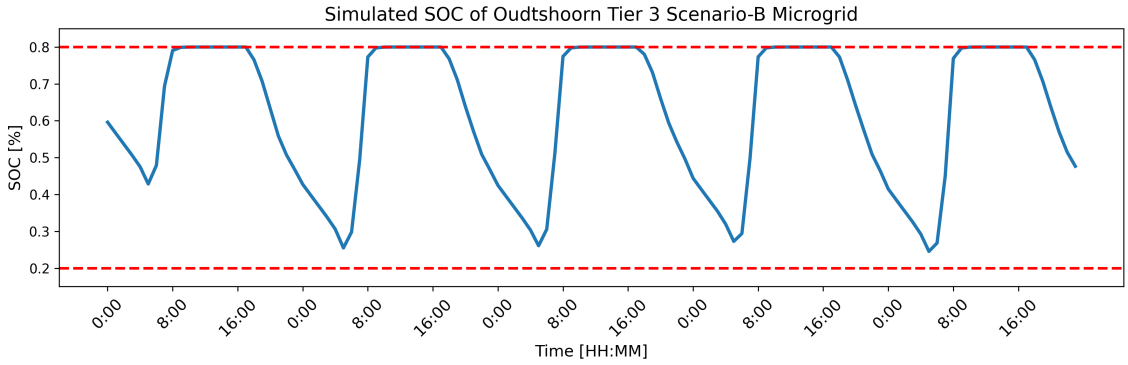

Figure 5.21: SOC levels for the Tier 3 Oudtshoorn Scenario-B distribution network using Canadian Solar 550W PV modules. The red dashed lines represent the 20% and 80% ideal operational limits.

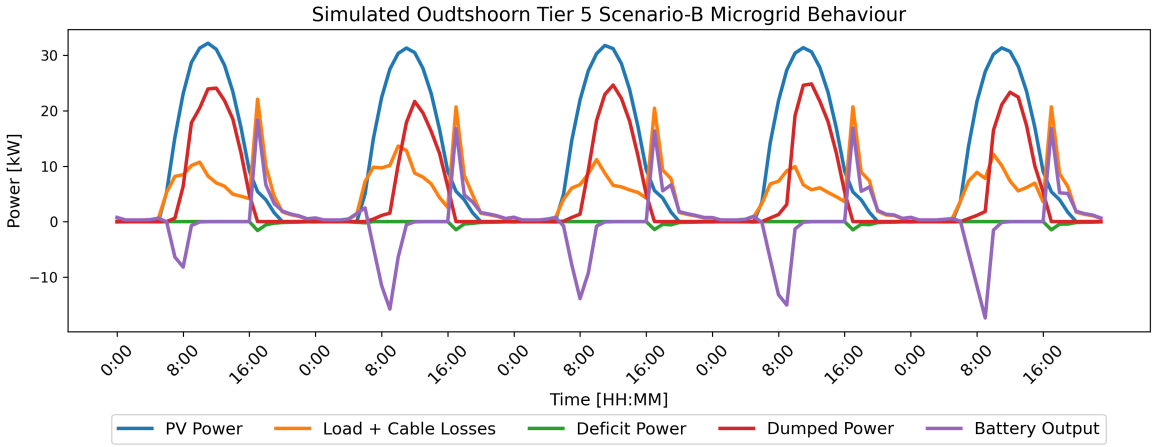

Figure 5.22: Simulated system behavior for the Tier 5 Oudtshoorn Scenario-B distribution network using Canadian Solar 550W PV modules.

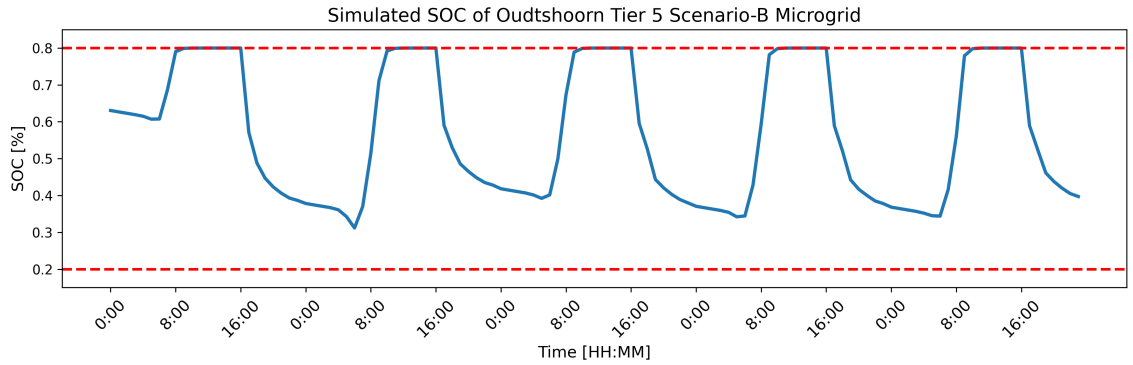

Figure 5.23: SOC levels for the Tier 5 Oudtshoorn Scenario-B distribution network using Canadian Solar 550W PV modules. The red dashed lines represent the 20% and 80% ideal operational limits.

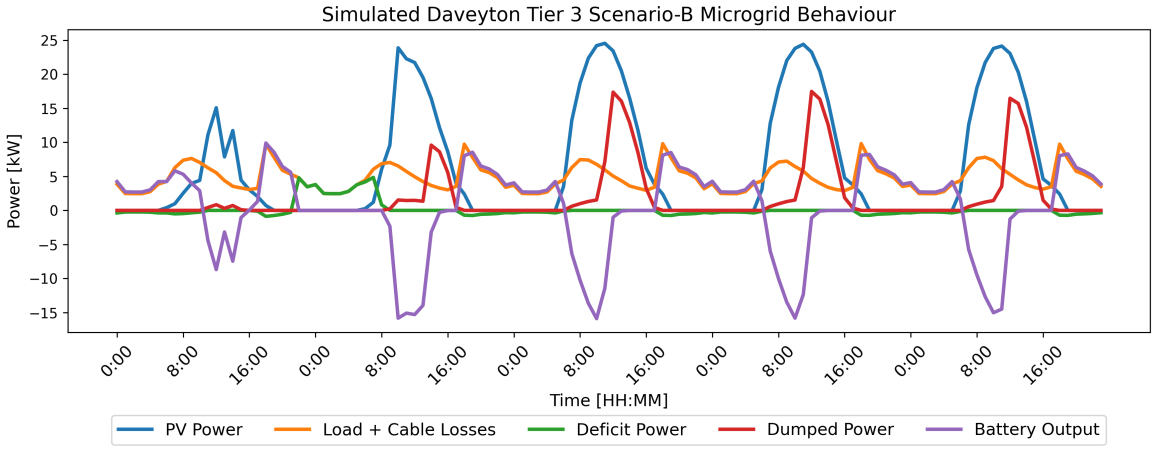

Figure 5.24: Simulated system behavior for the Tier 3 Daveyton Scenario-B distribution network using Canadian Solar 550W PV modules.

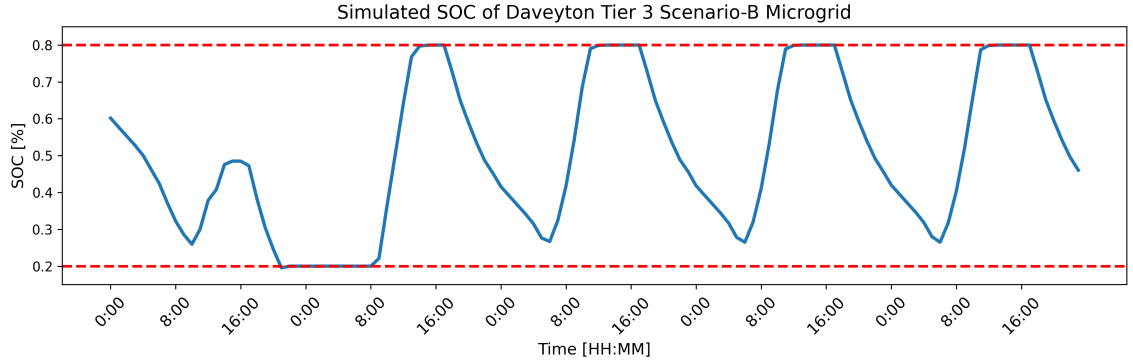

Figure 5.25: SOC levels for the Tier 3 Daveyton Scenario-B distribution network using Canadian Solar 550W PV modules. The red dashed lines represent the 20% and 80% ideal operational limits.

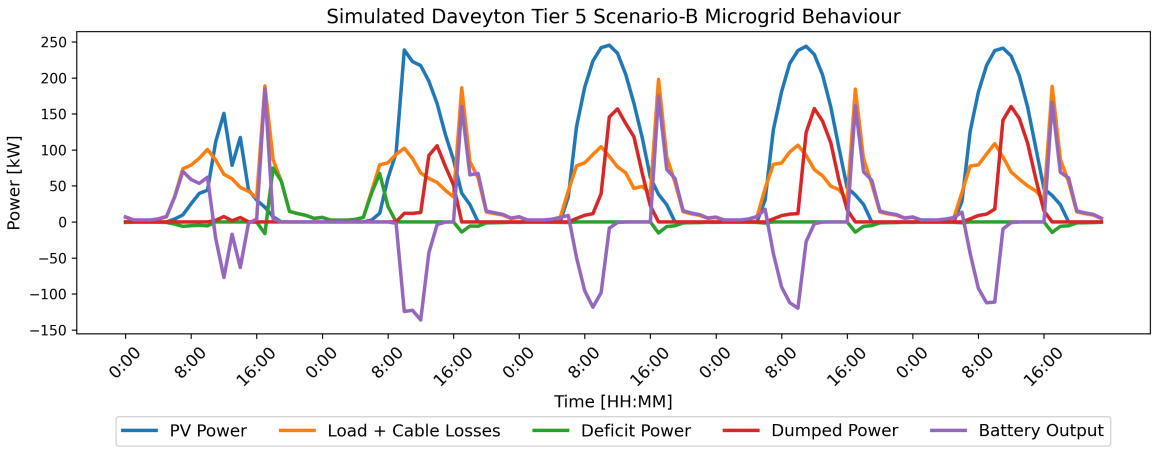

Figure 5.26: Simulated system behavior for the Tier 5 Daveyton Scenario-B distribution network using Canadian Solar 550W PV modules.

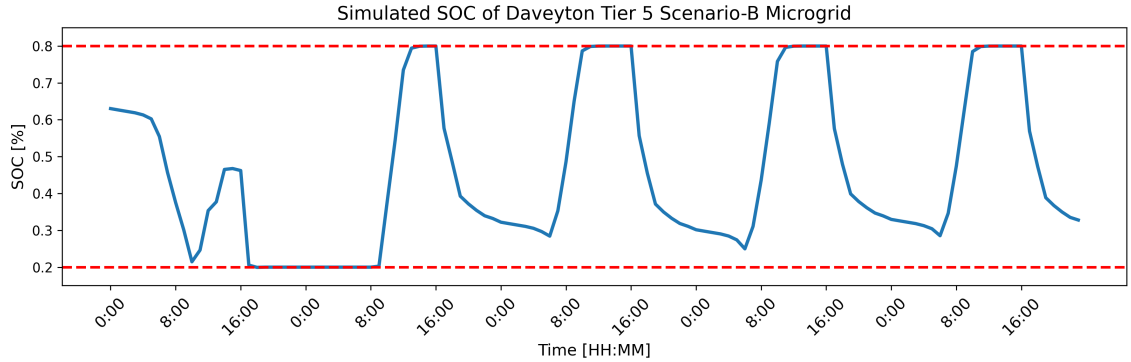

Figure 5.27: SOC levels for the Tier 5 Daveyton Scenario-B distribution network using Canadian Solar 550W PV modules. The red dashed lines represent the 20% and 80% ideal operational limits.

It is observed that the SOC levels are widely fluctuating within the ideal 20-80% operational range for all cases. It is also noticed that most days the SOC levels hit the upper 80% threshold, indicating that the battery systems gets full during peak solar production hours, resulting in excess energy being dumped. Table 5.17 presents the annual dumped energy, its percentage relative to the annual produced PV energy, and its percentage relative to the annual consumed energy, for the scenario-B distribution network using Canadian Solar 550W PV modules for both Oudtshoorn and Daveyton.

Table 5.17: Annual dumped energy for the cost-optimal system designs.

	Oudtshoorn Scenario-B with CS 550W modules		Daveyton Scenario-B with CS 550W modules	
	Tier 3	Tier 5	Tier 3	Tier 5
Annual Dumped Energy	9.88 MWh	28.49 MWh	15.56 MWh	176.08 MWh
Annual Dumped Energy as a Percentage of Annual Produced PV Energy	69.16%	39.88%	27.51%	31.12%
Annual Dumped Energy as a Percentage of Annual Consumed Energy	213.11%	63.24%	36.97%	42.87%

5.4.3. Overall Microgrid Material Costs

The overall material cost of the PV, battery and distribution network are summed and compared to identify the cost optimal Tier 3 and 5 microgrid designs for both sites. Figure 5.28 and Figure 5.29 present the material cost breakdown of all the considered design options for the Tier 3 and 5 microgrid for Oudtshoorn, respectively. The total costs are indicated at the top of each bar graph, with the cost optimal value highlighted in red. Both cost optimal options for Tier 3 and 5 were of the scenario-B distribution network, with the PV module selection of Canadian Solar 550 W modules.

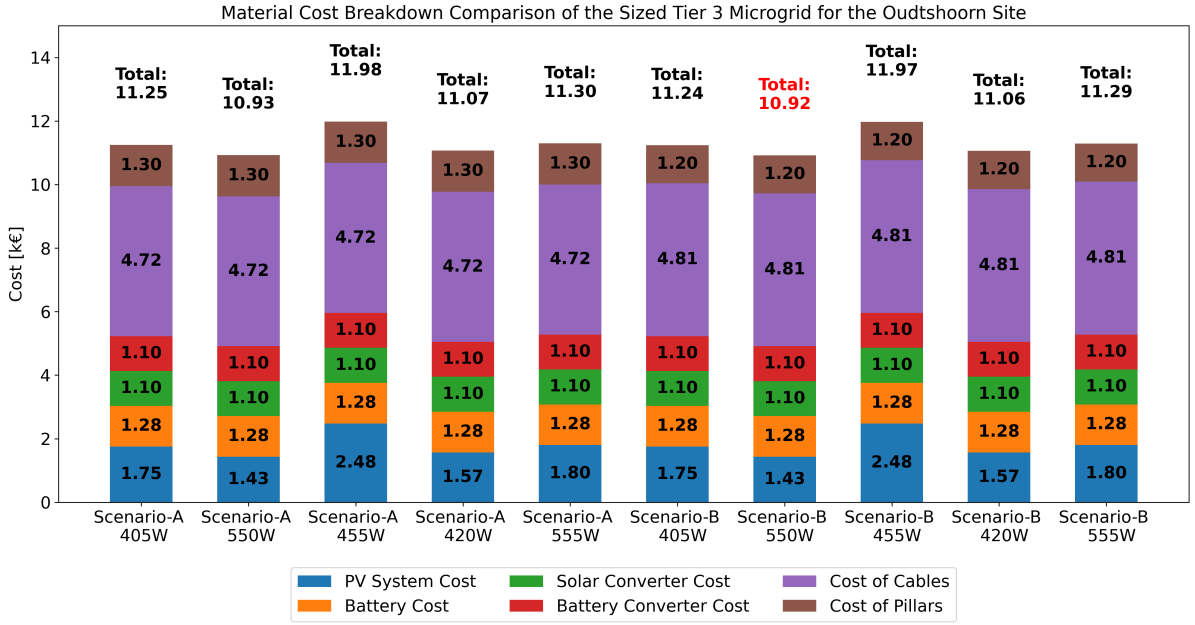

Figure 5.28: Material Cost Breakdown of the Tier 3 Oudtshoorn Microgrid Design Options

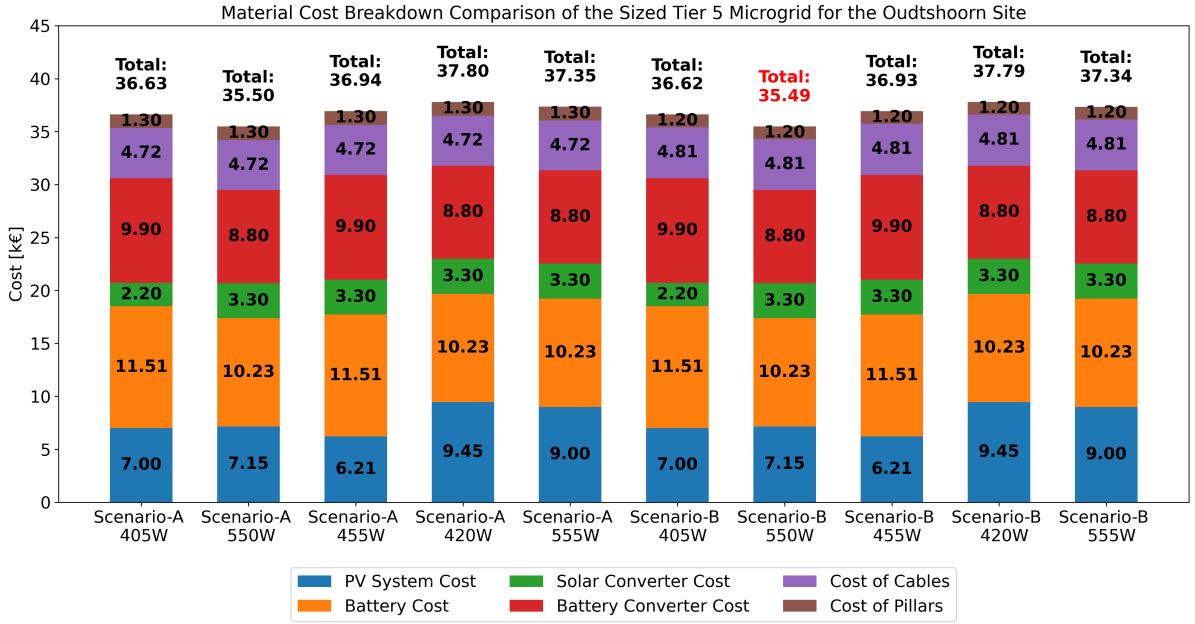

Figure 5.29: Material Cost Breakdown of the Tier 5 Oudtshoorn Microgrid Design Options

Figure 5.30 and Figure 5.31 now presents the material cost breakdown of all the considered design options for the Tier 3 and 5 microgrid for Daveyton, respectively. The scenario-B distribution network with the Canadian Solar 550W modules resulted as the cost optimal option for both tier microgrid designs.

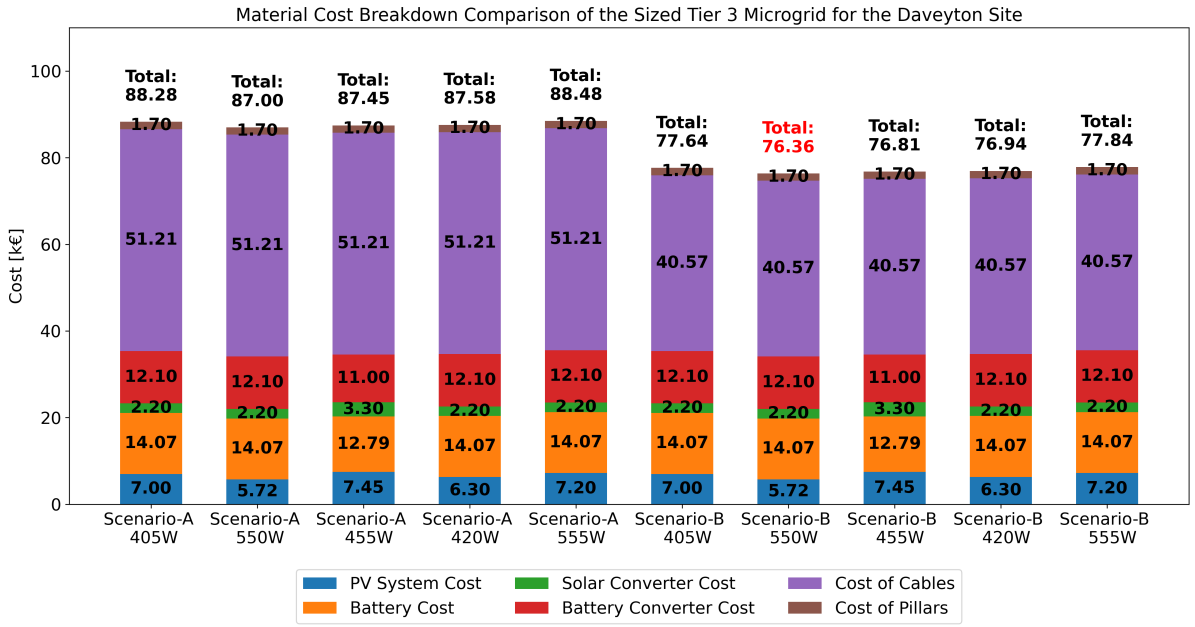

Figure 5.30: Material Cost Breakdown of the Tier 3 Daveyton Microgrid Design Options

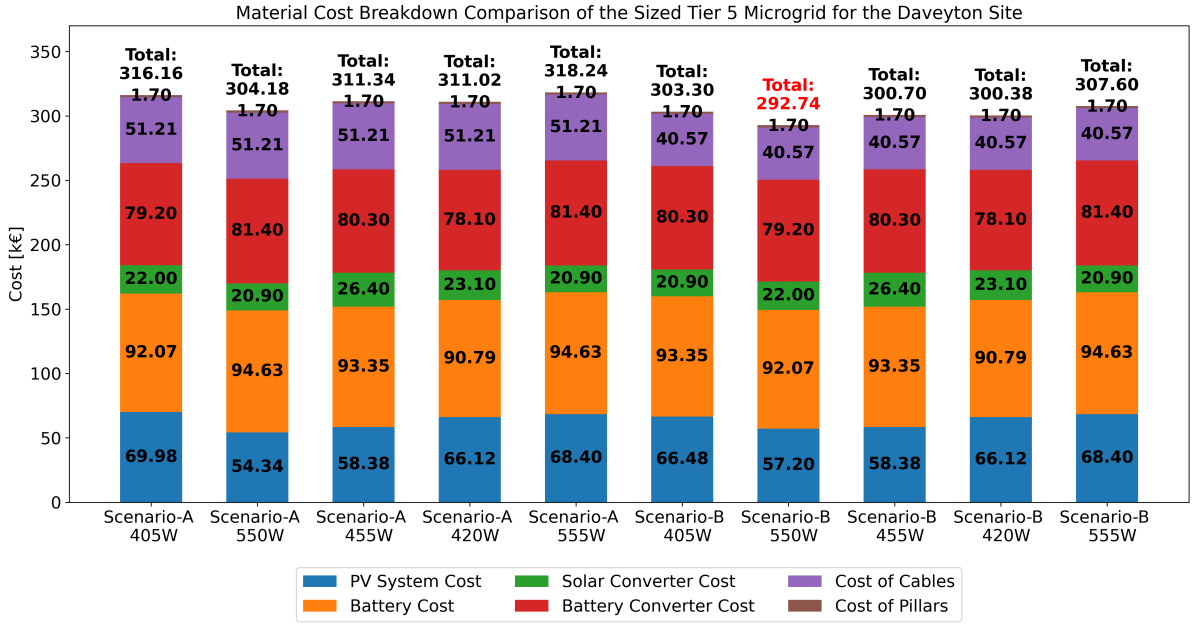

Figure 5.31: Material Cost Breakdown of the Tier 5 Daveyton Microgrid Design Options

5.4.4. Levelized Cost of Energy

Lastly, the Levelized Cost of Energy (LCOE) calculation assesses the benefits of starting with a distribution network sized for Tier 5, compared to beginning with a Tier 3 network and upgrading to a Tier 5 network when increasing PV and battery capacity as the community advances through the tiers. Table 5.18 and Table 5.19 show the cable sizing and cable cost difference between a distribution network sized for Tier 3 and Tier 5 load levels for the Oudtshoorn and Daveyton sites, respectively.

Table 5.18: Comparison of Cable Sizing for Oudtshoorn Scenario-B Distribution Network Sized for Tier 3 and Tier 5 Load Levels.

	Distribution Network Sized for Tier 3	Distribution Network Sized for Tier 5
Total Cable Cost	1.60 k€	4.81 k€
Total Cable Length	605.31 m	605.31 m
Required Length of 2.5 mm^2 Cable	605.31 m	341.63 m
Required Length of 6 mm^2 Cable	0.00 m	29.71 m
Required Length of 10 mm^2 Cable	0.00 m	88.30 m
Required Length of 16 mm^2 Cable	0.00 m	86.53 m
Required Length of 25 mm^2 Cable	0.00 m	59.14 m
Required Length of 35 mm^2 Cable	0.00 m	0.00 m
Required Length of 50 mm^2 Cable	0.00 m	0.00 m
Required Length of 70 mm^2 Cable	0.00 m	0.00 m
Required Length of 90 mm^2 Cable	0.00 m	0.00 m

Table 5.19: Comparison of Cable Sizing for Daveyton Scenario-B Distribution Network Sized for Tier 3 and Tier 5 Load Levels.

	Distribution Network Sized for Tier 3	Distribution Network Sized for Tier 5
Total Cable Cost	7.36 k€	40.57 k€
Total Cable Length	2634.7 m	2856.3 m
Required Length of 2.5 mm^2 Cable	2554.16 m	2169.46 m
Required Length of 6 mm^2 Cable	50.69 m	59.28 m
Required Length of 10 mm^2 Cable	29.93 m	110.71 m
Required Length of 16 mm^2 Cable	53.39 m	24.98 m
Required Length of 25 mm^2 Cable	83.00 m	84.17 m
Required Length of 35 mm^2 Cable	56.14 m	46.80 m
Required Length of 50 mm^2 Cable	27.68 m	0.00 m
Required Length of 70 mm^2 Cable	84.46 m	139.38 m
Required Length of 90 mm^2 Cable	363.85 m	221.53 m

For the LCOE analysis, it is assumed that the initial investment for the Tier 3 microgrid occurs at year 0, and the secondary investment for upgrading to the Tier 5 microgrid takes place at year 10, with operations continuing until year 25. Although in reality, scaling up to a fully Tier 5 microgrid for the entire community may not occur all at once, this assumption serves as a reference for the calculation.Table 5.20 shows the initial investment at year 0 (I_0), the investment at year 10 (I_{10}), annual energy delivered between years 1 to year 10 (E_{0-10}), and annual energy delivered between years 11 to year 25 (E_{11-25}). Analysis revealed that a discount rate (r) of less than 2% results in a lower LCOE for starting with a Tier 5 distribution network design, compared to switching from a Tier 3 to a Tier 5 design. This finding is illustrated by the LCOE values shown in the last row of Table 5.20, where r is set at 2%. Conversely, a higher discount rate would favor the alternative approach. It is crucial to note, however, that this calculation solely considers material costs. If the secondary cable installation costs, incurred only in year 10 when switching from a Tier 3 to a Tier 5 network, were included, the LCOE for this approach would increase. This would make starting with the Tier 5 distribution network design the more cost-effective option for even higher r values.

$$\text{LCOE} = \frac{I_0 + \frac{I_{10}}{(1+r)^{10}}}{\sum_{t=1}^{10} \frac{E_{0-10}}{(1+r)^t} + \sum_{t=11}^{25} \frac{E_{11-25}}{(1+r)^t}} \tag{5.1}$$

Table 5.20: Investment and energy delivery scenarios. Note that only material costs are included.

	Oudtshoorn Scenario-B with CS 550W modules		Daveyton Scenario-B with CS 550W modules	
	Tier 3	Tier 5	Tier 3	Tier 5
Material Cost of Initial Distribution Network	2.80 k€	6.01 k€	9.06 k€	42.27 k€
Material Cost of Initial PV, Batteries and Converters	4.91 k€	4.91 k€	34.09 k€	34.09 k€
Initial Investment Cost	**7.71 k€**	**10.92 k€**	**43.15 k€**	**76.36 k€**
Annual Energy Delivered by T3 Microgrid	4.41 MWh		39.99 MWh	
Material Cost of Secondary Distribution Network	4.81 k€	0.00 k€	40.57 k€	0.00 k€
Material Cost of Secondary PV, Batteries and Converters	24.57 k€	24.57 k€	216.38 k€	216.38 k€
Secondary Investment Cost	**29.38 k€**	**34.57 k€**	**256.95 k€**	**216.38 k€**
Annual Energy Delivered by T5 Microgrid	42.80 MWh		390.16 MWh	
LCOE	**69.00 €/MWh**	**67.40 €/MWh**	**60.44 €/MWh**	**60.43 €/MWh**

6

Discussion

In this chapter, the results from Chapter 5 are further analysed. Reflection on the methodology and the implications of the findings on the project's objectives are discussed.

6.1. Forecasted Demand

As mentioned in Section 5.1, the load profiles for both sites and both tier levels exhibited a wide morning peak and a narrow evening peak. This pattern aligns with typical consumer behavior, where electricity usage is concentrated in the mornings and evenings, with a dip during midday when residents are often away for school, work, or errands. However, it was observed that the evening peak values are significantly higher than the morning peak values for the Tier 5 load profiles compared to Tier 3. This can be attributed to the increase in the number and variety of appliances (e.g., kettles and laptops newly introduced in Tier 5) and the higher number of existing appliances (e.g., more phone chargers and fans in Tier 5) used during the evenings. It is uncertain if the Tier 5 evening peak levels in reality will be as high as the simulation results of this study, due to the lack of local consumption data and the uncertain effect of scaling electricity access has on the consumption behavior of the targeted sites. However, the peak loads determine the sizing of the distribution network cables and also impact the sizing of PV and battery capacities. Validating these evening peak load values would enhance the reliability of the cable, PV and battery sizing of this study. Thus, it is recommended to do so via surveys and interviews to account for the consumption behaviour of the targeted communities into the model to enhance the accuracy of not only the load simulation, but of the overall microgrid design.

Additionally, the Oudtshoorn site shows more variance in daily profiles, while the daily profiles for the Daveyton site are more consistent. This difference is likely due to the size of the communities. In the smaller Oudtshoorn community, variations in household-level daily load profiles have a greater impact on the shape of the aggregated load profile compared to the larger Daveyton site. This implies that systems for a larger sized community is sized for more stable consumption patterns, while systems for smaller sized communities are more susceptible to consumption behaviour variations.

6.2. PV String Power Production

The high POA global irradiation at both sites reaffirms the potential for utilizing South Africa's abundant solar resources for this project.

Additionally, the results from current curtailment due to DCO's solar converter showed that the Oudtshoorn site experienced slightly greater losses compared to the Daveyton site. This is due to the higher ambient temperatures in Oudtshoorn, which increase the current levels of the PV strings more than in the slightly cooler Daveyton site. However, it was also revealed that this current curtailment had only little impact on the overall annual power production, even for the PV modules that have rated currents exceeding the maximum operational current of the solar converter. This highlights that PV modules operate below their I_{mpp} for the majority of the year. Consequently, there may be a reduced need to select larger solar converters with maximum operational currents greater than the I_{mpp} of the PV strings, potentially leading to cost savings.

For both sites, the cost-optimal microgrid design utilized the Canadian Solar 550W modules, as they offered the lowest cost per rated string capacity. Interestingly, these modules also experienced the greatest impact of curtailment. Although the losses due to curtailment were low, it may still be

worth exploring a solar converter with a slightly higher maximum operational current, to further mitigate losses and enhance the PV power production, especially when coupled with installation sites with higher temperatures and PV modules with higher rated currents.

Lastly, the limitations of the simulation methodology for the PV string power production are acknowledged. Firstly, the use of TMY meteorological data introduce inaccuracies, as this data represents average weather conditions rather than the specific variations that may occur in any given year. This can lead to discrepancies between simulated and actual PV performance. Additionally, the use of the less accurate Sandia King transposition model in this study, due to the lack of the meteorological data required by more commonly used and accurate models, may have slightly impacted the accuracy and validity of the simulated power production of the PV strings. Despite these limitations, the simulated PV string power remains a valuable and necessary reference for determining the required system size to meet the load, given the available resources.

6.3. Distribution Network

It was anticipated that for the Oudtshoorn site, scenario-B, with a denser grid of potential pillar points, would result in a more optimal layout than Scenario-A. Though it did reduced the number of nodes, reducing the grid spacing from 10 m to 8 m was found to be insignificant, as it still resulted in non-direct cable routes. This issue arises from the insufficient number of potential pillar points. To resolve this, a significant reduction in spacing to values between 0.5 and 1 m might be necessary. However, such a reduction would generate larger datasets, leading to increased computational times, which is not feasible with the current methodology that required roughly 2 days for the 8 and 10 m spaced pillar point grids. Further investigation into alternative methods to address the computation time versus data size conflict is needed, as detailed in Section 7.3.

For the Daveyton site, a large difference between the two distribution network scenarios, regarding the number of households connected to a single edge, was observed. Figure 6.1 highlights the heavy load carrying cables coming out of the central container with dashed pink lines. Figure 6.1a shows two heavy load carrying cables for scenario-A, and Figure 6.1b shows three. The edge carrying the most loads are identified by the green arrow. The most load carrying edge of scenario-A carried 77 loads, while that of scenario-B only carried 59, as presented in Table 5.9. This significant difference in centralization of the cable routs caused the most load carrying edge of scenario-A to consist of more and larger sized cables.

(a) Daveyton Scenario-A Distribution Network

(b) Daveyton Scenario-B Distribution Network

Figure 6.1: Comparison of the Daveyton distribution network scenarios, with heavy load-carrying edges highlighted in pink dashed lines. The green arrows indicate the edges carrying the highest load. The dedicated cable route for a single household is shown with red dashed lines, with the red square representing the dedicated pillar for this household and the light blue square indicating the neighboring pillar.

Additionally, it was also identified that the produced distribution network layouts do not follow along the roads. The industry prefers cable routes along roads rather than over households due to the ease of installation. An attempt was made to enforce this preference, via introducing an additional cost to cable routs that cross over households. However, the cutoff value of the pathfinding algorithm, which was minimized in this study to improve computational time, did not allow paths requiring additional node

connections to avoid over-household cabling, to be considered in the ILP optimization. This leads back to the computation time versus data size conflict mentioned above.

Furthermore, the Daveyton scenario-A distribution network includes a dedicated pillar point and cable route for a single household, which is not ideal for cost optimization. This dedicated node is outlined in a red square, and the dedicated cable route is shown in dashed red lines in Figure 6.1a. The maximum cable length threshold set in this study prevented the option of connecting the household via the neighboring pillar point outlined by the light blue square. Introducing another pillar point option within the cable length threshold of all connecting nodes of the two pillar points outlined in squares would allow the household currently necessitating the dedicated cable route to share the same pillar point as its neighboring households. Thus, increasing the number of possible pillar points would prevent such incidents of non-ideal dedicated cable routes for a single households to be selected, however, this circles back to the trade-off between computational time and data size.

To summarize, the computational complexity of the methodology used in this study has imposed limitations on the distribution network designs. The designs produced by the current methodology are thus suboptimal due to limiting computational complexity via reduced pillar points and restricting cutoff values for pathfinding. Thus, as detailed in Section 7.3, adaptation to computationally less complex alternative methodologies is worth investigating. Alternatively, incorporating an additional step to refine the designed distribution network layout through engineering intuition could increase the cost optimality of the given layouts.

6.4. PV, Battery & Cable Sizing

It was observed that the LLP decrease is more pronounced with the addition of battery units, then the number of PV strings. This suggests that batteries, which address the mismatch between generated PV power and load, play a crucial and influential role in achieving an LLP of less than 5%.

In terms of PV and battery sizing, only a few cases showed differences between the two distribution network scenarios for both sites. This indicates that variations in cable losses between the two scenarios did not significantly impact PV and battery sizing, as the losses were of similar levels. However, this might not always be the case. For the case of Oudtshoorn site, if a finer possible pillar point grid is used and the optimal network layout resulted in both significantly reduced pillars and cable length, the cable losses are expected to also be reduced, impacting the PV and battery sizing. For the Daveyton site, the location of the container did not significantly impact cable losses for the two considered scenarios. However, in a non-symmetrical area, variations in container location could affect cable losses and, consequently, PV and battery sizing.

The observed annual dumped energy mentioned in Subsection 5.4.2 are of significance. The PV system is intentionally oversized to ensure reliability on days with lower solar production, thereby maintaining a low LLP. This design choice represents a trade-off between reliability and cost. By increasing the LLP threshold, the need for oversized PV systems can be reduced, which would lower both the annual dumped energy and the overall material costs. Conversely, increasing the battery capacity would reduce the annual dumped energy and further decrease the LLP, but this comes with the trade-off of increased costs. Additionally, for the Tier 3 Oudtshoorn case, the extremely high percentage of annual dumped energy relative to the annual consumed energy indicates that the single PV string is oversized for the consumption needs. Therefore, it may be beneficial to explore reducing the PV string size for this particular case to better align with actual energy consumption needs.

Moreover, the sized systems, particularly for Tier 5, are substantial in scale. Initially, the plan was to store all batteries and converters in a single storage container and install PV modules only on the roof of this central container. However, this approach is not feasible given the number of components required. Instead, multiple containers will be needed, and the PV system installation will have to utilize available space within the community, either on open land or on mounting structures.

6.5. System Cost

An interesting finding was that the cable cost of the distribution network of scenario-A was smaller than scenario-B for the Oudtshoorn site. It was anticipated that scenario-B, with a finer grid of possible pillar points, would lead to a more optimal layout, as discussed in Section 6.3, resulting in reduced costs for both pillars and cables. However, although Scenario-B reduced the number of nodes and thus node costs, Scenario-A required slightly less cable length, leading to lower cable costs. As explained in Section 6.3, it is anticipated that a much finer grid of potential pillar points would allow for the selection of a network with both reduced pillars and total required cable length, and that the small reduction in grid

spacing from 10m to 8m was not significant enough to showcase this.

For Daveyton, the scneario-B distribution network resulted in roughly 20% reduction in cable cost. This is attributed to the discussion from Section 6.3, in that the heavy centralization of the cable routes in Scenario-A necessitated multiple and large-sized cables, leading to an increased cost.

It is also observed that the distribution network costs (i.e., cable and pillar costs), designed for Tier 5 loads, occupy roughly half of the Tier 3 microgrid costs. While this initially increases the investment required, opting for a Tier 5 distribution network from the start can ultimately reduce the overall system cost by eliminating the need for a separate Tier 3 network, depending on the discount rate. Furthermore, as discussed in Subsection 5.4.4, when accounting for cable instillation fees (i.e., cost of installation personnel), in addition to material costs, the difference in LCOE between the two scenarios is likely to be even more pronounced. However, the discount rate and the timing of transitioning from Tier 3 to Tier 5 have a significant impact on this calculation. Since the rate of scaling up and the timing of this transition are hard to predict—being influenced by economic growth and increased electricity access within the community—further detailed analysis is recommended. This analysis should also consider installation costs and the cost of containers that were not accounted for in this study. Such an approach would refine LCOE calculations and better inform decisions on energy bundle offerings.

Additionally, the risks associated with starting with a Tier 5 network is acknowledged, as there is a possibility that the demand for Tier 5 electricity access may not be realized within the project's lifetime. However, site visit findings suggest a strong demand and willingness to pay for higher tiers of electricity access. Although there are greater uncertainties associated with scaling up from Tier 3 to Tier 5 compared to the transition from Tier 0 to Tier 3, this study displays the potential benefits of initially investing in a Tier 5 distribution network, providing an effective electrification pathway in bridging the current electricity access gap.

7

Conclusion

In this final chapter of this report, the research questions of this project are answered and recommendations for future work are presented.

7.1. Answers to Research Questions

The following section provides answers to the research questions introduced in Subsection 1.3.1:

1. **Are market-available open-source design tools applicable for designing feasible PV-powered DC microgrid systems in South African informal settlements?**

   A review of available tools revealed that existing open-source design tools do not offer a comprehensive solution for sizing PV systems, batteries, and distribution networks tailored to specific sites and component selections within fully DC microgrids. The lack of such a comprehensive open-source tool that can address the entire system's design requirements cohesively, is likely due to the specialized nature of DC microgrid solutions for residential community electricity use. Purely DC microgrids are relatively uncommon compared to integrated AC systems, leading to less focus on their design and implementation. There is also limited research in the field of electricity access that address these needs comprehensively.

   This gap necessitated an approach where available open-source tools were utilized independently for each design domain and then integrated to form a cohesive and holistic design solution.

2. **How can a comprehensive design methodology for the desired PV-Powered DC Microgrid be developed, utilizing open-source market-available design tools?**

   For each design domain—demand forecasting, PV system design, distribution network design, and PV-battery sizing—market-available open-source tools were exploited. In the case where open-source tools were not suitable, Python scripts were developed based on established design methodologies :

   - Demand Forecasting:
     The free-to-use load profile model established by Dr. Narayan was utilized for generating tier-specific load profiles. This model was chosen due to its alignment with the MTF's energy access classifications, its focus on DC appliances, and its incorporation of real-world variability in load usage, making it well-suited for PV, battery, and cable sizing for the application of this study.
   - PV String Sizing & Modelling:
     The open-source Python library, PV Lib, was employed for PV system modeling and sizing using local meteorological data. PV Lib was selected for its open-source nature, its flexibility in modeling purely DC systems, and its demonstrated accuracy in predicting DC power output, as supported by relevant studies.
   - Distribution Network Design:
     A Python script was developed to facilitate the sequential process, which includes GIS-based data processing, identification of feasible cable paths using a pathfinding algorithm, and ILP

optimization to select the most cost-effective cable paths for achieving an optimal layout. Additionally, a custom Python script was created for calculating DC network cable losses, addressing the absence of suitable open-source tools for this specific task.

- PV and Battery Sizing:
  A python script adapting the analytical sizing method with LLP as the performance indicator was created to determine optimal PV and battery capacities that minimize material costs while achieving the desired level of reliability.

By combining these tools and methodologies, a unified approach that addresses the challenges of designing an effective PV-powered DC microgrid for informal settlements in South Africa is proposed. Specifically, a microgrid design that accommodates and scales with increasing electricity access from Tier 3 to Tier 5, that incorporates theft prevention, designs for ease of O&M, and limits user interface for preventing any misuse through a centralized system is designed. It also prioritizes cost optimality of the distribution network and system sizing for an economically feasible solution.

3. **How can the developed design process be generalized and applied to diverse scopes?**

   The developed design process was successfully applied to two diverse sites—Oudtshoorn and Daveyton—varying in geographical locations, size, and density. Despite these variations, the methodology proved effective in generating feasible microgrid designs for both sites. This comprehensive design methodology can be further generalized for applications beyond South Africa or informal settlements. By acquiring load profiles for specific uses (e.g., public lighting, EV charging stations, industrial areas) instead of designing the system in reference to the residential MTF load profiles, the PV-powered DC microgrid can be tailored to these various purposes. The selection of PV modules and cable sizes can be adjusted to utilize locally available or preferred components for specific applications.

   Though the size of the scope may be a limiting factor due to currently limited large datasets for the distribution network domain, the methodology remains highly versatile. By applying the current methodology to subgroups within a large area, multiple microgrids can be generated, thereby extending its applicability. Furthermore, improvements on the current distribution network design process can be transferred back to this comprehensive microgrid design framework and enlarge its scope.

7.2. Summary and Implications of Conducted Study

The goal of this project was to develop a robust framework for designing DC microgrids aimed at electrifying South African informal settlements. This objective was pursued by first identifying specific design considerations through site visits and consultations with local developers, which highlighted the unique challenges faced by the targeted communities. This foundation was essential for assessing the applicability of existing open-source design tools, revealing that no single tool could comprehensively address the needs for sizing the proposed PV-powered Dc microgrid solution. As a result, a comprehensive design framework was created, combining available open-source tools with custom Python scripts based on established design methodologies. Applying this framework to the informal settlements of Oudtshoorn and Daveyton proved its effectiveness in producing feasible microgrid designs that are both scalable and adaptable to increasing electrical demands. This approach not only meets technical requirements but also accommodates the practical constraints of these communities.

The implications of this project extends to the future of microgrid deployment. The methodology's flexibility in adapting to different geographical and community contexts underscores its potential for broader application. Implementing the recommended future work, as outlined in Section 7.3, will further refine the design process and enhance the framework's effectiveness and applicability. Overall, this project lays a solid foundation for advancing electrification efforts in South African informal settlements.

7.3. Future Work

The recommendations for future work are enclosed in the following:

1. **Conduct interviews / surveys to validate load profiles**
   To improve the accuracy of the load profiles specific to the targeted sites, it is recommended to conduct interviews and surveys to better understand local consumption behaviors. While surveys and interviews alone are insufficient for demand forecasting, as discussed in Subsection 2.4.1,

gathering detailed information on daily routines—such as when most family members are out of the house—and appliance usage, including usage duration and timing, can help refine the input parameters of the simulation model to be more specific to the targeted communities. This approach can be achieved for the starting tier levels, however, estimating future tier consumption behavior is challenging. Therefore, surveying or referencing load data from a similar community that is more advanced in tier levels can provide valuable insights for improving the simulated load profiles.

2. **Consider PV system orientations that shift the PV power production curve**
   For designing the PV system, only the optimal tilt at North facing orientation was considered for this work. However, alternative orientations that reshape the PV production curve may benefit by reducing battery sizing. Specifically, East-West orientations could flatten but widen the PV production curve to cover more of the two morning and evening load peaks. Alternatively, a fully West facing orientation could shift the PV production curve to the highest evening peak. These alternative orientation options, which could easily be implemented into the design process, could potentially reduce the necessary battery capacity, leading to a reduced system cost.
3. **Consider PV system mounting logistics**
   The mounting method of the PV system was not fully addressed in this study. Originally, the plan was to install PV modules solely on the roof of the central container. While feasible for smaller communities at lower tiers, larger communities and higher tier levels would necessitate a substantial amount of space. Site visits revealed that larger informal settlements, such as Diepsloot and Daveyton, have main streets lined with containers housing various shops and services. For installations in similar large-scale informal settlements, it is worth exploring the possibility of installing a roof structure between the rows of containers along these main streets. This approach would integrate the PV system into the community center and should be discussed with local community leaders and the owners of the shop and service containers.
4. **Enhancing computational power allowing for increased data sets**
   As discussed in Section 6.3, the methodology used for designing the distribution network in this study faces a trade-off between computation time and data size. While a finer grid of possible pillar points is desirable for identifying an optimal layout and increasing the cutoff value of the pathfinding algorithm can facilitate layouts that avoid crossing over households, this increases the data size and thus the computation time. Investigating the use of multithreading for the pathfinding algorithm could enhance computation speed for smaller communities. However, this issue is likely to persist for larger communities. Therefore, alternative approaches are recommended for further research. One such alternative is the multiplier-accelerated A* algorithm introduced in [45], which reduces computational effort with only a minor trade-off in optimality. Implementing this algorithm, or employing hierarchical clustering algorithms, could improve computational efficiency while accepting a slight reduction in the overall optimality of the design.
5. **Enabling multiple central containers for a single microgrid**
   The current design methodology does not consider the input of multiple central container locations, as a centralized system is preferred for theft prevention and ease of O&M measures. However, for larger communities that require significant space for PV and container installations, a centralized system may not be feasible. In such cases, the flexibility to place multiple container points could be beneficial. Therefore, it is recommended to adapt the distribution network design process to accommodate multiple container locations and to account for the cable losses in this more complex network.
6. **Account for 3D topology**
   The current design methodology assume a flat, two-dimensional plane, which overlooks the complexities introduced by varying terrain elevations and obstacles. Incorporating 3D topology would allow for more accurate modeling of cable lengths, potential physical barriers, and the impact of elevation changes on the distribution network. This enhancement would lead to more precise cost estimations, better planning for installation, and improved overall network performance by considering the actual physical environment in which the microgrid will operate.
7. **Detailed LCOE Analysis**
   Conducting a more detailed LCOE analysis and integrating it into the system sizing process as a financial performance indicator could lead to system sizing that is better optimized for cost-effectiveness, ensuring that the design not only meets technical requirements but also aligns with financial viability. This comprehensive analysis should consider all relevant costs, including installation fees, container costs, and maintenance expenses, which were not fully accounted for in this study.

Bibliography

[1] International Energy Agency. *Access to electricity improves slightly in 2023, but still far from the pace needed to meet SDG7*. https://www.iea.org/commentaries/access-to-electricity-improves-slightly-in-2023-but-still-far-from-the-pace-needed-to-meet-sdg7. Licence: CC BY 4.0. 2023.

[2] World Bank Group. *State of Electricity Access Report 2017 (Vol. 2): Full Report (English)*. Washington, D.C.: World Bank Group, 2017.

[3] Sustainable Energy for All. *Sustainable Development Goal 7 (SDG7) - Sustainable Energy for All*. Accessed: 2024. URL: https://www.seforall.org/our-work/sustainable-development-goal-7-sdg7#:~:text=Sustainable%20Development%20Goal%207%20(SDG7)%20calls%20for%20%E2%80%9Caffordable%2C,energy%20for%20all%E2%80%9D%20by%202030..

[4] African Climate Foundation. *Energy Access and Transitions*. https://africanclimatefoundation.org/programmes/energy-access-and-transitions/. Accessed: May 4, 2024.

[5] Hannah Ritchie, Pablo Rosado, and Max Roser. "Access to Energy". In: *Our World in Data* (2019). https://ourworldindata.org/energy-access.

[6] Department of Minerals and Energy, Republic of South Africa. *National Electrification Programme Evaluation: Summary Report*. Nov. 2001.

[7] Sandeep Mahajan. *Economics of South African Townships: Special Focus on Diepsloot*. Ed. by Sandeep Mahajan. World Bank Studies. License: Creative Commons Attribution CC BY 3.0 IGO. Washington, DC: World Bank, 2014. DOI: 10.1596/978-1-4648-0301-7.

[8] Department of Energy South Africa. *Integrated National Electrification Programme*. Department of Energy. Available at: http://www.energy.gov.za/files/INEP/inep_overview.html (Accessed 8 June 2020). 2018.

[9] Louise Tait. "Towards a multidimensional framework for measuring household energy access: Application to South Africa". In: *Energy for Sustainable Development* 38 (2017), pp. 1–9. ISSN: 0973-0826. DOI: https://doi.org/10.1016/j.esd.2017.01.007. URL: https://www.sciencedirect.com/science/article/pii/S0973082616310924.

[10] Debendra Chandra Baruah and Christopher Chintua Enweremadu. "Prospects of decentralized renewable energy to improve energy access: A resource-inventory-based analysis of South Africa". In: *Renewable and Sustainable Energy Reviews* 103 (2019), pp. 328–341. ISSN: 1364-0321. DOI: https://doi.org/10.1016/j.rser.2019.01.006. URL: https://www.sciencedirect.com/science/article/pii/S1364032119300085.

[11] Energy Sector Management Assistance Program (ESMAP). *Multi-Tier Framework*. https://mtfenergyaccess.esmap.org/methodology/electricity. The World Bank, Accessed: May 4, 2024.

[12] *South Africa - Country Commercial Guide - Energy*. Last published date: 2024-01-26. International Trade Administration, U.S. Department of Commerce. URL: https://www.trade.gov/country-commercial-guides/south-africa-energy.

[13] The Centre for Renewable and Sustainable Energy Studies (Stellenbosch University). *SA Energy Made Visual: Visualisation of South African Energy Data*. https://www.crses.sun.ac.za/sa-energy-stats/#load-shedding. Last updated: April 2024. 2024.

[14] Eskom Holdings SOC Ltd. *Loadshedding Clips*. Eskom Holdings SOC Ltd. Available at: https://www.eskom.co.za/loadshedding/ (Accessed 8 June 2020). 2024.

[15] Sean Moolman. *2022 Update: Eskom Tariff Increases vs Inflation Since 1988*. PowerOptimal. Available at: https://poweroptimal.com/2021-update-eskom-tariff-increases-vs-inflation-since-1988/. Aug. 2022.

[16] World Bank, Development Research Group. *Gini index (World Bank estimate) - Sub-Saharan Africa*. https://data.worldbank.org/indicator/SI.POV.GINI. Accessed: 2024-07-01.

[17] Jan Corfee-Morlot et al. *Financing Climate Futures: Rethinking Infrastructure*. Case Study for the OECD, UN Environment, World Bank project. OECD Publishing, 2018. URL: https://www.oecd.org/environment/cc/climate-futures.

[18] N. Narayan. “Solar home systems for improving electricity access: An off-grid solar perspective towards achieving universal electrification”. Dissertation. Delft University of Technology, 2019. URL: https://doi.org/10.4233/uuid:aa29b04f-4cd7-41fa-b48b-5edc75fef104.

[19] IEA. *Energy Access Outlook 2017: From Poverty to Prosperity*. Paris: IEA, 2017. URL: https://doi.org/10.1787/9789264285569-en.

[20] GIZ. *Photovoltaics for Productive Use Applications- A Catalogue of DC-Appliances*. Deutsche Gesellschaft für Internationale Zusammenarbeit (GIZ) GmbH, 2016.

[21] Arno H.M. Smets et al. *Solar Energy: The Physics and Engineering of Photovoltaic Conversion, Technologies and Systems*. Copyright © 2016 UIT Cambridge Ltd. UIT Cambridge Ltd., 2016. ISBN: 978-1-906860-75-2.

[22] C.B. Honsberg and S.G. Bowden. *Photovoltaics Education Website*. http://www.pveducation.org. 2019.

[23] Fraunhofer Institute for Solar Energy Systems, ISE. *PHOTOVOLTAICS REPORT*. Freiburg: Fraunhofer Institute for Solar Energy Systems, ISE with support of PSE Projects GmbH, May 2024. URL: www.ise.fraunhofer.de.

[24] *International Technology Roadmap for Photovoltaic (ITRPV)*. 15th. VDMA, 2023.

[25] Jan Haschke et al. “The impact of silicon solar cell architecture and cell interconnection on energy yield in hot & sunny climates”. In: *Energy Environ. Sci.* 10 (5 2017), pp. 1196–1206. DOI: 10.1039/C7EE00286F. URL: http://dx.doi.org/10.1039/C7EE00286F.

[26] ENF Ltd. *Solar Cell Directory 158mm Topcon Cells 5BB*. https://www.enfsolar.com/pv/cell-datasheet/2998. Accessed: 2024-07-14. 2024.

[27] Matthew Lave et al. “Evaluation of Global Horizontal Irradiance to Plane-of-Array Irradiance Models at Locations Across the United States”. In: *IEEE Journal of Photovoltaics* 5.2 (2015), pp. 597–606.

[28] Aron P. Dobos. “An Improved Coefficient Calculator for the California Energy Commission 6 Parameter Photovoltaic Module Model”. In: *Journal of Solar Energy Engineering* 134.2 (May 2012). DOI: 10.1115/1.4005759. URL: https://www.osti.gov/biblio/1043759.

[29] Jay A Kratochvil, William Earl Boyson, and David L King. “Photovoltaic array performance model.” In: (Aug. 2004). DOI: 10.2172/919131. URL: https://www.osti.gov/biblio/919131.

[30] Olindo Isabella. *PV systems components: MPP Tracking*. Course ET4378 Photovoltaic Systems (2022/2023). Lecture slides. 2023.

[31] P. Gilman. *SAM Photovoltaic Model Technical Reference*. Technical Report NREL/TP-6A20-64102. Contract No. DE-AC36-08GO28308. National Renewable Energy Laboratory (NREL), May 2015. URL: https://www.nrel.gov/docs/fy15osti/64102.pdf.

[32] PVsyst. *PVsyst 7 Help*. https://www.pvsyst.com/help.

[33] Mac Elvina. *Modeling 101: Performance Modeling Overview*. https://help-center.helioscope.com/hc/en-us/articles/13804165205395-Modeling-101. HelioScope Help Center. Mar. 2024.

[34] National Renewable Energy Laboratory. *PVWatts*. https://www.esig.energy/wiki-main-page/pvwatts-d1/#Plane-of-Array_Irradiance. ESIG Energy Wiki.

[35] EU Science Hub Joint Research Centre. *PVGIS data sources & calculation methods*. https://joint-research-centre.ec.europa.eu/photovoltaic-geographical-information-system-pvgis/getting-started-pvgis/pvgis-data-sources-calculation-methods_en.

[36] Valentin Software GmbH. *2024 PV*SOL Help*. https://help.valentin-software.com/pvsol/en/. 2024.

[37] HOMER Energy. *HOMER Pro 3.15: HOMER's Calculations*. https://homerenergy.com/products/pro/docs/3.15/homers_calculations.html.

[38] K. S. Anderson et al. “pvlib python: 2023 project update”. In: *Journal of Open Source Software* 8.92 (2023), p. 5994. DOI: 10.21105/joss.05994. URL: https://doi.org/10.21105/joss.05994.

[39] A Zuiker. “A comparative study of PV simulation and machine learning models on a macrolevel and microlevel”. MA thesis. 2019.

[40] Inkwood Research. *Size of the global battery market from 2018 to 2021, with a forecast through 2030, by technology (in million U.S. dollars) [Graph]*. In Statista. Retrieved July 14, 2024, from https://www-statista-com.tudelft.idm.oclc.org/statistics/1339880/global-battery-market-size-by-technology/. Sept. 2022.

[41] Faruk A. Bhuiyan and Amirnaser Yazdani. “Energy storage technologies for grid-connected and off-grid power system applications”. In: *2012 IEEE Electrical Power and Energy Conference*. 2012, pp. 303–310. DOI: 10.1109/EPEC.2012.6474970.

[42] Eliseo Zarate-Perez et al. “Battery energy storage performance in microgrids: A scientific mapping perspective”. In: *Energy Reports* 8 (2022). Technologies and Materials for Renewable Energy, Environment and Sustainability, pp. 259–268. ISSN: 2352-4847. DOI: https://doi.org/10.1016/j.egyr.2022.06.116. URL: https://www.sciencedirect.com/science/article/pii/S2352484722012598.

[43] Yuqing Yang et al. “Battery energy storage system size determination in renewable energy systems: A review”. In: *Renewable and Sustainable Energy Reviews* 91 (2018), pp. 109–125. ISSN: 1364-0321. DOI: https://doi.org/10.1016/j.rser.2018.03.047. URL: https://www.sciencedirect.com/science/article/pii/S1364032118301436.

[44] Graeme Vanderstar and Petr Musilek. “Optimal Design of Distribution Overhead Powerlines Using Genetic Algorithms”. In: *IEEE Transactions on Power Delivery* 37.3 (2022), pp. 1803–1812. DOI: 10.1109/TPWRD.2021.3099007.

[45] J. C. Li, D. Zimmerle, and P. M. Young. “Effective rural electrification via optimal network: Optimal path-finding in highly anisotropic search space using multiplier-accelerated A* algorithm”. In: *Energy and AI* 7 (2022), p. 100119. ISSN: 2666-5468. DOI: 10.1016/j.egyai.2021.100119. URL: https://www.sciencedirect.com/science/article/pii/S2666546821000689.

[46] Aric A. Hagberg, Daniel A. Schult, and Pieter J. Swart. “Exploring network structure, dynamics, and function using NetworkX”. In: *Proceedings of the 7th Python in Science Conference (SciPy2008)*. Ed. by Gäel Varoquaux, Travis Vaught, and Jarrod Millman. Pasadena, CA USA, Aug. 2008, pp. 11–15.

[47] Courtney Blodgett et al. “Accuracy of energy-use surveys in predicting rural mini-grid user consumption”. In: *Energy for Sustainable Development* 41 (2017), pp. 88–105.

[48] National Fire Protection Association. *National Electrical Code, Article 310—Conductors for General Wiring*. 2014. URL: https://www.nfpa.org/Codes-and-Standards/All-Codes-and-Standards/List-of-Codes-and-Standards/detail?code=70.

[49] Olindo Isabella. *PV Systems Components - Cables and batteries*. Course ET4378 Photovoltaic Systems (2022/2023). Lecture slides. 2023.

[50] L. Thurner et al. “pandapower — An Open-Source Python Tool for Convenient Modeling, Analysis, and Optimization of Electric Power Systems”. In: *IEEE Transactions on Power Systems* 33.6 (Nov. 2018), pp. 6510–6521. ISSN: 0885-8950. DOI: 10.1109/TPWRS.2018.2829021.

[51] Jijian Lian et al. “A review on recent sizing methodologies of hybrid renewable energy systems”. In: *Energy Conversion and Management* 199 (2019), p. 112027. ISSN: 0196-8904. DOI: https://doi.org/10.1016/j.enconman.2019.112027. URL: https://www.sciencedirect.com/science/article/pii/S0196890419310337.

[52] Tamer Khatib, Ibrahim A. Ibrahim, and Azah Mohamed. “A review on sizing methodologies of photovoltaic array and storage battery in a standalone photovoltaic system”. In: *Energy Conversion and Management* 120 (2016), pp. 430–448. ISSN: 0196-8904. DOI: https://doi.org/10.1016/j.enconman.2016.05.011. URL: https://www.sciencedirect.com/science/article/pii/S0196890416303776.

[53] N. O. Shokoya and A. K. Raji. “Electricity Theft: A Reason to Deploy Smart Grid in South Africa”. In: *2019 International Conference on the Domestic Use of Energy (DUE)*. 2019, pp. 96–101.

[54] Author. *The Safety of Township Tourists in Cape Town, South Africa: A Customer Orientation Approach*. https://www.researchgate.net/publication/351903999_The_Safety_of_Townships_Tourists_in_Cape_Town_South_Africa_A_Customer_Orientation_Approach. Accessed: 2024-06-07. 2024.

[55] Simon Tindemans. *Low Carbon London smart meter data (refactored)*. Version 1. 2023. DOI: 10.4121/fbbe775b-48d8-469f-a39b-b64488bfd6fd.v1. URL: https://doi.org/10.4121/fbbe775b-48d8-469f-a39b-b64488bfd6fd.v1.

[56] PV Performance Modeling Collaborative (PVPMC). *Simple Sandia Sky Diffuse Model*. https://pvpmc.sandia.gov/modeling-guide/1-weather-design-inputs/plane-of-array-poa-irradiance/calculating-poa-irradiance/poa-sky-diffuse/simple-sandia-sky-diffuse-model/. Accessed: 2024-07-03. Sandia National Laboratories.

[57] Adam Sparks. “nasapower: A NASA POWER Global Meteorology, Surface Solar Energy and Climatology Data Client for R”. In: *Journal of Open Source Software* 3.30 (2018), p. 1035. DOI: 10.21105/joss.01035.

[58] QGIS.org. *QGIS Geographic Information System*. Open Source Geospatial Foundation Project. 2024. URL: http://qgis.org.

[59] Stuart Mitchell. *PuLP: A Linear Programming Toolkit for Python*. Available at https://github.com/coin-or/pulp. 2011.

[60] Eduardo Lorenzo. *Solar electricity: engineering of photovoltaic systems*. Progensa, 1994, p. 207.

[61] BloombergNEF. *Lithium-ion battery price worldwide from 2013 to 2023 (in 2023 U.S. dollars per kilowatt-hour) [Graph]*. In Statista. Retrieved July 15, 2024, from https://www-statista-com.tudelft.idm.oclc.org/statistics/883118/global-lithium-ion-battery-pack-costs/. 2023.

A

Input Parameters for the Load Profile Generating Model

Load j	Rating P [W]					T_{min}	T_{max}	T_m [h]					n_{min}	n_{max}	W1 start time	W1 length [h]	W2 start time	W2 length [h]	Quantity q [-]				
	T-1	T-2	T-3	T-4	T-5	[min]	[min]	T-1	T-2	T-3	T-4	T-5	[-]	[-]					T-1	T-2	T-3	T-4	T-5
LED Lighting	2	2	2	2	2	30	240	6	8	8	12	12	1	12	4	2	18	6	3	5	5	8	12
Mobile Phone Charging	3	3	3	3	3	5	120	6	8	8	8	8	1	12	0	1	6	18	2	3	3	5	5
Radio	0	3	3	3	3	5	240	0	8	8	12	12	1	10	7	13	0	0	0	2	2	2	2
Fan	0	15	20	35	35	5	600	0	8	8	12	16	1	10	7	12	0	0	0	1	2	4	4
TV	0	12	18	29	29	5	240	0	8	8	12	12	1	10	7	7	17	6	0	1	1	2	2
Fridge	0	0	54	54	54	5	30	0	0	3	8	24	5	15	5	19	0	0	0	0	1	1	1
Tablet	0	0	18	18	18	5	120	0	0	6	12	12	1	10	0	1	6	18	0	0	1	1	1
Kettle	0	0	0	400	400	5	15	0	0	0	1	1	1	8	7	14	0	0	0	0	0	1	1
Laptop	0	0	0	60	60	5	240	0	0	0	6	6	1	10	0	1	6	18	0	0	0	1	1
Rice Cooker	0	0	0	200	200	30	30	0	0	0	1.5	1.5	1	3	10	2	17	3	0	0	0	1	1
Clothes Iron	0	0	0	150	150	5	20	0	0	0	2	2	1	2	6	16	0	0	0	0	0	1	1
Washing machine	0	0	0	70	70	15	120	0	0	0	2	2	0	1	6	14	0	0	0	0	0	1	1
Air cooler	0	0	0	500	500	30	120	0	0	0	4	12	0	8	9	9	0	0	0	0	0	1	1
Power tools	0	0	0	0	100	5	60	0	0	0	0	10	2	10	6	14	0	0	0	0	0	0	1
Grinders/Millers	0	0	0	0	750	10	120	0	0	0	0	10	2	10	6	14	0	0	0	0	0	0	1
Sewing Machine	0	0	0	0	40	5	120	0	0	0	0	10	3	20	6	14	0	0	0	0	0	0	1
Water Pump	0	0	0	0	750	5	30	0	0	0	0	4	0	2	5	12	0	0	0	0	0	0	1

Figure A.1: The operational constraints and inputs to the load profile simulation model [18]. DC appliance specifications from those listed in [20].